

DISSERTATION

SOLUTE TRANSPORT BY A VOLATILE SOLVENT

Submitted by

Glenn Owen Brown

Civil Engineering Department

In partial fulfillment of the requirements

for the Degree of Doctor of Philosophy

Colorado State University

Fort Collins, Colorado

Summer 1987

LIBRARIES  
COLORADO STATE UNIVERSITY  
FORT COLLINS, COLORADO

QC  
175.2  
.B76  
1987

COLORADO STATE UNIVERSITY

Summer 1987

WE HEREBY RECOMMEND THAT THE THESIS PREPARED UNDER OUR SUPERVISION  
BY Glenn Owen Brown

ENTITLED SOLUTE TRANSPORT BY A VOLATILE SOLVENT

BE ACCEPTED AS FULFILLING IN PART REQUIREMENTS FOR THE DEGREE OF  
Doctor of Philosophy

Committee on Graduate Work

James W. Warner  
Deanna Quinlan  
J. D. Stone

Co-Adviser

Deil B. McWhorter

Adviser

J. D. Stone

Department Head

COLORADO STATE UNIVERSITY LIBRARIES

ABSTRACT OF DISSERTATION  
SOLUTE TRANSPORT BY A VOLATILE SOLVENT

Reclamation and impact analysis of retorted oil shale piles will require prediction of water and solute transport rates over the entire solution content range, down to and including the relatively dry region. In such dry materials, vapor transport of water affects the transport of solutes. Experimental measurements of transport coefficients in relatively dry oil shale have brought forward long-standing questions concerning the mechanics of combined liquid-vapor flow. Principal among these is the apparent inability of porous media to transport solutes at low solution contents.

In an attempt to ensure proper interpretation of experimental data, a new theory of solute transport by combined liquid-vapor flow has been developed, and new analytical solutions for transient flow have been obtained. The solutions show that the relative magnitudes of the separate transport coefficients produce many of the flow features seen in experimental data, and significant liquid transport can occur in regions without apparent solute transport. This development is new and represents an addition to the understanding of solute transport. These methods and results can be applied to other problems in multiple phase transport, such as hazardous waste disposal, mine reclamation, and soil leaching.

Glenn Owen Brown  
Civil Engineering Department  
Fort Collins, Colorado 80523  
Summer 1987

#### ACKNOWLEDGMENTS

The author extends his sincere gratitude to his advisor, Dr. D.B. McWhorter. Dr. McWhorter's support, advice, and encouragement were invaluable to this study.

Thanks are also due the author's co-advisor Dr. John D. Nelson, and committee members Drs. James W. Warner and Deanna S. Durnford. Their time, counsel and cooperation are appreciated.

Special thanks are due Mr. John A. Brookman, who aided in the experimental program and drafted many of the figures. The effort and patience of Mrs. Elaine Dean in the preparation of this manuscript are deeply appreciated. Drs. Arnold Klute and Mark E. Grismer provided very helpful advice.

Support for this research was provide by three sources. The research was initiated by funding from the AMOCO Research Center, Naperville, Illinois. Mr. George Watson was the AMOCO project officer. The majority of support was provided by the U.S. Environmental Protection Agency, under Cooperative Agreement CR812225. Mr. Edward R. Bates, Office of Research and Development, Hazardous Waste Engineering Research Laboratory, Cincinnati, Ohio was the EPA project officer. A thesis award funded by the U.S. Department of the Interior, Office of Surface Mining, and awarded by the Minerals Research Institute at the Colorado School of Mines, helped in the preparation of the dissertation.

DEDICATION

To Barbara McColl Brown. She is surely the best wife a professional student could wish for.

## TABLE OF CONTENTS

<u>Chapter</u>		<u>Page</u>
1	INTRODUCTION . . . . .	1
	MOTIVATION . . . . .	1
	OBJECTIVES . . . . .	5
2	LITERATURE REVIEW . . . . .	6
	LIQUID TRANSPORT . . . . .	6
	Flow Theory and Analysis . . . . .	7
	Liquid State at Low Solution Contents . . . . .	9
	VAPOR AND LIQUID TRANSPORT . . . . .	11
	Flow Theory and Analysis . . . . .	11
	Theoretical Concerns . . . . .	19
	SOLUTE TRANSPORT . . . . .	20
	Solute Transport Processes . . . . .	20
	Non-Piston Displacement . . . . .	24
	Solute Transport by a Volatile Solvent . . . . .	26
	SUMMARY . . . . .	29
3	GOVERNING EQUATIONS . . . . .	30
	CONDITIONS OF INTEREST AND TERMINOLOGY . . . . .	30
	SOLVENT TRANSPORT . . . . .	33
	Liquid Solvent . . . . .	33
	Solvent Vapor . . . . .	37
	Gas Phase Bulk Flow . . . . .	41
	Total Solvent Flow . . . . .	46
	Gas Phase Dispersion . . . . .	52
	SOLUTE TRANSPORT . . . . .	53
4	SOLUTIONS TO TRANSPORT EQUATIONS . . . . .	56
	CONSTANT SOLUTION CONTENT BOUNDARIES . . . . .	56
	Total Solvent Transport . . . . .	56
	Liquid Phase Solvent Transport . . . . .	63
	Solute Transport . . . . .	66
	CONSTANT INLET SOLUTION FLUX . . . . .	72
	Total Solvent Transport . . . . .	72
	Liquid Phase Solvent Transport . . . . .	77
	Solvent Transport . . . . .	77
	Numerical Particle Tracking . . . . .	79
5	EXPERIMENTAL PROCEDURES AND RESULTS . . . . .	83
	MATERIAL AND PREPARATION . . . . .	83
	PARTICLE SIZE AND DENSITY . . . . .	85
	WATER CHARACTERISTIC . . . . .	85
	Procedures . . . . .	85
	Results . . . . .	90
	SPECIFIC SURFACE . . . . .	94

<u>Chapter</u>		<u>Page</u>
	SURFACE CONDUCTIVITY . . . . .	96
	SOLUTE TRANSPORT BY LIQUID-VAPOR FLOW . . . . .	97
	Theory . . . . .	97
	Apparatus . . . . .	102
	Procedures . . . . .	104
	Interpretation and Results . . . . .	105
6	ANALYSIS . . . . .	117
	DIFFUSIVITIES . . . . .	118
	CONSTANT SOLUTION CONTENT BOUNDARY . . . . .	121
	Sorpton into a Dry Column . . . . .	121
	Gas Convection Effects . . . . .	135
	Sorpton with a Resident Solution . . . . .	140
	CONSTANT INLET FLUX SORPTION . . . . .	152
	Assumed $F(\theta)$ . . . . .	152
	Sorpton into a Dry Material . . . . .	153
	Sorpton with a Resident Solution . . . . .	162
7	SUMMARY, CONCLUSIONS AND RECOMMENDATIONS . . . . .	170
	SUMMARY . . . . .	170
	CONCLUSIONS . . . . .	172
	RECOMMENDATIONS . . . . .	175
	REFERENCES . . . . .	177
	APPENDIX - EXPERIMENTAL DATA . . . . .	183

LIST OF TABLES

<u>Table</u>	<u>Page</u>
5.1. Saturated salt solutions used in vapor sorption . . . .	92
A.1. Grain size distribution of Lurgi retorted oil shale . .	183
A.2. Vapor sorption isotherms for Lurgi retorted oil shale. .	184
A.3. Water characteristic for Lurgi retorted oil shale . . .	185
A.4. Liquid content and solute concentration for Run 1 . . .	186
A.5. Liquid content and solute concentration for Run 2 . . .	189

LIST OF FIGURES

<u>Figure</u>	<u>Page</u>
1.1. Leachate evaporating oil shale pile (after Golder and Associates, 1983) . . . . .	3
2.1. Liquid, vapor and total vapor diffusion (after Jackson, 1965) . . . . .	16
2.2. Rose's stages of water transport (after Rose, 1963b.) . . . . .	18
2.3. $\theta(\lambda)$ and $C_s/C_{sn}(\lambda)$ data from two experiments (after Smiles et al., 1978) . . . . .	22
2.4. $SrCl_2$ solution injection into dry Ritzville silt loam (after Grismer, 1984) . . . . .	27
2.5. $SrCl_2$ solution injection into moist Ritzville silt loam (after Grismer, 1984) . . . . .	28
3.1. Macroscopic control volume of porous media . . . . .	31
3.2. Phase transfer and induced gas phase convection during sorption into a dry porous media . . . . .	44
4.1. Constant solution content boundary sorption profiles . . . . .	58
4.2. $F(\theta)$ relationships . . . . .	64
4.3. Constant flux boundary sorption profiles . . . . .	74
5.1. Grain size distribution of Lurgi retorted oil shale . . . . .	86
5.2. Pressure cell apparatus . . . . .	88
5.3. Water characteristic for Lurgi retorted oil shale . . . . .	91
5.4. Water vapor sorption isotherms for Lurgi retorted oil shale . . . . .	93
5.5. B.E.T. plot of vapor adsorption data . . . . .	95
5.6. Falling head permeameter analysis . . . . .	98
5.7. Dual source gamma system . . . . .	103
5.8. Idealized depiction of dry column behavior . . . . .	106

<u>Figure</u>	<u>Page</u>
5.9. Solution and solute profiles for wetting in Run 1 . . . .	109
5.10. Solution and solute profiles for redistribution in Run 1 . . . . .	110
5.11. Solution and solute profiles for wetting in Run 2 . . . .	111
5.12. Range of solution contents at salt front in Run 1 . . . .	112
5.13. Range of solution contents at salt front in Run 2 . . . .	114
5.14. Total diffusivity for Lurgi retorted shale . . . . .	115
5.15. Unsaturated conductivity for Lurgi retorted shale . . . .	116
6.1. Assumed normal divisions of diffusivity . . . . .	119
6.2. Total diffusivity for cases 1, 2, and 3 . . . . .	122
6.3. Fractional flow function for cases 1, 2, and 3 . . . . .	123
6.4. Liquid content profiles for cases 1, 2, and 3 . . . . .	125
6.5. Seepage velocity for cases 1, 2, and 3 . . . . .	126
6.6. Water phase transfer versus $\lambda$ for cases 1, 2, and 3 . . .	128
6.7. Water phase transfer versus $\theta$ for cases 1, 2, and 3 . . .	129
6.8. Invading solute concentration profiles for cases 1, 2, and 3 . . . . .	130
6.9. Velocity ratio, B versus $\theta$ for cases 1, 2, and 3 . . . .	132
6.10. Relative liquid flux versus $\lambda$ , for cases 1, 2, and 3 . . .	133
6.11. Relative liquid flux versus $\theta$ , for cases 1, 2, and 3 . . .	134
6.12. Gas convection for case 3 . . . . .	137
6.13. Gas convection ratio for case 3 . . . . .	138
6.14. Gas convection derivative for case 3 . . . . .	139
6.15. Fraction flow function for cases 4 and 5 . . . . .	141
6.16. Liquid content profiles for cases 4 and 5 . . . . .	142
6.17. Water phase transfer versus $\lambda$ for cases 4 and 5 . . . . .	144
6.18. Water phase transfer versus $\theta$ for cases 4 and 5 . . . . .	145
6.19. Relative liquid flux for cases 4 and 5 . . . . .	146

<u>Figure</u>	<u>Page</u>
6.20. Seepage velocity for cases 4 and 5 . . . . .	147
6.21. Velocity ratio B, for cases 4 and 5 . . . . .	148
6.22. Invading solute concentration profiles for cases 4 and 5 . . . . .	149
6.23. Resident solute concentration profiles for cases 4 and 5 . . . . .	150
6.24. Measured constant flux fractional flow functions . . .	154
6.25. Liquid content profiles for case 6 . . . . .	155
6.26. Time to inlet liquid content for case 6 . . . . .	157
6.27. Seepage velocity for case 6 . . . . .	158
6.28. Phase transfer for case 6 . . . . .	159
6.29. Solute Concentration for case 6 . . . . .	160
6.30. Liquid content at the solute front in case 6 . . . . .	161
6.31. Liquid content profile for case 7 . . . . .	163
6.32. Time to inlet liquid content for case 7 . . . . .	164
6.33. Seepage velocity for case 7 . . . . .	165
6.34. Phase transfer for case 7 . . . . .	166
6.35. Invading solute concentration for case 7 . . . . .	167
6.36. Resident solute concentration for case 7 . . . . .	169

## LIST OF SYMBOLS

Variable	Definition	Dimensions
A	Sample area	$L^2$
a	Reservoir area	$L^2$
b	Attenuation slope coefficient	$L^{-1}$
$C_a$	Carrier gas concentration	$M/L^3$
$C_m$	Solid matrix concentration	$M/L^3$
$C_r$	Adsorbed solute concentration	$M/L^3$
$C_s$	Liquid solute concentration	$M/L^3$
$C_v$	Solvent vapor gas concentration	$M/L^3$
$C_{vs}$	Saturated solvent vapor concentration	$M/L^3$
$C_w$	Liquid solvent concentration	$M/L^3$
c	B.E.T. adsorption constant	none
$w_i$	Component mass fraction	none
$D_l$	Liquid hydraulic diffusivity	$L^2/T$
$D_m$	Free space molecular diffusion coefficient	$L^2/T$
$D_s$	Solute dispersion coefficient	$L^2/T$
$D_t$	Total solvent diffusivity	$L^2/T$
$D_v$	Vapor solvent effective diffusion coefficient	$L^2/T$
$D_w$	Liquid solvent dispersion coefficient	$L^2/T$
d	Particle size	L
E	Solvent phase transfer	$M/L^3T$
e	Normalized phase transfer	none
e'	Transformed phase transfer	$T/L^2$
F	Fractional flow function	none

Variable	Definition	Dimensions
$F_a$	Carrier gas mass flux	$M/L^2T$
$F_s$	Solute mass flux	$M/L^2T$
$F_{so}$	Solute mass influx	$M/L^2T$
$F_t$	Total solvent mass flux	$M/L^2T$
$F_v$	Mass flux of vapor solvent	$M/L^2T$
$F_w$	Mass flux of liquid solvent	$M/L^2T$
$g$	Acceleration of gravity	$L/T^2$
$h$	Pressure head	$L$
$H_o$	Initial reservoir head	$L$
$H_t$	Reservoir head	$L$
$h_c$	Capillary head	$L$
$h_o$	Osmotic head	$L$
$h_t$	Thermodynamic head	$L$
$I$	Count rate	$T^{-1}$
$I'$	Unadjusted count rate	$T^{-1}$
$I_a$	Americium count rate	$T^{-1}$
$I_c$	Cesium count rate	$T^{-1}$
$I_o$	Initial count rate	$T^{-1}$
$I_{oa}$	Initial americium count rate	$T^{-1}$
$I_{oc}$	Initial cesium count rate	$T^{-1}$
$I_s$	Standard adsorbed count rate	$T^{-1}$
$I_{so}$	Initial standard absorbed count rate	$T^{-1}$
$i$	B.E.T. intercept	none
$K$	Hydraulic conductivity	$L/T$
$KI$	Integration constant	undefined
$K_s$	Saturated hydraulic conductivity	$L/T$
$k$	Intrinsic permeability	$L^2$

Variable	Definition	Dimensions
$k_d$	Source constant	none
$L$	Sample length	$L$
$M_w$	Molar weight	$M/\text{mole}$
$m$	Molar solute concentration	$M/M$
$P_e$	Peclet number	none
$P_g$	Gas pressure	$M/LT^2$
$P_l$	Liquid pressure	$M/LT^2$
$P_s$	Standard pressure	$M/LT^2$
$p$	Solvent vapor partial pressure	$M/LT^2$
$Q_l$	Relative liquid flux	none
$q_g$	Volumetric gas flux	$L/T$
$q'_g$	Normalized gas convection	$L/T^{3/2}$
$q_l$	Volumetric liquid flux	$L/T$
$q_{l0}$	Inlet volumetric liquid flux	$L/T$
$q_t$	Total equivalent volumetric flux	$L/T$
$q_{to}$	Total solvent inlet volumetric flux	$L^3/L^2T$
$R$	Solute phase transfer	$M/L^3T$
$SS$	Specific surface	$L^2/M$
$s$	B.E.T. slope	none
$T$	Transformed temporal coordinate	$L^2/T$
$T_a$	Absolute temperature	$^{\circ}K$
$T_o$	Transformed time to inlet liquid content	$L^2/T$
$T_s$	Standard temperature	$^{\circ}K$
$v_s$	Seepage velocity	$L/T$
$v'_s$	Normalized seepage velocity	$L/T^{1/2}$
$v_{\theta}$	Liquid content velocity	$L/T$
$X$	Transformed spatial coordinate	$L^2/T$

Variable	Definition	Dimensions
$x$	Spatial coordinate	L
$\beta$	Attenuation coefficient	$L^{-1}$
$\beta^*$	Ratio of molecular weights	none
$\beta'$	Carrier-vapor coefficient	$L^3/M$
$\beta_a$	Americium attenuation coefficient for water	$L^{-1}$
$\beta_c$	Cesium attenuation coefficient for water	$L^{-1}$
$\beta_w$	Attenuation coefficient for water	$L^{-1}$
$\theta$	Normalized volumetric liquid content	none
$\theta$	Volumetric liquid content	$L^3/L^3$
$\theta_m$	Monolayer volumetric liquid content	$L^3/L^3$
$\theta_n$	Initial liquid content	$L^3/L^3$
$\theta_o$	Inlet liquid content	$L^3/L^3$
$\lambda$	Boltzman variable	$L/T^{1/2}$
$\mu$	Dynamic viscosity	M/TL
$\mu_w$	Water mass adsorption coefficient	$L^2/M$
$\mu_s$	Solute mass adsorption coefficient	$L^2/M$
$\nu$	Mass flow correction factor	none
$\rho_g$	Gas phase density	$M/L^3$
$\rho_{gs}$	Standard gas density	$M/L^3$
$\rho_l$	Liquid phase density	$M/L^3$
$\rho_s$	Solid phase density	$M/L^3$
$\phi$	Porosity	$L^3/L^3$
$\alpha$	Tortousity	none

## Chapter 1

### INTRODUCTION

#### MOTIVATION

The rise in the environmental ethic in this country has brought with it the demand that natural physical processes, not only be understood in a general sense, but also be quantifiable and predictable. There is a concern among the public and technical communities that today's economic activities, such as mining, farming and waste disposal, may produce their most significant environmental impacts not today, but many years from now. This attitude is based on the assumption that while most impacts are rapid, obvious, and usually manageable, any slow process at work may not express itself until it is too late for prevention. The subject of this thesis, solute transport by volatile solvent, which occurs in relatively dry porous media, is one such process. It is a process that is generally slow, qualitatively understood, but lacking in quantifiable solutions for even simple flow conditions.

Questions concerning the disposal of retorted oil shale provided the direct motivation for this research. A possible source of future liquid fuels are the large deposits in the Western U.S. of "oil shale", which is actually a marlstone containing kerogen, a high molecular weight hydrocarbon. Presently, the most popular means of removing the kerogen is to mine the oil shale, and heat it in surface retorts. Upon heating in the retort vessel, much of the kerogen vaporizes, is

recovered, and condensed back to a liquid. The retorted oil shale is then removed from the retort. Depending on the specific process, the retorted shale can have large amounts of soluble salts, and lesser quantities of heavy metals and organics. Disposal of this material in a manner which protects the environment is of great concern, especially since a mature oil shale industry could produce  $9 \times 10^5$  metric tons of solid waste a day (Heistand, 1985). That rate translates into a cube, one kilometer to a side, in only three years. Piles may be about 100 meters in height and will cover several square kilometers.

Accurate prediction of water and salt movement through disposal piles will require measurements of both water and solute transport over the entire range of solution content, down to and including the relatively dry region. Dry region transport phenomenon is of concern for two reasons. First, retorting produces a solid that is bone dry (drier than standard oven drying). It is expected that only enough water to control dust will be added before placement, and much of that may rapidly be lost to evaporation. Thus a pile's initial condition, before infiltration of precipitation, will probably be relatively dry. Leaching may be strongly influenced by transport processes near the initial condition. Second, an earlier study by Golder Associates (1983) has proposed that piles be designed to eliminate leachate by evaporating all excess infiltration. Figure 1.1 presents a conceptual picture of the pile. Any leachate moving through the pile would be intercepted by a layer of coarse overburden. By natural or artificial means, dry air would be passed through the coarse layer. This air would evaporate the leachate and then exhaust from rock chimneys. Such evaporation would, of course, require the portion of the pile near the evaporation interface to remain quite dry.

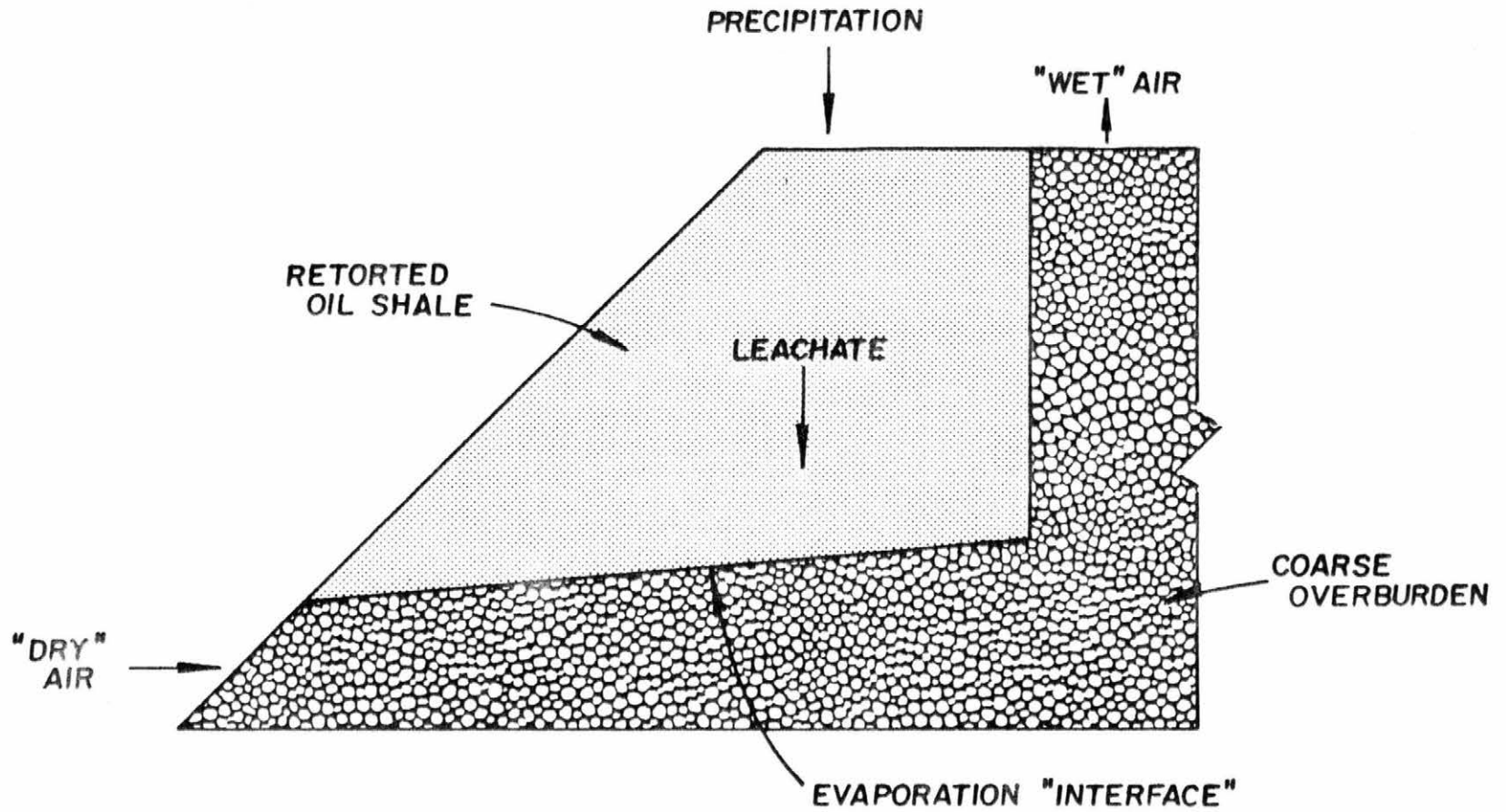


Figure 1.1. Leachate evaporating oil shale pile (after Golder and Associates, 1983).

It is known that in relatively dry media vapor transport of water plays an important role, but it has not been impossible to directly separate liquid and vapor water transport. In an attempt to do so, Grismer (1984) developed a dual source gamma ray attenuation system which can accurately measure both water and solute transport rates. It was hoped that analysis of the data would shed light on the two-phase transport of water. Grismer's measurements in soils and the writer's measurements in retorted oil shale produced rather unexpected results. Principal among these is the apparent inability of porous media to transport solutes at low solution contents. Specifically, during the transient sorption of solution into an initially dry column, a region of solute-free water (at low volumetric solution contents) was observed to develop at the front of the sorption profile.

The regularity, and strength of the observed process convinced the writer that something of importance was occurring. At first it was thought that a "critical" water content, was being observed; a critical water content being a solution content below which solute is not transported. But the limitations of existing theory prevented the exact analysis of the experimental data. After many failed attempts to analyze the experimental data it became obvious that existing theory and solutions were inadequate. Specifically, existing theories did not account for the effect of solvent vaporization on the distribution of nonvolatile solutes. Thus, it was decided that an expanded theory and new solutions of the governing equations were necessary if the experimental results were to be adequately explained.

## OBJECTIVES

Within the broad motivation of this research, this dissertation will pursue six somewhat narrow objectives. The objectives are:

- 1) Review the present theory of combined liquid flow and solute transport under isothermal conditions.
- 2) Expand the theory of combined liquid-vapor flow, such that phase transfer and the contributions of each phase to water transport is explicitly shown.
- 3) Develop a theory for solute transport in a volatile solvent.
- 4) Develop analytical and numerical solutions of the solvent and solute transport in specific transient flow problems.
- 5) Experimentally measure water and solute transport in a relatively dry retorted oil shale.
- 6) Apply theoretical developments to interpret experimental data obtained from both experiments and the literature.

The dissertation is organized as follows: Chapter 2 presents a review and synthesis of the literature; and Chapter 3 contains the development of a theory for liquid, vapor and solute transport. Several special solutions to the flow systems of interest are presented in Chapter 4. In Chapter 5 experimental procedures and results obtained for Lurgi retorted oil shale are presented, while Chapter 6 contains an analysis of the data obtained and other data found in the literature. Finally, Chapter 7 summarizes and reviews the study conclusions.

## Chapter 2

### LITERATURE REVIEW

This chapter will present current concepts and applications in solute transport by a volatile solute. To develop these concepts it will be necessary to look at a relatively broad range of literature. The material includes unsaturated flow theory, vapor flow, combined liquid-vapor flow, solute transport, ionic effects and transient flow solution methods. The chapter divides the material into three main sections; liquid flow, combined liquid-vapor flow and solute transport. Each section will address theoretical, experimental and solution methods that have been advanced.

In addition to reviewing the previous work this chapter will attempt a synthesis, or more accurately a Hegelian dialectic, which will reconcile the apparently contradictory theses in the literature. This synthesis is necessary because, without it, the results and conclusions of this research could be unfairly criticized.

#### LIQUID TRANSPORT

In this section two points will be addressed. The first subsection will examine the theory and analysis of transient, liquid flow in porous media. Governing equations and solution methods will be presented. The second subsection will examine the range of liquid content over which the theory should apply. Specifically, it will

address if it is reasonable to expect hydraulic flow of water in relatively dry porous media.

#### Flow Theory and Analysis

The first significant advancements relative to this study are the work of Childs and George (1950), and Klute (1952). They showed for unsaturated horizontal flow, Darcy's law could be transformed to a diffusional form. This is accomplished by defining a liquid diffusivity,  $D_1$ ,

$$D_1 = K dh/d\theta \quad , \quad (2.1)$$

where  $K$  is the hydraulic conductivity, (a function of  $\theta$ ),  $h$  is the pressure potential and  $\theta$  is the volumetric solution content. Darcy's law is then stated as

$$q_1 = -D_1 \partial\theta/\partial x \quad , \quad (2.2)$$

where  $q_1$  is the liquid volume flux and  $x$  is the spatial coordinate. This diffusional form has two advantages. First, it is generally easier to measure solution contents than pressure head, and second, the linear diffusion equation has been solved for many special cases of interest. The principal disadvantage to this form is that the water characteristic,  $h$  versus  $\theta$ , must be single valued during the flow process. For most porous media, the water characteristic is hysteretic and will only be single valued for processes that are entirely wetting or entirely drying.

For transient flow problems, a control volume balance will yield

$$\partial\theta/\partial t = \partial/\partial x(D_1 \partial\theta/\partial x) \quad , \quad (2.3)$$

where  $t$  is time. Klute also determined values of  $D_1$  by finite difference methods on horizontal column data, by solving Eq. (2.3) for  $D_1$ .

Bruce and Klute (1956) showed experimentally and theoretically that for the constant-solution-content boundary conditions,  $(\theta(x,0)=\theta(\infty,t)=\theta_0; \theta(0,t)=\theta_n)$ , Eq. (2.3) could be "transformed" to an ordinary differential equation by the Boltzman variable,  $\lambda=x/t^{1/2}$ . This allowed for convenient measurements of  $D_1$ .

McWhorter (1971) and Phillip (1973) showed that Eq. (2.3) could be solved by a method of fractional flow. The flux at any  $\theta(x,t)$  is defined as a fraction,  $F(\theta,t)$ , of the influx at  $x=0$ , or

$$q_1(x,t) = F(\theta,t) q_{t_0}(t) \quad , \quad (2.4)$$

where  $q_{t_0}(t)$  is the inlet volumetric flux. Phillip proved that for constant solution content boundary conditions,  $F(\theta)$  was not a function of time. Thus, an exact solution for the flow with known  $D_1$  can be found using the Boltzman transform and a semi-analytical calculation of  $F(\theta)$ , where  $\theta$  is equal to  $(\theta-\theta_n)/(\theta_0-\theta_n)$ .

White et al. (1979) and White (1979) showed that for a constant-volume-flux boundary condition, the time dependence of measured  $F(\theta,t)$  was weak except for early times. They found the transforms  $X=q_{t_0}x$  and  $T=q_{t_0}^2t$  simplified treatment of the system. The transforms showed that water content profiles, at any value of  $T$  are unique in terms of

X. This is regardless of the value of  $q_{to}$ . While no method was found to compute  $F(\theta)$ , experiments showed it to lie between  $F(\theta)$  computed for constant solution content boundaries, and the linear function,  $F=\theta$ .

Boulier et al. (1984) have recently extended constant-flux fractional flow concepts to nonuniform initial solution contents. With these fractional flow methods it is possible to analyze many one-dimensional diffusional flow situations in a semi-analytical manner.

#### Liquid State at Low Solution Contents

The final point to address in this section is the range of solution contents where these principles apply. Several workers including Phillip and DeVries (1957), Porter et al. (1960), Rose (1963), Krupp et al. (1972) and Grismer et al. (1986b) have speculated on the existence of a critical solution content, below which the liquid phase is discontinuous or immobile. In those papers, the unproven concept of an immobile liquid phase at the microscopic scale was used to explain macroscopic observations that indicated the existence of a critical water content. The general justification for the theory is that at low humidities (and therefore low water contents) most of the water is in thin films that are only a few molecular layers thick. This water is held to the solid surface by large adsorptive forces. There are two points to examine: are thin films continuous, and is water close to the solid surface still a fluid, able to respond to hydraulic forces?

Classical vapor adsorption theory can address the first point. The B.E.T. equation (Brunauer et al., 1938) describes the adsorption of vapors on solid surfaces and is widely used to measure the specific surface of porous media. Stated simply, the theory assumes:

1. There is a dynamic equilibrium between free vapor and adsorbed liquid.
2. The vapor is adsorbed in uniform molecular-layers and is unlimited by pore geometry.
3. The energy of adsorption of the first molecular layer is greater than the second.
4. The energy of adsorption of the second and subsequent molecular layers are equal and equivalent to the energy of condensation of the bulk liquid.

The B.E.T. equation is limited to low vapor pressures due to capillary effects at higher vapor pressures which limit the number of uniform layers.

Much work has been done on the experimental measurement of water vapor adsorption on soils (Emmett et al., 1937; Mooney et al., 1952; Orchisten, 1953, 1954, 1955; Quirk, 1955; Anderson and Low, 1958; and Karathanasis and Hajek, 1982). There is evidence that the first molecular layer is slightly less dense than bulk water, and that at less than a monolayer, adsorption is localized at specific sites of hydrated cations. Nevertheless, there is general consensus that the B.E.T. assumptions are satisfied in soils-water systems. Most important for this work is the proof of assumption 2, that uniform adsorption occurs at coverage above a monolayer.

The mobility of water adjacent to solid surfaces has been addressed by Kemper et al. (1964). They measured self diffusion of water in saturated clay systems. Thermodynamic theory was used to compute the viscosity at various coverages of water. They found there was an increase in viscosity as the solid surface was approached but outside of the first layer the viscosity did not exceed 2.5 times the

bulk water value. Stigter (1980) performed a more detailed theoretical analysis of diffusion near solid surfaces. He examined the wall effect on self-diffusion of water and concluded

"...the wall effects partially explain the reported decrease of the self-diffusion in thin interlamellar water layers. The residual decrease corresponds to the immobilization of a small amount of water, of the order of half a monolayer at the clay-water interface. This is about equal to the commonly assumed hydration of the exchangeable cations. The present interpretation of available data implies that there is no significant increase of the viscosity of the remaining interlamellar water and that there is no significant viscoelectric effect near charged clay surfaces."

From the preceding discussion it is concluded that even in relatively dry soils, adsorbed water is uniformly distributed and has about the density and viscosity as the bulk fluid. It is reasonable to assume (though not adequately proven), that water will respond to hydraulic forces and obey the equations of hydraulic flow presented in this section down to monolayer coverage. Thus, it appears that an apparent critical solution content cannot be explained on the basis of zero hydraulic flow at low solution contents.

## VAPOR AND LIQUID TRANSPORT

As in the liquid transport section, this section will address two points. The first will be the existing theory and analysis of combined liquid and vapor flow. The second section will address theoretical concerns that have been raised about the existing theory.

### Flow Theory and Analysis

The transport of water by combined liquid and vapor processes has received a small but continuous interest in the literature through the years. Unfortunately, the majority of the research has been aimed at

nonisothermal systems. Nonisothermal systems can operate under greatly different conditions. The range of vapor concentrations is much greater, and in some cases, liquid and vapor will flow in opposite directions. Therefore, much of the nonisothermal work is not directly applicable to this research. While some of the nonisothermal work is presented here, no attempt has been made to review all such materials. This chapter will concentrate on the few papers that address isothermal conditions.

Rollins et al. (1954) reviewed the earliest works in vapor transport. The early works, including Rollins', are only qualitative in nature due to the limits of the existing theory. Starting with DeVries (1950a,b), Phillip (1955), and Phillip and DeVries (1957) theoretical points were addressed. In their landmark work, Phillip and DeVries expressed the vapor flux as

$$F_v = -D_m \nu \alpha (\phi - \theta) \nabla C_v, \quad (2.5)$$

where  $F_v$  is the vapor mass flux,  $D_m$  is the free space molecular diffusion coefficient,  $\alpha$  is a tortuosity factor,  $\phi$  is the porosity, and  $C_v$  is the vapor density. The variable  $\nu$ , is a mass flow factor introduced to account for the convection of vapor due to the counter diffusion of air. Quoting Phillip and DeVries:

"...for steady diffusion in a closed system between a evaporating source and a condensing sink

$$\nu = P/(P-p), \quad (2.6)$$

where  $p$  is the partial pressure of water vapor (and  $P$  is the total pressure). It is by no means obvious that  $\nu$  will assume this value under nonstationary (transient) conditions. However, the order of magnitude of the deviation of  $\nu$  from unity follows from (Eq. (2.6));  $\nu$  is clearly quite close to 1 at normal soil temperatures."

In a similar fashion Phillip and DeVries also noted that Eq. (2.5) was developed for nonadsorbing gases.

"We therefore remark at this stage that the failure of this theory of moisture transfer should occasion no surprise..."

In porous media, water vapor is adsorbable and few problems of interest are steady state. Thus, researchers were not developing an original theory of adsorbable vapor transport but were adapting a less than perfect analogy of inert gas diffusion. Likewise, assumptions were being made, but not explicitly stated. This is demonstrated by the fact Eq. (2.5) can only be obtained from classical diffusion theory by assuming constant gas phase density. But with variable water vapor concentration, the gas phase density will vary even in isobaric systems.

Phillip and DeVries also showed for isothermal transport, that thermodynamic relations can be used to transform the gradient of vapor concentration to a gradient of liquid solution content. Therefore, with the liquid flux transformed to the diffusional form, liquid and vapor diffusivities can be added to obtain a total diffusivity, or

$$D_t = D_m \frac{\nu}{\rho_l} \alpha (\phi - \theta) \frac{dC_v}{d\theta} + D_l \quad , \quad (2.7)$$

where  $\rho_l$  is the liquid phase density. The sum of the two functions would have a secondary maximum at low water contents. They recognized that, with a total diffusivity, experimental and mathematical solutions developed for liquid flow could be applied to combined liquid-vapor processes.

Phillip and DeVries also hypothesized the existence of "liquid islands" in relatively dry porous media. These islands of water were

assumed held in pendular rings around solid particle contact points. The islands would be connected by films of adsorbed liquid incapable of liquid flow. The solution content below which such conditions prevail was denoted as  $\theta_k$ . They qualitatively argued that under such conditions that vapor transport could be enhanced by the condensation and evaporation through the liquid islands. They provided no quantitative experimental or theoretical data to substantiate this theory.

Phillip (1957) using a steady state isothermal model based on Eq. (2.5) described evaporation rates from soils. While he principally addressed total evaporation to the atmosphere, he also showed relative rates of local evaporation as a function of water content. His analysis showed that most evaporation occurred at intermediate volumetric water contents, between 0.10 and 0.06 for light clay.

Jackson (1964a,b,c) and (1965) and Rose (1963a,b and 1968a,b) performed landmark research in isothermal water and vapor transport. Jackson tested the isothermal transport theory of Phillip and DeVries. He placed uniformly packed columns, open at one end, in chambers held at a constant vapor density. The column geometry and boundary conditions complied with the transient testing requirements of Bruce and Klute (1956). He found that experimental results obeyed the Boltzman transform, and the total diffusivity for adsorption followed the trend predicted by Phillip and DeVries (1957). He also found the diffusivity differed for adsorption and desorption. He explained the difference on the basis of hysteresis of the sorption isotherms. Jackson concluded that classical diffusion theory adequately described isothermal sorption of water vapor. Thus, there is no need to introduce special effects, such as liquid islands.

Jackson (1964c) also performed steady state transport experiments. Columns, open at each end, were placed between two chambers, held at different vapor densities. The vapor densities were maintained by saturated salt solutions. Equilibrium was determined when the rate of mass loss from one solution equaled the gain of the other. Jackson found the steady state experiments gave comparable, but less accurate results than the transient experiments.

Attempting to separate liquid and vapor components, Jackson (1965) performed a series of transient isothermal experiments at varying temperatures and pressures. He used thermodynamic arguments to show the free space vapor diffusion coefficient was a function of pressure and temperature, while liquid diffusion was only a function of temperature. With his experimental results he was able to show the vapor diffusion varied as expected. With the exact knowledge of the vapor diffusion he was able to calculate the liquid diffusion down to less than one monolayer of coverage. While vapor transport was the dominant process at low coverages, liquid transport was still the same order of magnitude. Figure 2.1 presents some of his results.

Rose (1963a) measured liquid and vapor water diffusion with a small steady state cell. The sample was separated by air gaps from two pads wetted with saturated salt solutions. Water was transported from one pad over an air gap, through the sample, over the next air gap, to the second pad. Mass transport was determined by weight gain and loss in the pads. Diffusivities were calculated from a series flow analysis. The analysis assumed an average solution content within the sample. Calculated conductivities were quite reasonable. Total diffusivities were reasonable at low contents, but apparently questionable at higher contents.

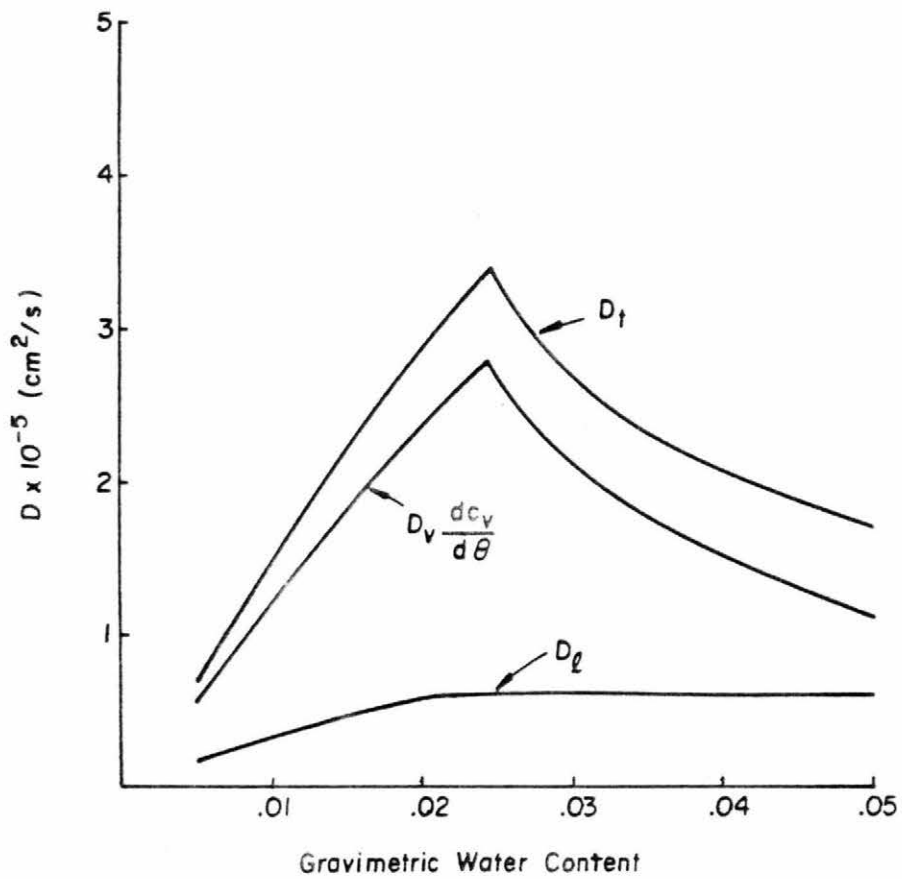


Figure 2.1 Liquid, vapor and total vapor diffusion (after Jackson, 1965).

Rose (1963b) presented a very detailed theory of four stages and two substages of water movement. Figure 2.2 depicts his transport stages. His stages, which are an elaboration of Phillip and DeVries ideas, assume immobile adsorbed vapor films at low coverages, liquid enhanced vapor transport, a distinction between surface creep and hydraulic flow and the two phases usually acting in series. That is, water is transported by only one phase at any position. He presented no evidence that these states exist, and was uncertain himself about the two substages. It is not clear why he considered liquid and vapor in series, and neglected parallel flow, as is assumed by combining both mechanisms into a total diffusivity (Eq. (2.7)).

Grismer (1984) and Grismer et al. (1986a) developed a method to determine the total diffusivity and hydraulic conductivity in soils at low solution contents by nondestructive transient flow observations. They used a small horizontal column with a constant mass influx boundary condition, and determined solution contents by gamma ray attenuation. They started with Jackson's (1964a) equation for the total flow of water

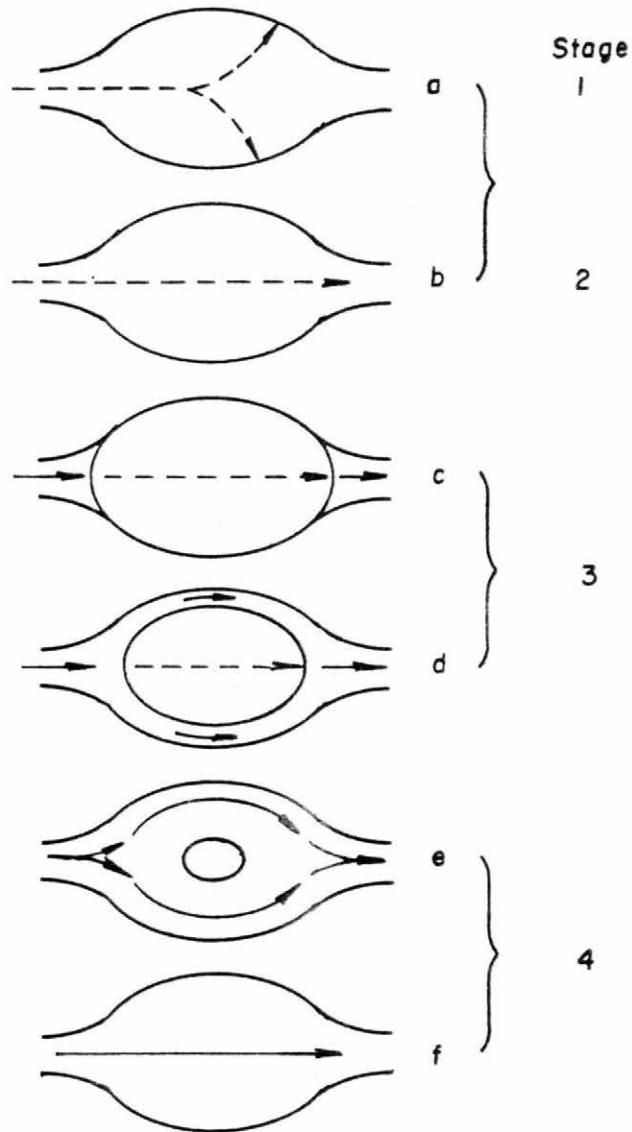
$$\frac{\partial \theta}{\partial t} = \frac{\partial}{\partial x} \left( D_t \frac{\partial \theta}{\partial x} \right) \quad (2.8)$$

Then solving for  $D_t$  they obtained

$$D_t(\theta) \Big|_{x'} = \frac{\partial x}{\partial \theta} \Big|_{x'} \left[ \int_0^{x'} \frac{\partial \theta}{\partial t} dx - q_{t0} \right] \quad (2.9)$$

where  $q_{t0}$  is the inlet flux and  $x'$  is a particular value of  $x$ . Actual values of  $D_t$  were computed by using successively measured flow

- - - - -> Vapor Phase Movement  
 -----> Liquid Phase Movement



a. Adsorption b. Vapor Transfer, c. Distillation,  
 d. Surface Creep, e. Unsaturated Hydraulic Flow,  
 f. Saturated Hydraulic Flow.

Figure 2.2. Rose's stages of water transport (after Rose, 1963b).

profiles and a finite difference form of Eq. (2.9). The method was successful in measuring total diffusivity down to less than 0.01 volumetric solution content.

#### Theoretical Concerns

To conclude this section, it is noted that several authors have expressed concerns over the classical theory of Phillip and DeVries, usually under nonisothermal conditions. Jury and Letey (1979) found the theory under predicts vapor transport, Cass et al. (1984) found it required an empirical calibration and Nakano and Miyazaki (1979) concluded, based on a theoretical argument, it was only valid when the total water potential is larger than  $-10^6$  cm. Nakano and Miyazaki presented a more detailed theoretical development, but still made limiting assumptions in its development. In the defense of the Phillip and DeVries theory, Hadas (1977) found that when applied consistently, with the assumptions it was based upon, its predictions are reasonable, and the discrepancies reported are due to difficulties in measuring accurately all the parameters involved.

To some extent, most of the criticism of Phillip and DeVries are based on the implicit assumption that the effective vapor diffusion coefficient in the porous media is predicted as in Eq. (2.2), by the quantity  $D_m \nu \alpha(\phi - \theta)$ . There is no known conclusive proof that this is the case. Van Brakel and Heertjes (1974) who studied gas diffusion in several soils, presented detailed data and proposed a different approximation. Their empirical approximation gives significantly different results at intermediate solution contents. Because of this lack of concensus it is concluded that the vapor diffusion coefficient should be measured, not predicted. Once it is assumed that the vapor

diffusion coefficient cannot be predicted most of the criticism of Phillip and DeVries becomes moot.

## SOLUTE TRANSPORT

While some qualitative and empirical work in solute transport with a volatile solvent has been performed, no known quantitative or theoretical research has been published. It will thus be necessary to build the base of this section from works which have investigated solute transport in nonvolatile systems. This limitation is not as severe as it may seem at first glance. A basic assumption of this thesis is that solute is transported only in the liquid phase. Therefore, the work in nonvolatile systems is directly applicable to the liquid phase processes of interest here. This section will address two questions; what are the solute transport processes in unsaturated porous media, and are ion adsorption or exclusion processes significant to the systems of interest here? At the end of the section, the recent research in solute transport by a volatile solvent will be reviewed.

### Solute Transport Processes

Solute transport in porous media at the macroscopic scale is assumed to be the result of two processes; dispersion and convection. Bear (1972) presents a general equation for the solute transport. In one dimension it states

$$\frac{\partial}{\partial t}(\theta C_s) + \frac{\partial}{\partial x}(q_1 C_s) + \frac{\partial}{\partial x}(-D_s \frac{\partial C_s}{\partial x}) = R \quad , \quad (2.10)$$

where  $C_s$  is the solute concentration,  $D_s$  is the solute dispersion coefficient and  $R$  is a source term. With the notation of  $q_1$ , the liquid volume flux, (not the total water flux), this equation is valid for volatile solvent systems, (as will be shown in the next chapter). Implicit in its development is the assumption that solute is uniformly distributed over all cross-sections as observed from the macroscopic point of view and that all liquid is mobile and accessible by solute. These assumptions generally limit application of Eq. (2.10) to homogeneous porous media without dead end pores or dual porosity. The form of the dispersion flux assumes that a dispersion coefficient can be defined as a function of the diffusion coefficient, solution content and convective velocity.

Smiles et al. (1978) provided the first significant experimental evidence that Eq. (2.10) describes the solute distribution for transient unsaturated solution sorption. They assumed that for the low Peclet number flows found in typical infiltration studies,  $D_s$  is principally a function of  $\theta$  and not  $q_1$ . For horizontal flow subject to constant solution content ( $\theta(x,0)=\theta(\infty,t)=\theta_n$ , and  $\theta(0,t)=\theta_o$ ), and constant solute concentration boundary conditions ( $C_s(x,0)=C_s(\infty,t)=C_{sn}$ , and  $C_s(0,t)=C_{so}$ ), they were able to obtain an analytical solution for the solute concentration distribution. Using the Boltzman transform,  $\lambda = x/t^{1/2}$ , they showed  $C_s$  to be only a function of  $\theta$  (or  $\lambda$ ). Smiles et al. tested their theory by displacing, in a horizontal column, a resident solution of KCl with distilled water. After a period the columns were sectioned, and the solution content and solute concentration determined as functions of  $\lambda$ . Figure 2.3 presents some of their results. The solute profile agreed well with the theory in most respects. First the solute was displaced piston-like in the sense

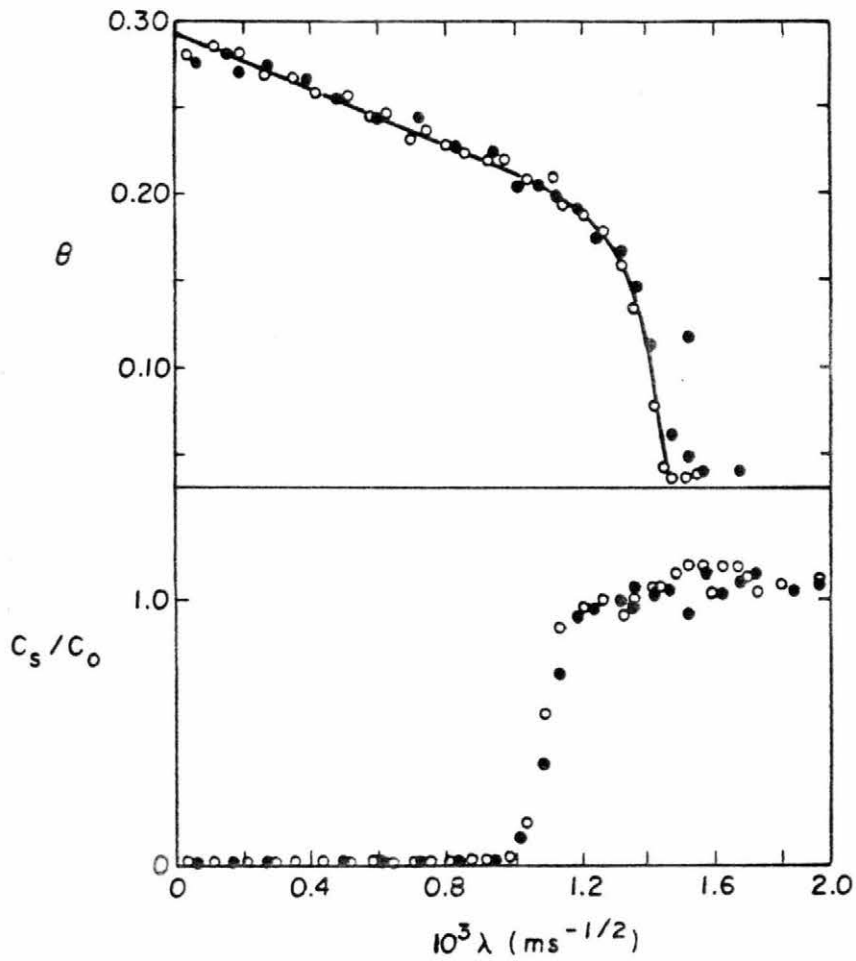


Figure 2.3.  $\theta(\lambda)$  and  $C_s/C_{sn}(\lambda)$  data from two experiments;  $\circ$ ,  $t = 7.2 \times 10^{-3} \text{ s}$ ,  $\bullet$   $t = 2.68 \times 10^4 \text{ sec}$  (after Smiles et al., 1978).

that all water was mobile. A small dispersive front was observed. Also, the position of the front ( $C_s/C_{sn}=0.5$ ) corresponded to the position,  $x^*$ , where the volume of water in the column from the inlet to the front equals the total volume inflow (i.e. where the following equation is satisfied):

$$\int_0^t q_{to} dt = \int_0^{x^*} \theta dx \quad (2.11)$$

The approximate solution of Wilson and Gelhar (1974; 1981) predicts precisely this result. Smiles et al., also concluded that the assumption that  $D_s = D_s(\theta)$  was consistent with the data. Their data indicated that the function  $D_s/\theta$  had a minimum value at the front about equal to the molecular diffusion. At solution contents less than or greater to the solution content,  $D_s/\theta$  increased, but they questioned the accuracy of the data.

One exception to the apparent piston displacement occurred at the farthest reach of the wetting front. At about  $\lambda = 1.6 \text{ m/s}^{1/2}$  the solute concentration was observed to exceed the initial value. They examined the data and were convinced of its accuracy, but could not explain it.

Smiles and Phillip (1978) repeated the experiments of Smiles et al. They also found piston displacement,  $D_s$  independent of  $q_1$ , and that  $D_s$  is roughly equal to the product of  $\theta$  and  $D_m$ . They state that there was no basis to subdivide the water into 'mobile' and 'immobile' fractions. Interestingly, the same anomaly of Smiles et al. (1978), is again apparent in the data of Smiles and Phillip (1978).

Elrick et al. (1979) and Watson and Jones (1982) examined the concentration of invading solute under the constant concentration boundary conditions. They also found similitude in respect to  $\lambda$  and piston displacement. Smiles et al. (1981) performed infiltration experiments with constant inlet flux boundary. Following White (1979), they normalized all data by  $T=q_{t0}^2 t$  and  $X=q_{t0} x$ . They again found piston displacement and  $D_s$  independent of  $q_1$ .

Bond and Smiles (1983) developed a theory of  $D_s$  dependent on  $q_1$ . They showed that at early times the velocity dependence of  $D_s$  is significant. They were unable to demonstrate the dependence experimentally.

#### Non-Piston Displacement

There seems to be good evidence of the adequacy of Eq. (2.10) to describe unsaturated solute transport, but there are exceptions. Several authors have written about the failure of piston displacement. Porter et al. (1960); Kemper (1961); and Van Schaik and Kemper (1966) have shown salt sieving and anion exclusion due to double layer effects. They speculated on the inability of thin films to transmit solute. Krupp et al. (1972); Bond et al. (1982); Laryea et al. (1982); and Smiles and Gardiner (1982) have reported experimental results which they have explained as anion exclusion, or immobile solution. While the accuracy of these experiments is not challenged, the interpretation and significance of the results are questioned by the writer.

The materials used to obtain these results are generally unusual, and conclusions may have overreached the results. Both Bond, and Smiles and Smiles and Gardiner used a soil, termed "sub-plastic", which contained 60 percent of strongly aggregated clay. The aggregates

produce very significant dual porosity, and probably dead end pore space. Thus, the conclusions on anion exclusion are open to debate. Laryea et al., used a soil which was 35 percent clay and had a specific surface area of  $300 \text{ m}^2/\text{g}$ . Again, the question arises as to the homogeneity of the soil or if equilibrium existed on a microscopic scale during their short one to six hour experiments. Examination of their data shows that anion exclusion diminishes with time. Porter and, Van Schaik and Kemper used pure bentonite to obtain their anion exclusion salt sieving data. The use of a material with high surface charge density makes the transfer of their results to normal soils questionable. Krupp et al., used a soil with 41 percent clay packed to a dry bulk density of only  $1.13 \text{ g}/\text{cm}^3$  and a porosity of 0.58. This may have created a dual porosity system which could explain some of their results without invoking immobile solution or double layer effects.

Of greater interest is the work of Porter et al. (1960). They used soils with 26 to 53 percent clay to measure chloride diffusion in half cell experiments. They showed by extrapolation that chloride diffusion goes to zero at nonzero solution contents. They thus argued that "the moisture phase becomes practically discontinuous" at low moisture contents. However their data can be explained by another theory. As mentioned before, Stigter (1980) showed that wall effects significantly reduce the self diffusion coefficient of water near solid surfaces. This general analysis and conclusion is also applicable to any soluble molecule charged or uncharged. Therefore, the results of Porter et al., may only show that the diffusion coefficient, for whatever reason, is zero at low coverages. No conclusion should be made about the ability of liquid films to convect solute.

### Solute Transport by a Volatile Solvent

Grismer (1984) and Grismer et al. (1986b) provide the most relevant work published concerning solute transport with a volatile solvent. They measured the transient transport of water and solutes in relatively dry soils with a dual source gamma ray attenuation system. Solution was injected at a constant flux into horizontal columns. The tests used a loamy sand and a silt loam packed at moderate densities. Their materials are not open to the criticism made of the previous papers. Figures 2.4 and 2.5 present some of their results. Figure 2.4 presents the results of injecting  $\text{SrCl}_2$  solution into a dry soil. Solution profiles developed as could be expected when vapor plays a role. Solution content fell rapidly from the inlet to a relatively low value and then remained near a constant value in a "vapor nose" before going to zero. Solute behaved quite differently. From the injection value the solute concentration rose to values 1.5 times the injection concentration. From the maximum, the solute concentration fell to zero at nonzero solution content. Figure 2.5 presents the results of injecting  $\text{SrCl}_2$  into the same soil with a small initial water content ( $\theta_n = 0.035$ ). In that experiment no solute peak was formed and the vapor nose was less distinct. The reduction in the vapor nose was expected but no explanation was made for the reduction in the solute peak. As in the other case, the solute concentration fell to zero at nonzero solution contents. They concluded that salt was only transported at volumetric solution contents greater than 0.04 in their soil. While they used the data to calculate total water diffusivities, they did not attempt solution of the solute transport equation. Their conclusion concerning solute transport was empirical and based on the fact salt was not observed in the flow profile at solution contents less than

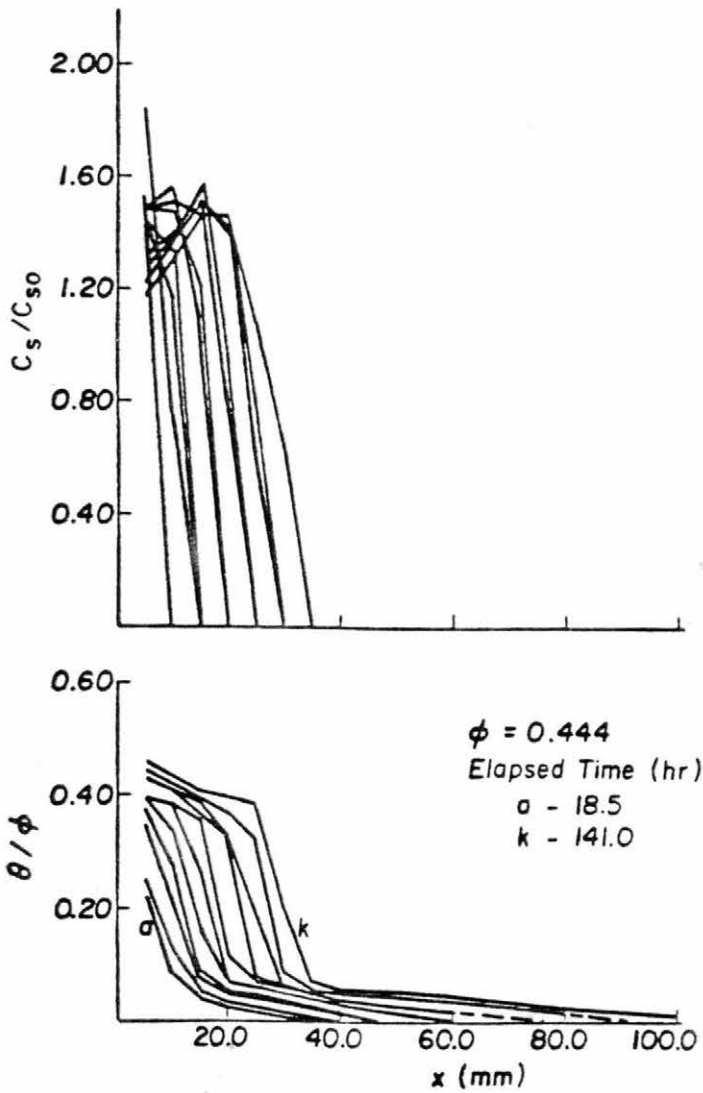


Figure 2.4.  $\text{SrCl}_2$  solution injection into dry Ritzville silt loam (after Grismer, 1984).

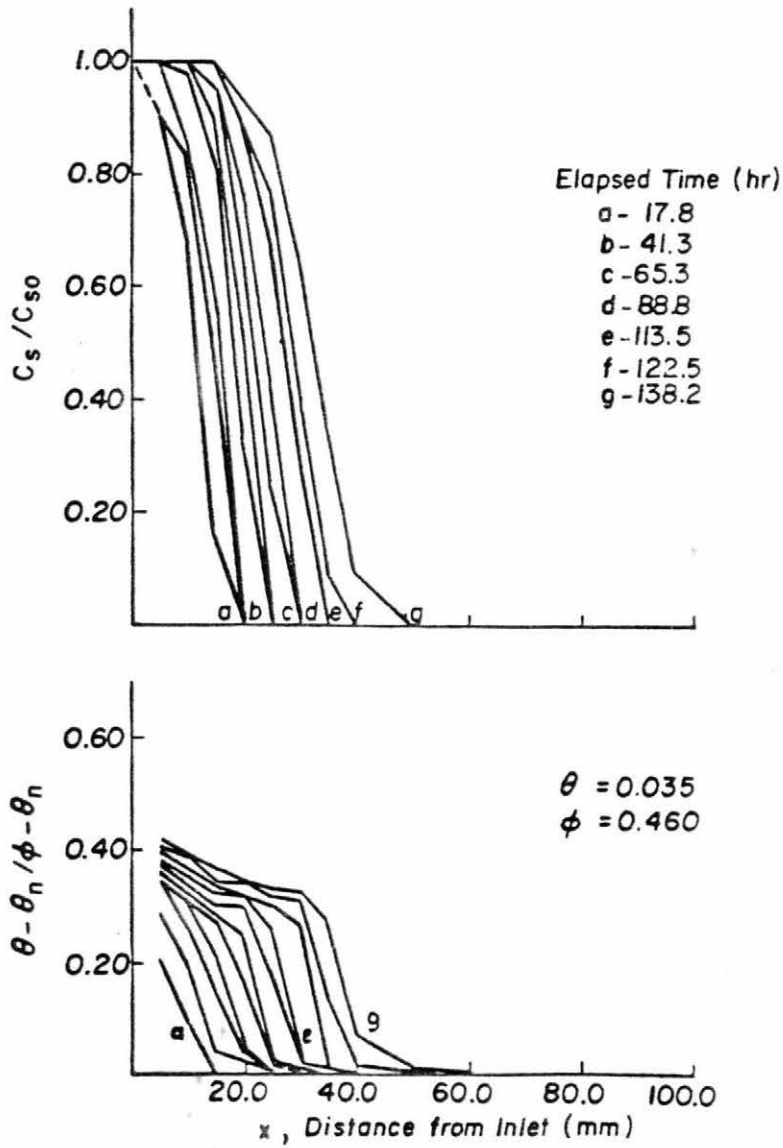


Figure 2.5.  $\text{SrCl}_2$  solution injection into moist Ritzville silt loam (after Grismer, 1984).

0.04. They did not investigate if a solution of the solute transport equation would predict such behavior.

#### SUMMARY

The theory of unsaturated liquid diffusive flow is well developed and several special analytical solution methods exist. It is reasonable to expect (though not adequately proven) that liquid convection occurs down to monolayer coverage. Combined liquid-vapor flow theory defines a total diffusivity which is the sum of the liquid and vapor diffusivities. Phase transfer and gas convection are generally neglected. Vapor diffusion coefficients should be measured, not predicted. While combined liquid-vapor flow has been studied for about 40 years no one has presented a thorough theoretical development for the isothermal system.

The theory of liquid solute transport is well-developed and several special analytical solutions exist for one-dimensional single-phase, transient flow. While it is reasonable to expect liquid convection of solute to occur down to monolayer coverage, anion exclusion and wall effects may eliminate solute dispersion and diffusion at nonzero solution contents. No theory exists which predicts the mechanics of solute transport when the solvent is volatile. Development of such a theory and solution for special flow cases should answer some of the questions raised by previous researchers.

## Chapter 3

### GOVERNING EQUATIONS

Chapter 2 has shown that the governing processes of combined liquid-vapor flow are well established, but to some extent, poorly justified. Solute transport in such systems has only been approached in a qualitative fashion. In this chapter the governing equations for solute transport by a volatile solvent are developed in a more complete manner than previously done. To obtain this level of completeness, it is necessary to start from the basic concepts of mass transport.

This chapter will examine the transport of the solvent in the liquid, gas and combined fluid phases. Then the transport of solute by a volatile solvent will be examined. While the water solvent system is of principal concern here, this development will be kept as general as possible.

#### CONDITIONS OF INTEREST AND TERMINOLOGY

Before the development of the governing equation, it will be beneficial to list the conditions of interest and to present the complete terminology to be used. There are a number of phases, components and fluxes. A detailed presentation at this time should minimize confusion later.

Consider the macroscopic control volume of porous media shown in Figure 3.1. The volume can be divided into three phases: solid, liquid, and gas. Each phase is comprised of one or more components. A

Phase	Volume Content (L <sup>3</sup> /L <sup>3</sup> )	Density (M/L <sup>3</sup> )	Volume Flux (L <sup>3</sup> /L <sup>2</sup> ·T)	Component	Concentration (M/L <sup>3</sup> )	Mass Flux (M/L <sup>2</sup> ·T)	Mass Transfer (M/L <sup>2</sup> ·T)
Solid	(1- $\phi$ )	$\rho_s$	-	solid	$C_m$	-	-
				solute	$C_r$	-	+R
Liquid	$\theta$	$\rho_l$	$q_l$	solvent	$C_w$	$F_w$	-E
				solute	$C_s$	$F_s$	-R
Gas	( $\phi-\theta$ )	$\rho_g$	$q_g$	solvent	$C_v$	$F_v$	+E
				carrier	$C_a$	$F_a$	-

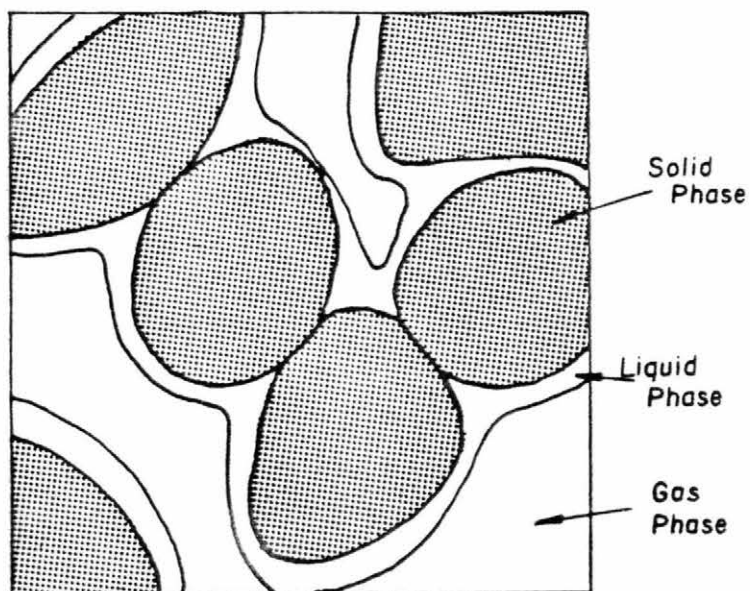


Figure 3.1. Macroscopic control volume of porous media.

component, such as molecular water, may reside in one or more phases and be transported in a phase or transferred between phases. Here the word "transport" refers to mass movement in a single phase while "transfer" implies mass exchange between phases. A distinction must also be made between phase density and component concentrations. Phase densities are the total mass of the phase per unit phase volume, while concentrations are component mass per unit phase volume. Phase densities are equal to the sum of component concentrations. Phase volume contents are based on volume of phase per unit volume of porous media.

The solid phase is assumed rigid, forming a homogeneous and isotropic pore space at a macroscopic scale. The solid phase is comprised of two components, the solid mineral and adsorbed solute. The density of the solid phase is  $\rho_s$  (M/L<sup>3</sup>) while its volume content is  $1-\phi$  (L<sup>3</sup>/L<sup>3</sup>) where  $\phi$  is the total porosity (volume of voids per volume of porous media). The solid matrix concentration is  $C_m$  and the adsorbed solute concentration is  $C_r$ .

The liquid phase is comprised of two components a solvent and a solute. The solvent has the concentration  $C_w$  (M/L<sup>3</sup>), and the solute concentration is  $C_s$ . The liquid phase density,  $\rho_l$  is equal to the sum of  $C_w$  and  $C_s$ . The volumetric liquid phase content is  $\theta$ .

The gas phase is comprised of two components; a vapor of the liquid phase solvent and a carrier gas. The vapor concentration is,  $C_v$  and the carrier concentration is  $C_a$ . The gas phase density  $\rho_g$  is equal to the sum of  $C_v$  and  $C_a$ .

Phase bulk flow volume fluxes are defined as volume of phase per unit area of porous medium per unit time (L<sup>3</sup>/L<sup>2</sup>·T). The phase volume fluxes are  $q_l$  for the liquid phase and  $q_g$  the gas phase.

Phase component mass fluxes are measured as mass of component per unit area of porous media per unit time ( $M/L^2 \cdot T$ ). The mass fluxes are;  $F_w$  the flux of solvent in the liquid phase,  $F_s$  the flux of solute in the liquid phase,  $F_v$  the flux of the solvent vapor in the gas phase and  $F_a$  the flux of carrier gas in the gas phase.

The only mass transfers allowed will be the solute transfer between liquid and solid phases,  $R$ , and the solvent transfer between liquid and gas phases,  $E$ . Both are defined on the basis of mass transferred per unit volume of porous media per time ( $M/L^3 \cdot T$ ).

#### SOLVENT TRANSPORT

This section will examine the mass transport of solvent in liquid and gas phases and the mass transfer of solvent between these phases. The first subsection will address the liquid phase, while the second subsection will address the gas phase. The third subsection will examine the influence of gas phase convection on mass transport of solvent. The fourth subsection will combine the results of the first three to provide a description of total solvent transport. The final subsection will discuss the possibility of bulk flow induced solvent vapor convection in the gas phase.

#### Liquid Solvent

Mass conservation of liquid solvent requires

$$\frac{\partial}{\partial t}(\theta C_w) + \frac{\partial}{\partial x} F_w = -E \quad (3.1)$$

The phase mass transfer,  $E$  is positive when solvent is lost to the gas phase. The mass flux can be expressed as the sum of phase convection and component dispersion or

$$F_w = C_w q_1 - \rho_1 D_w \frac{\partial}{\partial x} (C_w / \rho_1) \quad , \quad (3.2)$$

where  $D_w$  is the liquid phase solvent dispersion coefficient (Bird et al., 1960). With the phase density inside the gradient term of Eq. (3.2), allows for variable density solutions. The volume flux, of solution  $q_1$  can be obtained from Darcy's law which for horizontal, one-dimensional flow can be stated as

$$q_1 = - \frac{k}{\mu} \frac{\partial P_1}{\partial x} \quad , \quad (3.3)$$

where  $k$  is the intrinsic permeability,  $\mu$  is the dynamic viscosity, and  $P_1$  is the liquid phase pressure. Equations (3.2) and (3.3) can be substituted into Eq. (3.1) to yield a general equation of motion for the liquid solvent

$$\frac{\partial \theta}{\partial t} (\theta C_w) - \frac{\partial}{\partial x} \left[ \frac{C_w k}{\mu} \frac{\partial P_1}{\partial x} + \rho_1 D_w \frac{\partial}{\partial x} (C_w / \rho_1) \right] = -E \quad . \quad (3.4)$$

Equation (3.4) is limited to one-dimensional horizontal flow but is valid for variable solution content, phase density, and solvent concentrations. By assuming dilute, incompressible solutions, the derivatives of  $C_w$  and  $\rho_1$  can be cancelled to leave

$$\frac{\partial \theta}{\partial t} - \frac{\partial}{\partial x} \left( \frac{k}{\mu} \frac{\partial P_1}{\partial x} \right) = \frac{-E}{C_w} \quad . \quad (3.5)$$

Note that the dispersive flux has vanished, and the term remaining in the parentheses is simply  $q_1$ . With constant density the volume flux can be transformed to the more traditional form by relating  $P_1$  to a capillary pressure,  $P_c$ , and  $k$  to the conductivity,  $K$ ,

$$P_1 = P_g - P_c \quad , \quad (3.6)$$

$$K = k\rho_1 g / \mu \quad , \quad (3.7)$$

where  $P_g$  is the gas phase pressure and  $g$  is the acceleration of gravity. With these relations Eq. (3.5) becomes

$$\frac{\partial \theta}{\partial t} - \frac{\partial}{\partial x} \left\{ K \frac{\partial}{\partial x} \left[ (P_g - P_c) / \rho_1 \right] \right\} = \frac{-E}{C_w} \quad . \quad (3.8)$$

With the introduction of the capillary pressure, the analysis is limited to unsaturated systems.

Equation (3.8) is still not at the desired form. In relatively dry porous media, gas permeabilities are much greater than liquid values (Corey, 1977). Thus, it is reasonable to expect,  $VP_g \ll VP_c$ . With this assumption, Eq. (3.8) becomes;

$$\frac{\partial \theta}{\partial t} + \frac{\partial}{\partial x} \left[ K \frac{\partial}{\partial x} (P_c / \rho_1 g) \right] = \frac{-E}{C_w} \quad . \quad (3.9)$$

The quantity  $P_c / \rho_1 g$  is the capillary pressure head,  $h_c$ . Since capillary pressures or heads are difficult to measure, the "water characteristic" will be introduced

$$\frac{\partial}{\partial x} (P_c / \rho_l g) = \frac{\partial h_c}{\partial x} = \frac{dh_c}{d\theta} \frac{\partial \theta}{\partial x} \quad (3.10)$$

The use of the ordinary derivative for the water characteristic implicitly assumes a unique equilibrium relation between capillary pressure and solution content. In porous media the relation is hysteretic, and a single-valued relation only occurs under pure wetting or drying.

Following Childs and George (1950), and Klute (1952) a liquid diffusivity is defined as

$$D_l = -K \frac{\partial h_c}{\partial \theta} \quad (3.11)$$

The diffusivity is, of course, a function of solution content. Substituting Eqs. (3.10) and (3.11) into Eq. (3.9) produces the desired result

$$\frac{\partial \theta}{\partial t} - \frac{\partial}{\partial x} (D_l \frac{\partial \theta}{\partial x}) = \frac{-E}{C_w} \quad (3.12)$$

A diffusional form for liquid transport has now been obtained. Jackson (1964) and Rose (1963) started their analyses with this equation obtained from a less rigorous derivation. The assumptions made to obtain Eq. (3.12) are:

1. 1-D, horizontal flow,
2. unsaturated conditions prevail,
3. incompressible liquid phase,
4. dilute solution,
5.  $\nabla P_g \ll \nabla P_c$ , and

6. the water characteristic is single valued.

The fifth assumption should not be mistaken for the more restrictive assumption of constant gas pressure. In a relatively dry porous media the capillary pressure can easily range over a thousand atmospheres. Thus, gas phase pressure changes of several atmospheres could occur while still meeting the fifth assumption.

With the flux identities Eq. (3.3) and (3.11), Eq. (3.12) can be rewritten in terms of the solution volume flux

$$\frac{\partial \theta}{\partial t} + \frac{\partial q_1}{\partial x} = \frac{-E}{C_w} \quad (3.13)$$

This relation will be useful in later sections. Now the solvent vapor will be examined.

#### Solvent Vapor

Continuity on the control volume of porous medium requires

$$\frac{\partial}{\partial t} \{(\phi - \theta)C_v\} + \frac{\partial}{\partial x} F_v = E \quad (3.14)$$

Again the mass flux of solvent is assumed to be the sum of convective and dispersive components

$$F_v = C_v q_g - \rho_g D_v \frac{\partial}{\partial x} (C_v / \rho_g) \quad (3.15)$$

where  $D_v$  is the vapor diffusivity which is a function of the molecular diffusion, convective dispersion, pore geometry and solution content.

Substituting Eq. (3.15) into Eq. (3.14) yields

$$\frac{\partial}{\partial t} (\phi - \theta) C_v + \frac{\partial}{\partial x} [C_v q_g - \rho_g D_v \frac{\partial}{\partial x} (C_v / \rho_g)] = E \quad (3.16)$$

Expanding the derivatives produces

$$(\phi - \theta) \frac{\partial C_v}{\partial t} - C_v \frac{\partial \theta}{\partial t} + \frac{\partial}{\partial x} \left[ C_v q_g - D_v \left( \frac{\partial C_v}{\partial x} - \frac{C_v}{\rho_g} \frac{\partial \rho_g}{\partial x} \right) \right] = E \quad (3.17)$$

Similar to the introduction of the water characteristic the vapor density can be related to the solution content

$$\frac{\partial C_v}{\partial (\quad)} = \frac{dC_v}{d\theta} \frac{\partial \theta}{\partial (\quad)} \quad (3.18)$$

where  $dC_v/d\theta$  is the slope of the vapor adsorption isotherm. Again, the ordinary derivative implies a single value function, while the actual relation is hysteretic and is also a function of the solute content. Similar to the water characteristic, the process must be pure wetting or drying, and the solution must be dilute to minimize osmotic effects. With the isotherm Eq. (3.18), Eq. (3.17) is transformed to

$$\left[ (\phi - \theta) \frac{\partial C_v}{\partial \theta} - C_v \right] \frac{\partial \theta}{\partial t} + \frac{\partial}{\partial x} \left[ C_v q_g - D_v \left( \frac{dC_v}{d\theta} \frac{\partial \theta}{\partial x} - \frac{C_v}{\rho_g} \frac{\partial \rho_g}{\partial x} \right) \right] = E \quad (3.19)$$

The appearance of the gas density requires additional information or assumptions to be brought into the analysis. With a two component gas system, the gas density will be a function of both the gas pressure and the vapor concentration. Even at constant pressure, changes in vapor concentration will change the phase density. For any carrier gas-vapor

mixture, the ideal gas law and the law of partial pressures can be combined to show (CRC, 1986)

$$\rho_g = \rho_{gs} \frac{T_s}{T_a} \left( \frac{P_g - \beta^* p}{P_s} \right) , \quad (3.20)$$

where  $\rho_{gs}$  is the density of pure carrier gas at  $T_s$  and  $P_s$ ,  $T_a$  is the absolute temperature,  $T_s$  is a standard temperature,  $P_s$  is the standard pressure,  $p$  is the partial pressure of vapor, and  $\beta^*$  is the ratio of the molecular weights of vapor and carrier gas. In Eq. (3.20) all three pressures must be measured on an absolute scale. The vapor pressure can be determined from the ideal gas law and  $C_v$ . At an isothermal temperature of 22.5°C and an air-water vapor gas phase Eq. (3.20) reduces to

$$\rho_g = \rho_{gs} \left( \frac{P_g}{P_s} - \beta' C_v \right) , \quad (3.21)$$

where  $\rho_{gs} = 0.0012 \text{ g/cm}^3$  ,  
 $\beta' = 511 \text{ cm}^3/\text{g}$ , and  
 $P_s = 1030 \text{ cm of H}_2\text{O}$ .

With Eq. (3.21) two gas phase state assumptions can be evaluated. First, the traditional (though implicit), constant gas density assumption will be examined. With this assumption

$$P_g = P_s \beta' C_v + \rho_g / \rho_{gs} . \quad (3.22)$$

Differentiation of Eq. (3.22) with respect to  $C_v$  shows

$$\frac{dP_g}{dC_v} = P_s \beta' = 5.26 \times 10^5 \frac{\text{cm}^3}{\text{g}} \text{ cm H}_2\text{O} \quad (3.23)$$

Water vapor at 22°C will have a range in  $C_v$  of 0 to  $2 \times 10^{-5} \text{ g/cm}^3$ . This will require gas pressures differences of 10.5 cm of water (or 0.15 psi) to maintain constant phase density. This is a substantial value since the vapor density can go from saturation to zero in a few centimeters. It could be concluded at this point that constant gas density is a poor assumption.

Now examine a constant gas pressure assumption. Differentiation of Eq. (2.21) with respect to  $C_v$  shows

$$\frac{d\rho_g}{dC_v} = -\rho_{gs} \beta' = -0.613 \quad (3.24)$$

Thus, any gradient of  $C_v$  will produce an opposite gradient in the gas phase density equal to 0.613 of its magnitude. This gas phase gradient has implications in the mass transport by convection of the gas phase as will be shown later. Of course, the true gas phase state will be neither constant density or constant pressure. The actual state will be a function of both vapor concentration and resistance to gas phase bulk flow. Thus, to calculate the true gas state, Darcy's law for the gas phase must be solved; but to do so would complicate an already complex analysis. Therefore, it will be assumed that resistance to gas flow is negligible. This implies gas phase pressure is constant. With this assumption, Eq. (3.24) can be substituted into Eq. (3.19) and the chain rule applied to yield

$$\left[ (\phi - \theta) \frac{\partial C_v}{\partial \theta} - C_v \right] \frac{\partial \theta}{\partial t} + \frac{\partial}{\partial x} \left[ C_v q_g - D_v \frac{dC_v}{d\theta} \left( 1 + \rho_{gs} \beta' \frac{C_v}{\rho_g} \right) \frac{\partial \theta}{\partial x} \right] = E . \quad (3.25)$$

Now note that for an air-water system at atmospheric pressure the order of magnitude of  $C_v$ ,  $\rho_g$ , and  $\rho_{gs}$  is  $10^{-5}$ ,  $10^{-3}$  and  $10^{-3}$  in the cgs system. Thus the last term on the left can be neglected to produce, after dividing by  $C_w$

$$\left[ \frac{(\phi - \theta)}{C_w} \frac{\partial C_v}{\partial \theta} - \frac{C_v}{C_w} \right] \frac{\partial \theta}{\partial t} + \frac{\partial}{\partial x} \left[ \frac{C_v}{C_w} q_g - \frac{D_v}{C_w} \frac{dC_v}{d\theta} \frac{\partial \theta}{\partial x} \right] = \frac{E}{C_w} . \quad (3.26)$$

Interestingly, this is the same result as would be obtained if constant density had been assumed.

Equation (3.36) is the desired form for the solvent vapor equation of motion. It is not the traditional form in that gas phase convection has not been ignored. To obtain Eq. (3.26) it was necessary to assume;

1. 1-D horizontal unsaturated flow,
2. incompressible liquid phase,
3. dilute solution,
4. the vapor sorption isotherm is single valued, and
5. the gas phase pressure is constant.

Now the analysis will turn to the gas phase proper, to quantify the affects of gas phase bulk flow.

#### Gas Phase Bulk Flow

Continuity on the control volume of porous media requires

$$\frac{\partial}{\partial t} \left[ (\phi - \theta) \rho_g \right] + \frac{\partial}{\partial x} (\rho_g q_g) = E . \quad (3.27)$$

Equation (3.27) applies to the gas phase, thus dispersion does not contribute to mass transport. Following the vapor analysis, assumptions 1, 2, 3, 4 and 5 from above will be made. Applying the chain rule to Eq. (3.27) and dividing by  $\rho_g$  produces

$$-\left[ (\phi-\theta) \frac{\rho_{gs}\beta'}{\rho_g} \frac{dC_v}{d\theta} + 1 \right] \frac{\partial\theta}{\partial t} + \frac{\partial q_g}{\partial t} - \frac{q_g \rho_{gs}\beta'}{\rho_g} \frac{dC_v}{d\theta} \frac{\partial\theta}{\partial x} = \frac{E}{\rho_g} \quad (3.28)$$

It is possible to neglect three of the terms in Eq. (3.28). Note the first term on the left. In air-water-soil systems  $\partial C_v / \partial \theta \approx 10^{-4}$  g/cm<sup>3</sup>,  $\rho_g \approx 10^{-3}$  g/cm<sup>3</sup>, and  $(\phi-\theta) \approx 0.5$ , therefore, the first term is about 0.03 which is much less than 1, and can be neglected. Now note the last term on the left. Throughout the liquid profile, in almost all cases most soils will have a definite liquid content slope, thus  $\partial\theta/\partial x < 0.5$  cm<sup>-1</sup>. Therefore considering the variable magnitudes already mentioned, the last term on the left is less than  $0.03 q_g$ . Consistent with the length of the typical liquid-vapor zone, it can be expected that changes in the gas bulk flow will be spread over several centimeters, or  $\partial q_g / \partial x \approx 0.1 q_g$  cm<sup>-1</sup>. With these approximations, comparing the two terms indicates the change in gas bulk flow ( $\partial q_g / \partial x$ ) is more important to phase mass transport than the change in vapor concentration (the last term). With the approximations above, Eq. (3.28) will reduce to

$$-\frac{\partial\theta}{\partial t} + \frac{\partial q_g}{\partial x} = \frac{E}{\rho_g} \quad (3.29)$$

Interestingly, this is the same equation obtained if constant phase density had been assumed. Since the same result (the constant

phase pressure assumption equivalent to the constant phase density assumption), was obtained with the vapor component, it is concluded that the assumptions are equivalent for soil water systems near the condition tested, even if vapor concentration is variable.

Adding the liquid solvent and gas phase equations of motion (Eqs. (3.13), and (3.29)) results in

$$\frac{\partial}{\partial x} (q_g + q_l) = E \left( \frac{1}{\rho_g} - \frac{1}{C_w} \right) \quad (3.30)$$

Now note that  $1/\rho_g \gg 1/C_w$ , therefore

$$\frac{\partial}{\partial x} (q_g + q_l) = \frac{E}{\rho_g} \quad (3.31)$$

Integration of Eq. (3.31) yields

$$q_g + q_l = \frac{1}{\rho_g} \int E \, dx + KI \quad (3.32)$$

where  $KI$  is an integration constant which is evaluated from boundary conditions. If  $q_g(0,t) = 0$ ,  $KI = q_l(0,t)$  or  $q_{l0}$ . After rearranging Eq. (3.32) becomes

$$q_g = \frac{1}{\rho_g} \int_0^{x'} E \, dx + q_{l0} - q_l \quad (3.33)$$

The magnitude of gas bulk flow in the system can be evaluated. Consider the characteristics of wetting a dry porous media as shown in Figure 3.2. (Proof of the accuracy of the figure will await for

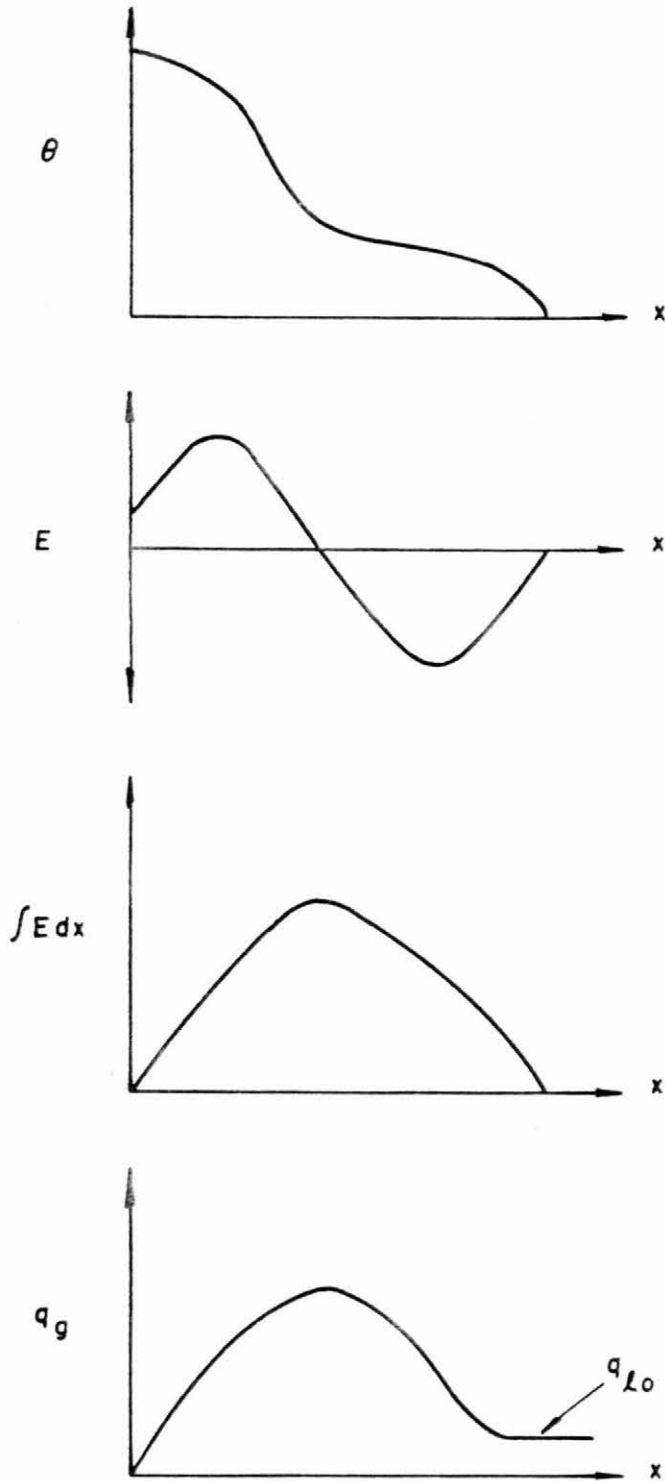


Figure 3.2. Phase transfer and induced gas phase convection during sorption into a dry porous media.

Chapter 6.) The solution content will be a maximum at the inlet and fall to zero at the wetting front. The phase transfer,  $E$ , will be positive at the inlet then pass through zero, reach a negative minimum and finally return to zero. The integral of  $E$  will start at zero, reach a maximum at the first zero of  $E$  and then fall back to zero at the wetting front. With Eq. (3.33) it is simple to sketch  $q_g$  for a no gas flux boundary condition. It will start at zero, rise to a maximum at the maximum of the integral and fall, not to zero, but to a value equal to  $q_{l0}$ . The maximum value of  $q_g$  can be estimated as a function of  $q_{l0}$ . For wetting conditions the total mass evaporation at a given instant ( $\int E dx$  evaluated over the entire evaporating region), will be greater than zero but less than  $C_w q_{l0}$ . Assume that one-tenth of the inlet flux evaporates. Then  $\int E dx \approx 0.1 C_w q_{l0}$ , and from Eq. (3.33) it can be stated

$$q_{gmax} \approx 0.1 \frac{C_w q_{l0}}{\rho_g} + q_{l0} - q_l$$

With  $\rho_g \approx 10^{-3} \text{ g/cm}^3$ , and  $C_w \approx 1 \text{ g/cm}^3$  the last two terms can be neglected. Then a rather surprising result is obtained,  $q_{gmax} \approx 100 q_{l0}$ . This relation shows approximately, that mass transfer from the liquid phase can induce a gas phase volumetric flux, two orders of magnitude greater than the liquid volume flux value.

Qualitatively, the integral of phase transfer in Eq. (3.33) arises from two processes; the generation of gas phase as water evaporates at the front of the column, and the diffusion of air toward the inlet. Due to the low gas density, evaporation will generate large volumes. Of course the generated volume will be approximately equaled by the

condensation and phase consumption at the dry end, but between source and sink a bulk flow cell will be induced. Likewise, as water vapor diffuses away from the inlet, air will diffuse in the opposite direction. Since the air has no sources or sinks, a forward gas phase bulk flow is induced in the column, which will balance the backward diffusion of air. These two processes are closely interrelated, and to some extent should not be considered separate. The phase transfer induced gas bulk flow exposed here is much greater than the convection implicit in Phillip and DeVries (1957) analysis, which was discussed in Chapter 2.

Again qualitatively, the term  $(q_{10} - q_1)$  in Eq. (3.33) arises from the effect of the gas phase being pushed forward as liquid is injected. This term is original to this analysis.

This section has demonstrated that when phase transfer occurs, significant gas phase convection is induced. It does not necessarily mean significant vapor transport occurs by convection. That point will be addressed in the next section.

#### Total Solvent Flow

Adding the equations of flow for the vapor and liquid solvent (Eqs. (3.12) and (3.26) produces

$$\left[ 1 + \frac{\phi - \theta}{C_w} \frac{\partial C_v}{\partial \theta} - \frac{C_v}{C_w} \right] \frac{\partial \theta}{\partial t} + \frac{\partial}{\partial x} \left[ \frac{C_v}{C_w} q_g - \frac{D_v}{C_w} \frac{\partial C_v}{\partial \theta} + D_1 \frac{\partial \theta}{\partial x} \right] = 0 \quad (3.34)$$

Note the phase transfer term cancels. Following Jackson (1964), note that  $C_w \approx 1 \text{ g/cm}^3$ ,  $(\phi - \theta) \approx 0.5$ ,  $\partial C_v / \partial \theta \approx 10^{-4} \text{ g/cm}^3$ , and  $C_v \approx 10^{-5} \text{ g/cm}^3$ .

Therefore, it can be stated that vapor storage is trivial compared to the liquid water storage and Eq. (3.34) reduces to

$$\frac{\partial \theta}{\partial t} + \frac{\partial}{\partial x} \left[ \frac{C_v}{C_w} q_g - \left( \frac{D_v}{C_w} \frac{\partial C_v}{\partial \theta} + D_1 \right) \frac{\partial \theta}{\partial x} \right] = 0 \quad . \quad (3.35)$$

Following Phillip and DeVries (1957), a total diffusivity,  $D_t$ , is defined

$$D_t = \left( \frac{D_v}{C_w} \frac{\partial C_v}{\partial \theta} + D_1 \right) \quad . \quad (3.36)$$

Substituting Eq. (3.36) into Eq. (3.35) yields

$$\frac{\partial \theta}{\partial t} + \frac{\partial}{\partial x} \left[ \frac{C_v}{C_w} q_g - D_t \frac{\partial \theta}{\partial x} \right] = 0 \quad . \quad (3.37)$$

Equation (3.37) is an approximate relation for the total flow of water. It is consistent with Jackson (1964a) and Rose (1963a) except for the vapor convection term.

The previous section has shown by qualitative analysis that even with zero gas phase flux at the boundaries, gas bulk flow orders of magnitude greater than the liquid volume flux is induced by the phase transfer. The gas bulk flow term destroys the diffusion form of the equation, thus it would be beneficial to remove it or combine it with the diffusional term. But simplifying Eq. (3.37) is not easy. Replacing  $q_g$  with its relation (Eq. (3.33)) and expanding terms does not aid in analysis.

The basic difficulty in simplifying Eq. (3.37) are the temporal derivatives ( $\partial(\ )/\partial t$ ) which are introduced when replacing  $q_g$  with Eq. (3.33). While the spatial terms ( $\partial(\ )/\partial x$ ) can be shown to be negligible, the temporal terms can not be quantified by the writer. Nevertheless, because of the mathematical benefit of simplifying Eq. (3.37) a rather difficult justification for neglecting  $q_g$  will be presented.

First, a total diffusive volume flux is defined

$$q_t = -D_t \frac{\partial \theta}{\partial x} \quad (3.38)$$

Substituting Eq. (3.38) into Eq. (3.37) yields

$$\frac{\partial \theta}{\partial t} + \frac{\partial}{\partial x} \left( \frac{C_v}{C_w} q_g + q_t \right) = 0 \quad (3.39)$$

Steady state conditions will be considered where the total mass flux of water is constant with respect to  $x$  and the solution content at a position is constant with respect to time. In Eq. (3.39),  $\partial \theta / \partial t$  is zero, while the terms within the parentheses are the total equivalent volume flux of water, a constant. Multiplying by  $C_w$  produces,

$$F_t = C_v q_g + C_w q_t \quad (3.40)$$

where  $F_t$  is the total mass flux of water.

Likewise, Eqs. (3.13) and (3.29) can be simplified for steady flow to yield

$$\frac{d}{dx} (q_1) = - \frac{E}{C_w} , \text{ and} \quad (3.41)$$

$$\frac{d}{dx} (q_g) = \frac{E}{\rho_g} , \quad (3.42)$$

respectively. Combining Eq. (3.41) and (3.42) to eliminate  $E$ , and integrating produces

$$q_g = - \frac{C_w}{\rho_g} q_1 + KI , \quad (3.43)$$

where  $KI$  is an integration constant. With the boundary condition  $q_g(0, t) = 0$ ,  $KI$  will equal  $+\frac{C_w}{\rho_g} q_{10}$ . This provides an expression for  $q_g$ ,

$$q_g = \frac{C_w}{\rho_g} (q_{10} - q_1) . \quad (3.44)$$

Substituting this expression for  $q_g$  back into Eq. (3.40) yields

$$F_t = \frac{C_v C_w}{\rho_g} (q_{10} - q_1) + C_w q_t . \quad (3.45)$$

The magnitude of the vapor convection in comparison to the diffusive flux can be determined. Note the order of magnitude of  $C_w$  and  $\rho_g$ , which are  $10^0$  and  $10^{-3}$ , respectively in cgs units. The vapor concentration will vary from  $10^{-5}$  at the inlet to  $10^{-6}$  in the vapor "nose" to zero at the dry end. Note also the liquid flux,  $q_1$ , will vary from  $q_{10}$  to zero such that the term in parenthesis will vary from

0 to  $q_{10}$ . Thus, the first term on the right (which is due to gas convection) is zero at both ends and has a maximum in between. Since  $q_{10} \leq q_{t0}$  it can be stated that the maximum value of the term will be less than  $10^{-2} C_w q_{t0}$ . The diffusive flux term will, of course, vary from  $C_w q_{t0}$  to 0. Thus, over the majority of the column, the water mass flux due to gas convection will be two order of magnitude less than the diffusive water mass flux. In the "vapor nose" the picture is not so clear. Both terms will be dropping to zero. The convective term reduction is due to the drop in  $C_v$ , and the diffusive term reduction is due to the drop in  $q_t$ . It is possible that vapor convection may be significant at the very tip of the "vapor nose". The significance, if any, would be dependent on boundary conditions and the slope of the vapor adsorption isotherm. If vapor convection is significant, it would tend to elongate the "vapor nose".

This discussion has shown that the gas convection of water vapor is probably insignificant. It is concluded that it is justifiable to drop the term if additional problem specific testing criteria can be developed. The specific criteria for such a test will now be developed.

The flux term inside Eq. (3.39) can be expressed as

$$\frac{\partial \theta}{\partial t} + \frac{\partial}{\partial x} \left[ q_t \left( 1 + \frac{C_v}{C_w} \frac{q_g}{q_t} \right) \right] = 0 \quad (3.46)$$

Applying the chain rule yields

$$\frac{\partial \theta}{\partial t} + \frac{\partial}{\partial x} \left( \frac{C_v}{C_w} q_g \right) + \left( 1 + \frac{C_v}{C_w} \frac{q_g}{q_t} \right) \frac{\partial q_t}{\partial x} = 0 \quad (3.47)$$

Now the vapor convection can be neglected if

$$\left| \frac{C_v q_g}{C_w q_t} \right| \ll 1 \quad (3.48)$$

and,

$$\left| q_t \frac{\partial}{\partial x} \left( \frac{C_v q_g}{C_w q_t} \right) \right| \ll \frac{\partial q_t}{\partial x} \quad \text{or,} \quad (3.49a)$$

$$\left| q_t \frac{\partial}{\partial x} \left( \frac{C_v q_g}{C_w q_t} \right) / \frac{\partial}{\partial x} (q_t) \right| \ll 1 \quad (3.49b)$$

These two tests assure that both the magnitude and relative change in the gas phase vapor convection is small.

There is no known a priori means to determine when these conditions are met for transient conditions. Thus, any solution which neglects the gas phase bulk flow term must test Eqs. (3.48) and (3.49). Neglecting the term transforms Eq. (3.37) to the traditional form

$$\frac{\partial \theta}{\partial t} + \frac{\partial}{\partial x} \left( -D_t \frac{\partial \theta}{\partial x} \right) = 0 \quad (3.50)$$

With Eq. (3.50) the water flow for several boundary conditions can be solved by the methods outlined in Chapter 2. While this form for the total flow of water allows the use of several powerful solution methods, it can only be developed by making several assumptions, some of which are not stated in the literature. In review, for Eq. (3.50) to hold all the assumptions made in the separate liquid and vapor analyses must be met and additionally;

1.  $(\phi - \theta) \partial C_v / \partial \theta - C_v / C_w \ll 1$ ,
2. Eqs. (3.48) and (3.49) must hold.

Before examining solute transport, one last aspect of gas phase convection will be explored. While it is assumed that gas convection of vapor solvent is negligible, it will be necessary to consider gas phase dispersion.

#### Gas Phase Dispersion

Up to this point the vapor diffusivity has not been explicitly defined. As stated before, it assumed to be a function of the molecular diffusion, convective dispersion, pore geometry and solution content. Traditional analyses that ignore the induced gas phase bulk flow assume no dispersion is present.

Even if the induced bulk flow is two or three orders of magnitude greater than the liquid volume flux, it will still be small in absolute terms. In systems such as of interest here, the liquid volumetric flux is usually around  $10^{-6}$  cm/s. Induced gas bulk flow could not exceed  $10^{-3}$  cm/s under such conditions. The Peclet number is used to classify dispersive flows. It is defined here as

$$P_e = v d / D_m \quad , \quad (3.51)$$

where  $v$  is the interstitial velocity, and  $d$  is a characteristic particle size. The Peclet number for the induced convection should be  $< 10^{-4}$ . Chemical Engineering literature contains extensive work on gas dispersion in packed beds, but that literature usually is only interested in flows with  $P_e > 1$ , and uniform particle size. At  $P_e > 1$  it is assumed that lateral diffusion will have an adequate effect to

eliminate axial dispersion (Langer et al., 1978; Ruthven, 1984). Therefore it would be reasonable to ignore convective dispersion. The work of Rolston et al. (1969) would seem to challenge this assumption.

They measured gas dispersion of  $O_2$ , He, and air in soils at  $P_e \ll 1$ . They found that measured gas dispersion coefficients doubled between volume flow rates of  $10^{-3}$  and  $5 \times 10^{-3}$  cm/s. These flow rates are approaching the range of interest here. Unfortunately, no additional work can be found in this subject, and the dispersive effect cannot be quantified. It will be necessary then, to ignore any dispersion that is induced by the induced gas convection.

The analysis of the solvent mass transport is complete. The significant transport terms for both phases have been defined. It is now possible to proceed to an analysis of the solute transport.

#### SOLUTE TRANSPORT

Continuity on the control volume requires

$$\frac{\partial(\theta C_s)}{\partial t} + \frac{\partial}{\partial x} F_s = R \quad , \quad (3.52)$$

where  $C_s$  is the solute concentration in the liquid phase,  $F_s$  is the mass flux of solute and  $R$  is the source term for adsorption of solute on the solid phase. The solute flux is assumed to be the sum of convective and dispersive fluxes

$$F_s = C_s q_1 - \frac{D_s}{\rho_1} \frac{\partial(C_s/\rho_1)}{\partial x} \quad . \quad (3.53)$$

where  $D_s$  is the dispersion coefficient for the solute. As in the liquid analysis, for dilute solutions the liquid density is assumed constant and cancels from the last term. Then placing Eq. (3.53) into Eq. (3.52) yields

$$\frac{\partial(\theta C_s)}{\partial t} + \frac{\partial}{\partial x} \left[ C_s q_1 - D_s \frac{\partial C_s}{\partial x} \right] = R \quad (3.54)$$

Applying the chain rule and regrouping produces

$$\theta \frac{\partial C_s}{\partial t} + q_1 \frac{\partial C_s}{\partial x} + \frac{\partial}{\partial x} \left[ -D_s \frac{\partial C_s}{\partial x} \right] + C_s \left( \frac{\partial \theta}{\partial t} + \frac{\partial q_1}{\partial x} \right) = R \quad (3.55)$$

From the liquid water analysis it can be stated that the last term on the left is equal to  $-E/C_w$  (Eq. (3.13)). The source term can also be removed by assuming it is proportional to the rate of change in solute concentration

$$R = (1-\phi) C_m k_d \frac{\partial C_s}{\partial t} \quad (3.56)$$

where  $k_d$  is a source constant and  $C_m$  is the solid component concentration. This relation assumes a linear equilibrium relation between liquid phase solute and adsorbed solute. With these two relations, Eq. (3.55) reduces to

$$\left[ \theta + (1-\phi) C_m k_d \right] \frac{\partial C_s}{\partial t} + q_1 \frac{\partial C_s}{\partial x} - \left[ D_s \frac{\partial C_s}{\partial x} \right] - C_s \frac{E}{C_w} = 0 \quad (3.57)$$

For nonadsorbing solutes,  $k_d = 0$ , and Eq. (3.57) can be simplified further

$$\theta \frac{\partial C_s}{\partial t} + q_1 \frac{\partial C_s}{\partial x} - \frac{\partial}{\partial x} \left( D_s \frac{\partial C_s}{\partial x} \right) - C_s \frac{E}{C_w} = 0 \quad . \quad (3.58)$$

This is the desired form of the equation of solute transport. The phase transfer has introduced a term that is in addition to the equation solved by Wilson and Gelhar (1974; 1981). Because the phase transfer has been introduced all previous assumptions must hold. Additional assumptions are;

1. fully miscible solute displacement occurs, and
2. solutes are nonadsorbing.

## Chapter 4

### SOLUTIONS TO TRANSPORT EQUATIONS

Two special mathematical solutions to the basic governing equations developed in Chapter 3, will now be obtained. The two solutions differ due to different inlet boundary conditions. The boundary conditions to be examined, are the constant solution content, and the constant solution flux. These two conditions serve to bracket the range that can be expected in experimental columns and many field applications.

The following sections are long and detailed. To keep each section in proper perspective, the general outline must be remembered. For each of two boundary conditions, a series of three steps is required. The steps are:

1. Solution of total solvent transport,
2. Solution of liquid solvent transport, and
3. Solution of solute transport.

Each step must be completed before the next is started.

#### CONSTANT SOLUTION CONTENT BOUNDARIES

##### Total Solvent Transport

The first problem to be addressed is the one-dimensional sorption of solution with constant solution content boundaries. These initial and boundary conditions are expressed mathematically as

$$\begin{aligned}
 \theta(x,0) &= \theta_n \quad , \\
 \theta(0,t) &= \theta_o \quad , \text{ and} \\
 \theta(\infty,t) &= \theta_n \quad .
 \end{aligned}
 \tag{4.1}$$

Constant solution content boundaries are obtained, by exposing one end of a long column, with an initially uniform solution content, to an unlimited supply of solution at a constant potential. At the wetting end the porous media will quickly reach a constant solution content, which is in equilibrium with the supply potential. The solution is imbibed into the column, producing a nonuniform solution profile. The column is effectively semi-infinite until the profile reaches the column end. Figure 4.1 shows typical adsorption profiles.

The total volume flux of water including both vapor and liquid was defined in the last chapter as

$$q_t = -D_t \partial\theta/\partial x \quad . \tag{4.2}$$

Following McWhorter (1971), the fractional flow,  $F$ , is now defined as

$$F = q_t/q_{t0} \quad , \tag{4.3}$$

where  $F$  is a function of  $\theta$  and time, and  $q_{t0}$  is the total flux at  $x=0$ . Examination of Eq. (4.3) shows  $F$  will have a value between 1 at  $\theta=\theta_o$  and zero at  $\theta=\theta_n$ . Combining Eq. (4.2) and (4.3) produces

$$Fq_{t0} = -D_t \partial\theta/\partial x \quad . \tag{4.4}$$

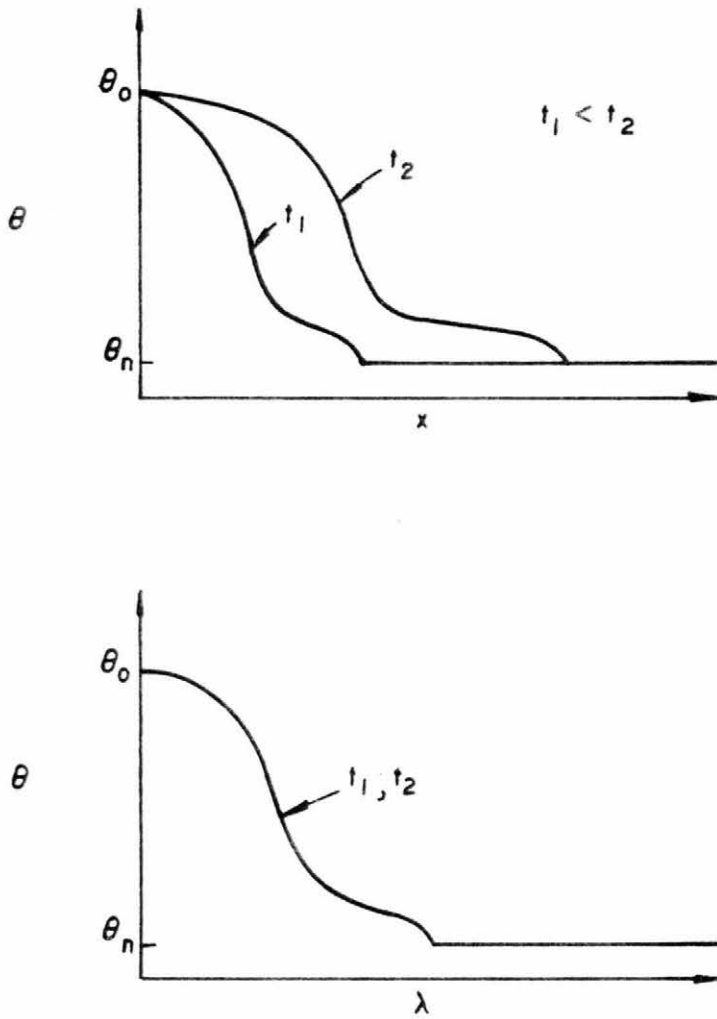


Figure 4.1. Constant solution content boundary sorption profiles. Top  $\theta$  vs.  $x$ , bottom  $\theta$  vs.  $\lambda$ .

Following Phillip (1974) it is possible to separate variables and integrate from  $x=0$  to  $x$

$$x = - \frac{1}{q_{t_0}} \int_{\theta_0}^{\theta} \frac{D_t}{F} d\theta \quad (4.5)$$

Eq. (4.5) is the desired form for the fractional flow analysis. Once  $F(\theta)$  and  $q_{t_0}$  are known, the position of any solution content can be calculated simply. The task that remains is the determination of  $F$  and  $q_{t_0}$ . The solution technique for  $F$  consists of using an iterative method, assuming a function  $F(\theta)$  and then using integral forms of the flux equation to estimate a new  $F(\theta)$ . Phillip and Knight (1974) have shown this method to converge to an exact solution of the flow for several situations.

The approximate equation of flow for the system obtained in Chapter 3 is

$$\frac{\partial \theta}{\partial t} = \frac{\partial}{\partial x} (D_t \frac{\partial \theta}{\partial x}) \quad (4.6)$$

Following Bruce and Klute (1956), the substitution of the Boltzman variable,  $\lambda = xt^{-1/2}$ , transforms Eq. (4.6) to

$$- \frac{\lambda}{2} \frac{d\theta}{d\lambda} = \frac{d}{d\lambda} (D_t \frac{d\theta}{d\lambda}) \quad (4.7)$$

Likewise, the initial and boundary conditions, Eq. (4.1), are transformed to

$$\theta(0) = \theta_0 \quad , \quad \text{and}$$

(4.8)

$$\theta(\infty) = \theta_n \quad .$$

Integration of Eq. (4.7) with respect to  $\lambda$  over the interval  $\lambda=\infty$  to  $\lambda$  ( $\theta_n$  to  $\theta$ ), yields

$$-\frac{1}{2} \int_{\theta_n}^{\theta} \lambda d\theta = D_t \quad d\theta/d\lambda \quad . \quad (4.9)$$

The transform of the flux relation, Eq. (4.2) also yields

$$q_t = -t^{-1/2} D_t \quad d\theta/d\lambda \quad . \quad (4.10)$$

Substituting Eq. (4.9) into (4.10) provides an integral equation for the volume flux at any position

$$q_t = \frac{1}{2} t^{-1/2} \int_{\theta_n}^{\theta} \lambda d\theta \quad . \quad (4.11)$$

This flux term can be substituted for both  $q_t$  and  $q_{t_0}$  in the definition of  $F$ , Eq. (4.3) to yield

$$F = \int_{\theta_n}^{\theta} \lambda d\theta / \int_{\theta_n}^{\theta_0} \lambda d\theta \quad . \quad (4.12)$$

From Bruce and Klute (1956) it is known that all solution profiles are normalized by the Boltzman variable as shown in Figure 4.1. Thus

for these boundary conditions,  $F=F(\theta)$  and is independent of time. Equation (4.12) is unsuitable for the evaluation of  $F$ , since it requires knowledge of the flow profile. Relations for  $\lambda$  must be developed. The denominator of Eq. (4.12) is the sorptivity,  $S$  (Phillip, 1973),

$$S = \int_{\theta_n}^{\theta_o} \lambda d\theta \quad . \quad (4.13)$$

The sorptivity of a soil, is a constant for the given boundary conditions. Mass continuity shows that  $q_{t0}$  is related to  $S$  by

$$q_{t0} = \frac{1}{2} St^{-1/2} \quad . \quad (4.14)$$

Likewise, the flux at any position can be related to  $S$  by Eq. (4.14) and the definition of  $F$ , Eq. (4.3),

$$q_t = \frac{1}{2} FSt^{-1/2} \quad . \quad (4.15)$$

The expression for  $q_t$  can be equated to that given previously in Eq. (4.10), and the result integrated to give

$$\lambda = \frac{2}{S} \int_{\theta}^{\theta_o} \frac{D_t}{F} d\theta \quad . \quad (4.16)$$

Equation (4.16) establishes the relationship between  $\lambda$  and  $\theta$  and is used in Eq. (4.12) to express  $F$  as a function of  $\theta$ . Making this substitution and integrating the denominator by parts yields

$$F = \frac{\int_{\theta_n}^{\theta} \left[ \int_{\theta}^{\theta_o} \frac{D}{F} d\theta \right] d\theta}{\int_{\theta_n}^{\theta_o} (\theta - \theta_o) \frac{D}{F} d\theta} \quad (4.17)$$

Now the iterative nature of the method can be seen. With the trial estimate of  $F$ , a new value of  $F$  can be calculated. Equation (4.17) is not yet suitable though for computation. Switching the limits of integration of the numerator and integration by parts produces

$$F_{i+1} = 1 - \frac{\int_{\theta}^{\theta_o} \frac{(\beta - \theta) D_t(\beta)}{F_i(\beta)} d\beta}{\int_{\theta_n}^{\theta_o} \frac{(\theta - \theta_n) D_t}{F_i} d\theta} \quad (4.18)$$

where  $\beta$  is an integration variable, and  $i$  indicates the iteration of  $F$ . Phillip and Knight (1974) showed this method converges rapidly and unconditionally for  $D_t$  increasing, or constant with  $\theta$ .

The solution of the total water transport equation is complete. With a known total diffusivity, the  $F(\theta)$  function can be calculated from Eq. (4.18). The calculation is iterative and requires an initial estimate of  $F(\theta)$ . Following Phillip and Knight (1973),  $F(\theta) = \frac{\theta - \theta_n}{\theta_o - \theta_n}$  is an adequate first guess. Once  $F(\theta)$  is calculated to an adequate precision, the liquid content profile can be calculated easily by Eq. (4.16). With the known liquid content profile the sorptivity can be calculated by Eq. (4.13). Finally, with the known sorptivity the inlet flux and the flux at any position and time can be calculated by Eqs. (4.14) and (4.15).

Equation (4.18) is solved numerically by a central, finite difference algorithm programed in Lotus 1-2-3, Verson 2.00, which runs

on an IBM PC/XT. The algorithm uses 50 steps in  $\theta$ . The solution is manually iterated until  $F$  is within 0.001 at all positions. With the final estimate of  $F$ , all other variables are calculated directly by central finite difference forms of their definition equations.

Figure 4.2 presents three  $F$  versus  $\theta$  functions. On the graph are shown three relations. The "linear" soil is Phillip's (1973) solution for porous media with a constant diffusivity that is not a function of  $\theta$ . The  $F=\theta$  relationship would be obtained for a material with a diffusivity at  $\theta=\theta_0$ , but with zero diffusivity for  $\theta<\theta_0$ . Phillip (1973) defines this case as a "delta function" soil, that corresponds to the so-called Green-Ampt wetting front. Also shown is the  $F(\theta)$  for a typical soil. All constant liquid content boundary  $F(\theta)$  will lie above the line  $F=\theta$ .  $F$  functions will exceed that for the linear soil only if diffusivity increases with decreasing liquid content. Such a situation occurs with vapor flow. The analysis will now turn toward an examination of the liquid phase.

#### Liquid Phase Solvent Transport

The equation of flow of the liquid phase was shown in Chapter 3 to be

$$\frac{\partial \theta}{\partial t} + \frac{\partial q_l}{\partial x} = - \frac{E}{C_w} \quad (4.19)$$

This equation of flow is also subject to the initial and boundary conditions of Eq. (4.1). The liquid flux can be related to the total flux by the ratio of their respective diffusivities

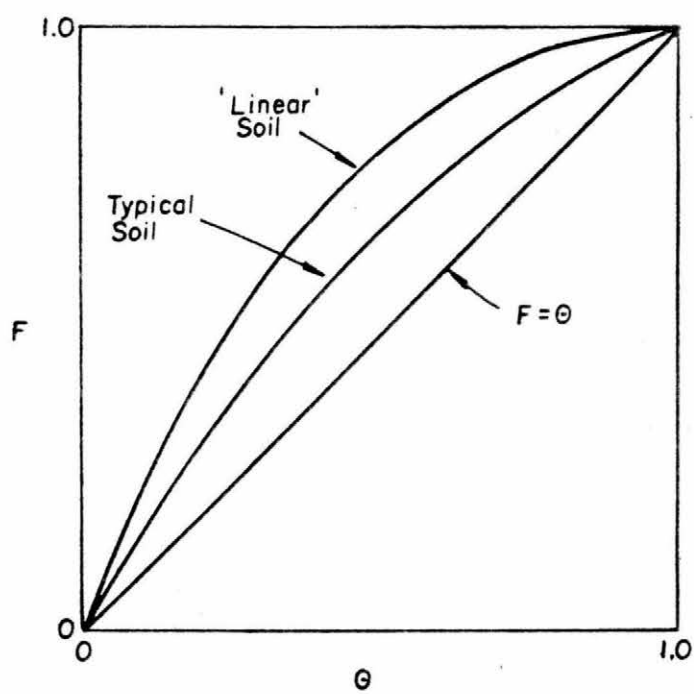


Figure 4.2.  $F(\theta)$  relationships.

$$q_1 = \frac{D_1}{D_t} q_t \quad (4.20)$$

Substitution of Eq. (4.15) into Eq. (4.20) expresses the liquid flux as a function of  $F$  and  $S$

$$q_1 = \frac{D_1 FS}{2D_t t^{1/2}} \quad (4.21)$$

Now substitution of Eq. (4.21) back into Eq. (4.19) and applying the Boltzman transform yields

$$-\frac{\lambda}{2} \frac{d\theta}{d\lambda} + \frac{S}{2} \frac{d}{d\lambda} \left[ \frac{D_1}{D_t} F \right] = -\frac{t E}{C_w} \quad (4.22)$$

With known values of  $D_t$ ,  $D_1$  and  $F$  the source term is the only unknown in Eq. (4.22). Thus, the phase transfer can be shown to be a function of the flow profile. Note the left-hand side of Eq. (4.21) is only a function of  $\theta$ . This would indicate

$$\frac{E}{C_w} = \frac{e(\theta)}{t} \quad (4.23)$$

where  $e$  is the normalized phase transfer. Just as  $\theta$  versus  $\lambda$  is a single-valued function,  $e$  versus  $\lambda$  will be single-valued. While Eq. (4.22) is a simple relation, a further reduction in terms is possible. Differentiation of Eq. (4.12) with respect to  $\theta$  shows

$$\lambda = S \, dF/d\theta \quad (4.24)$$

Substituting Eqs. (4.23) and (4.24) into Eq. (4.22) yields

$$e = \frac{S}{2} \frac{d}{d\lambda} \left[ F \left( 1 - \frac{D_1}{D_t} \right) \right] \quad (4.25)$$

With a known flow profile and diffusivities, Eq. (4.25) can be used to calculate the phase transfer at any point in the profile. All the characteristics of the liquid phase transport are now available to the analysis of the solute transport.

### Solute Transport

The equation of solute transport developed in Chapter 3 is

$$\theta \frac{\partial C_s}{\partial t} + q_1 \frac{\partial C_s}{\partial x} + \frac{\partial}{\partial x} \left( - D_s \frac{\partial C_s}{\partial x} \right) - C_s \frac{E}{C_w} = 0 \quad (4.26)$$

The initial and boundary conditions that apply are

$$\begin{aligned} C_s(x, 0) &= C_n \quad , \\ C_s(0, t) &= C_{s0} \quad , \text{ and} \\ C_s(\infty, t) &= C_{sn} \quad . \end{aligned} \quad (4.27)$$

With the proceeding analysis it is a simple matter to transform this equation to a similar form. Substituting Eq. (4.21) for  $q_1$ , Eq. (4.23) for  $E/C_w$ , applying the Boltzman transform and regrouping produces

$$\left( \frac{D_1 F S}{D_t 2} - \frac{\theta \lambda}{2} \right) \frac{dC_s}{d\lambda} - C_s e = \frac{d}{d\lambda} \left( D_s \frac{dC_s}{d\lambda} \right) \quad (4.28)$$

Applying the Boltzman transform to the initial and boundary conditions indicates

$$\begin{aligned} C_s(0) &= C_{so} \quad , \text{ and} & (4.29) \\ C_s(\infty) &= C_{sn} \quad . \end{aligned}$$

Care must be taken in defining the exact value of  $C_s(0,t)$ . Remember that the boundary condition requires a constant solution content, which produces a total water flux into the column. This implies that water will enter the column in both liquid and vapor phases. The fraction of water that enters as liquid is given by Eq. (4.20). In most cases the inlet content will be high enough that  $D_1 \approx D_t$  and the boundary concentration,  $C_s(0,t)$  will be equal to the concentration of the supply. However if the inlet content is low,  $D_1 < D_t$  and some water will evaporate at the inlet and enter the column as vapor, leaving the remaining liquid at a higher concentration, proportional to  $D_t/D_1$ .

Equation (4.28) is the basic equation of solute transport for the boundary conditions of Eq. (4.29). From inspection of Eq. (4.28) it can be stated that if the solute dispersion coefficient is only a function of the liquid content ( $D_s = D_s(\theta)$ ), then the solute concentration, likewise will be a function of liquid content only, ( $C_s = C_s(\theta)$ ). This is due to the ability of the Boltzman variable to "transform" the governing equation to an ordinary differential equation, reduce the boundary conditions to two, and that all other coefficients are only functions of liquid content. Drawing on the evidence presented in Chapter 2, it will be assumed

$$D_s = \theta D_m \quad , \quad (4.30)$$

where  $D_m$  is the free space molecular diffusion coefficient. Since Eq. (4.30) is only an approximate relation, the tortuosity is not included, but it could be inserted if desired. Substituting this relation into Eq. (4.29), applying the chain rule and regrouping gives

$$\left( \frac{D_1 F S}{D_t^2} - \frac{\theta \lambda}{2} - D_m \frac{d\theta}{d\lambda} \right) \frac{dC_s}{d\lambda} - eC_s = \theta D_m \frac{d^2 C_s}{d\lambda^2} \quad (4.31)$$

From the total flow analysis it is possible to eliminate  $d\theta/d\lambda$  and  $\lambda$ . Setting the two expressions for  $q_t$ , Eqs. (4.10) and (4.14) equal and solving for  $d\theta/d\lambda$  indicates

$$d\theta/d\lambda = -FS/2D_t \quad (4.32)$$

Substituting this relation and Eq. (4.24) for  $\lambda$ , reduces Eq. (4.31) to

$$\frac{S}{2} \left( \frac{D_1 F}{D_t} + \frac{D_m}{D_t} - \frac{\theta dF}{d\theta} \right) \frac{dC_s}{d\lambda} - eC_s = \theta D_m \frac{d^2 C_s}{d\lambda^2} \quad (4.33)$$

Equation (4.33) brings the complete solute transport equation to its simplest form. Examination shows the equation to be second order, linear, ordinary differential equation with variable coefficients. No general solution is known for this form. Attempts at special solutions using moving fronts and separation of variables have been fruitless.

Likewise attempts at numerical solutions of Eq. (4.33) have failed. The highly variable coefficients ( $D_1$ ,  $D_t$ ,  $\theta$ ,  $F$ , and  $e$ ) defeat simple iterative solutions while the boundary condition at the inlet ( $dC_s/d\lambda$  not specified), precludes use of step methods. Nevertheless, it will be beneficial to examine even a simplified solution to

Eq. (4.33), such that the effect of the phase transfer can be examined. Since the diffusion coefficient is quite small and as discussed in Chapter 2, may be zero at very low solution contents,  $D_m$  will be set to zero. With this assumption Eq. (4.33) reduces to

$$\frac{S}{2} \left( \frac{D_1 F}{D_t} - \frac{\theta dF}{d\theta} \right) \frac{dC_s}{d\lambda} - e C_s = 0 \quad (4.34)$$

Equation (4.34) represents the effects of the convective transport of the solute and the phase transfer of the solvent on the solute concentration. It applies to both invading solutes and any solutes present initially (resident) in the porous media. It can readily be solved for the constant concentration boundary conditions. Separation of variables and integration produces

$$\ln C_s \Big|_{C_s(\lambda_1)}^{C_s(\lambda_2)} = \int_{\lambda_1}^{\lambda_2} \frac{e d\lambda}{\frac{S}{2} \left( \frac{D_1 F}{D_t} - \frac{\theta dF}{d\theta} \right)} \quad (4.35)$$

where either  $\lambda_1$  or  $\lambda_2$  is a position of known concentration. Again, Eq. (4.35) applies for both invading and resident solute, but the limits of integration are as yet unspecified. Note only one boundary condition can be used in Eq. (4.35), but Eq. (4.29) specifies both  $C_s(0)$  and  $C_s(\infty)$ , thus each solute will use only one of the conditions. From inspection it can be concluded the invading solute calculation will use  $C_s(0)$  while the resident solute will use  $C_s(\infty)$ . Note, because dispersion has been neglected, resident and invading solute will not mix. That is, they are always segregated from one

another. It, therefore, does not matter if the resident and invading solutes are the same or different species. The resident solution is evaluated from the position  $\lambda_1$  to  $\lambda_2 = \infty$ , while the invading solution is evaluated from  $\lambda_1=0$  to  $\lambda_2$ . Applying these limits of integration and taking the exponential gives the final results. For the resident solution

$$\frac{C_s}{C_{sn}} = \exp \left[ \int_{\infty}^{\lambda} \frac{e \, d\lambda}{\frac{S}{2} \left( \frac{D_1 F}{D_t} - \frac{\theta dF}{d\theta} \right)} \right], \text{ and} \quad (4.36)$$

for the invading solution

$$\frac{C_s}{C_{so}} = \exp \left[ \int_0^{\lambda} \frac{e \, d\lambda}{\frac{S}{2} \left( \frac{D_1 F}{D_t} - \frac{\theta dF}{d\theta} \right)} \right]. \quad (4.37)$$

Note that Eqs. (4.36) and (4.37) only yield relative solute concentrations different from unity if  $e \neq 0$  somewhere in the profile. That is, the solvent must undergo phase transfer to produce nonuniform solute concentration. But likewise, solute concentration is also a function of  $F$  and the ratio  $D_1/D_t$ . Thus, the actual value of  $C_s$  at a position is a function of  $D_t$ ,  $D_1$ ,  $F$  and  $\theta$  throughout the profile.

As noted before, the invading and resident solutes will not mix due to the assumption that dispersion is zero. Thus the last remaining point is the evaluation of the position or front,  $\lambda_s$ , that separates the resident and invading solute. The integrals of Eqs. (4.36) and

(4.37) can both be evaluated from  $\lambda=0$  to  $\infty$  without a direct indication of where the invading solute ends and the resident begins. One way of determining the front position would be to apply Eqs. (4.36) and (4.37) through the entire domain, and then use mass balance calculations to determine  $\lambda_s$ . Those calculations show that mass balance is achieved at the position where  $\frac{D_1 F}{D_t} = \frac{\theta dF}{d\theta}$ . Inspection of Eqs. (4.36) and (4.37) show that position is the location of a singular point of the integrand. At that point the integrand is infinite. While the preceding is a direct method, the numerics of evaluating these integrals do not provide great accuracy, or insight. Instead, the following analysis examines more quantifiable processes.

At  $t=0$ , just after the start of adsorption, all the water contents between  $\theta_o$  and  $\theta_n$  are present at  $x=0$ . Likewise, solute will be present in all solution contents. As time increases, each solution content,  $\theta$ , will travel at a unique velocity,  $v_\theta(\theta, t)$ . Also, the solute at each solution content will have a unique velocity,  $v_s(\theta, t)$ . The solute front,  $\lambda_s$ , will be at the position where these two velocities are equal, or

$$B = \frac{v_s(\theta, t)}{v_\theta(\theta, t)} = 1 \quad (4.38)$$

The variable  $B$ , will be equal to 1 at only one position in a combined liquid-vapor flow. The velocity of a miscible solute is given by a seepage velocity,  $q_1/\theta$ . Using Eq. (4.21) for  $q_1$  shows

$$v_s = \frac{D_1 F S}{2D_t \theta t^{1/2}} \quad (4.39)$$

The  $\lambda$  value of a given solution content is given by Eq. (4.24), which after replacing the Boltzman variable, and differentiating produces

$$v_{\theta} = \partial x / \partial t = S / 2t^{-1/2} dF/d\theta \quad (4.40)$$

Dividing Eq. (4.39) by (4.40) provides the desired result

$$B(\theta) = \frac{D_1}{D_t} \frac{F}{\theta dF/d\theta} \quad (4.41)$$

Notice  $B$  is only a function of  $\theta$  and thus  $\lambda$ . With a computed flow profile,  $B$  can be determined exactly and easily. The solute front will be at the position where  $B(\theta)=1$ . This result checks with the location of the singular point noted before.

The analysis of the constant solution content boundary is complete. The constant flux boundary conditions will now be examined.

#### CONSTANT INLET SOLUTION FLUX

##### Total Solvent Transport

The second special case to be examined is sorption with a constant flux boundary at  $x=0$ . The mathematical expression of these conditions are:

$$\begin{aligned} \theta(x,0) &= \theta_n \quad , \\ \theta(\infty,t) &= \theta_n \quad , \text{ and} \\ q_t(0,t) &= -D_t \partial\theta/\partial x = q_{to} \neq q_{to}(t) \quad . \end{aligned} \quad (4.42)$$

In constant solution flux sorption, solution is injected at a constant rate into an effectively semi-infinite porous media with a uniform initial solution content. The solution content at the injection point will gradually increase with time. Within the porous media the solution profile will develop and advance. Profiles of constant flux adsorption are shown in Figure 4.3.

This case has the advantage of a known influx, but the disadvantage that the Boltzman transform cannot reduce the boundary conditions to two. This has prevented exact analytical solution of the flow profile, and implies that  $F=F(\theta,t)$  (White et al., 1979).

Experimental measurements by White (1979) indicate that if  $\theta$  is normalized by the transform

$$\theta = \left( \frac{\theta - \theta_n}{\theta_o - \theta_n} \right) , \quad (4.43)$$

that  $F(\theta,t)$  is only a weak function of time. The time dependence is greatest at early times. As an approximation it is assumed  $F=F(\theta)$ . White et al. showed that the transforms

$$X = xq_{t0} , \text{ and} \quad (4.44)$$

$$T = tq_{t0}^2 , \quad (4.45)$$

reduce all constant flux data into a set of normalized flow profiles. That is, data for different influx rates, but the same  $\theta_o$  will have the same profile in  $X$  as shown in Figure 4.3. With the first transformation (Eq. (4.44)) the equation of total water flux becomes a definition of the fraction flow

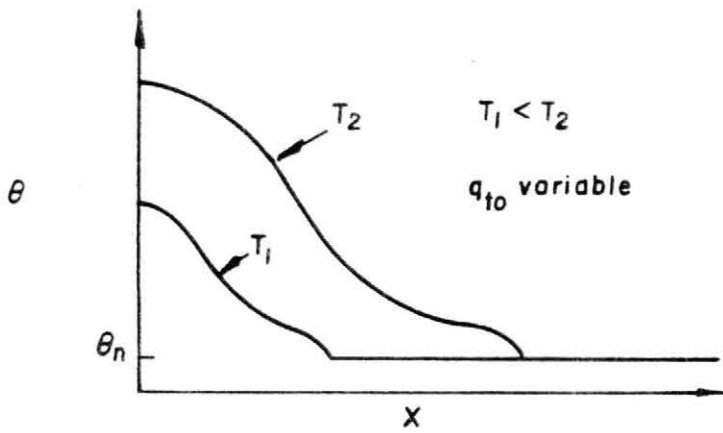
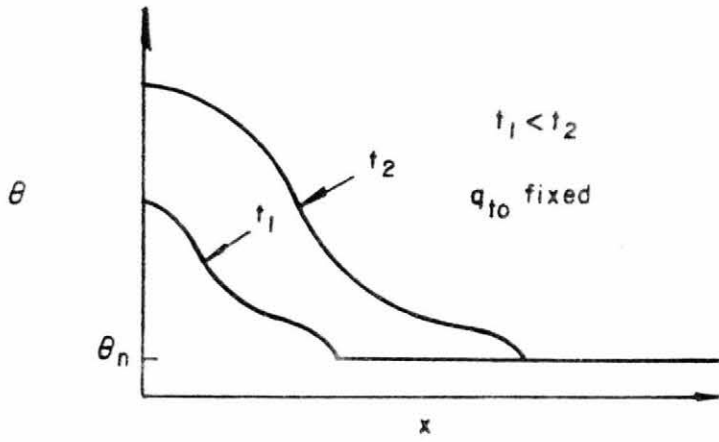


Figure 4.3. Constant flux boundary sorption profiles. Top  $\theta$  vs.  $x$ , bottom  $\theta$  vs.  $X$ .

$$F = q_t/q_{t_0} = -D_t \partial\theta/\partial X \quad . \quad (4.46)$$

This equation can be solved for  $X$  to yield

$$X(\theta) = - \int_{\theta_0}^{\theta} \frac{D_t(\theta)}{F(\theta)} d\theta \quad . \quad (4.47)$$

This result could also be obtained from transforming Eq. (4.4). The time dependence of  $\theta_0$  and therefore  $\theta$ , can be determined from a mass balance. Continuity from  $t=0$  to  $t$  produces

$$q_{t_0}t = \int_{\theta_n}^{\theta_0} X d\theta \quad . \quad (4.47)$$

Multiplying both sides by  $q_{t_0}$  yields

$$T(\theta_0) = \int_{\theta_n}^{\theta_0} X d\theta \quad . \quad (4.48)$$

Thus with Eqs. (4.47) and (4.48) and known values of  $D_t$  and  $F(\theta)$ , the profile for any  $\theta_0$ , and the  $T$  of that profile can be calculated. The last task is the determination of  $F(\theta)$ .

No solution is known to calculate  $F(\theta)$  for these boundary conditions, as was done for the constant content boundaries. White (1979) measured  $F(\theta)$  for a fine sand. He found that the measured  $F$  lay between  $F$  obtained for constant content boundaries, and  $F=\theta$ . He also showed that flow profiles calculated with  $F(\theta)$  measured from constant flux experiments, or the  $F(\theta)$  calculated for constant solution

content at  $\theta_o$ , gave equally good approximations to measured flow profiles. He concluded that  $F$  calculated with constant content boundaries over the range  $\theta_n$  to  $\theta_o$  was an adequate approximation for the constant flux flow.

With a known  $F$ , the total water transport, Eq. (4.6), can be transformed by dividing by  $q_{to}^2$  and noting the definition of  $F$ , given by Eq. (4.46) to yield

$$\frac{\partial \theta}{\partial T} = \frac{\partial}{\partial X} \left[ D_t \frac{\partial \theta}{\partial X} \right] = -\frac{\partial F}{\partial X} \quad (4.49)$$

The liquid phase volume flux as a function of  $F$  and  $X$  can be obtained by combining Eqs. (4.20) and (4.46) to obtain

$$q_l = \frac{D_l}{D_t} q_t = \frac{D_l}{D_t} F q_{to} \quad (4.50)$$

This completes the flow analysis for the constant flux boundaries. In summary, with an assumed or measured value of  $F(\theta)$ , the liquid content profile from a given  $\theta_o$  can be calculated by Eq. (4.47). The time at which a given  $\theta_o$  occurs then can be calculated by Eq. (4.48). The total flow or liquid flow at any value of  $\theta$  can be calculated with the use of Eq. (4.50). With this approximate total flow solution, the liquid phase transport can be examined. As for the other boundary condition, all calculations are performed in Lotus 1-2-3, Version 2.00 on an IBM PC/XT, with a central finite difference algorithm.

### Liquid Phase Solvent Transport

The liquid phase transport, Eq. (4.19) can be transformed to a constant flux basis by substituting Eq. (4.20) for the liquid flux, dividing by  $q_{t0}^2$ , and noting the denominator of F, Eq. (4.46), to produce

$$\frac{\partial \theta}{\partial T} + \frac{\partial}{\partial X} \left[ \frac{D_1}{D_t} F \right] = \frac{-E}{C_w q_{t0}^2} \quad (4.51)$$

Now a transformed phase transfer,  $e'$ , can be defined

$$e' = E/q_{t0}^2 C_w \quad (4.52)$$

Substituting Eqs. (4.49) and (4.52) into Eq. (4.51) and regrouping produces a simple relation for phase transfer

$$e' = - \frac{\partial}{\partial X} \left[ F(1-D_1/D_t) \right] \quad (4.53)$$

Note that  $e'$  is a function of both X and T. It, like the solution profiles will have a series of profiles that are constant for given  $\theta_0$ . The transport of solvent is now fully described. The analysis will turn to the solute transport.

### Solute Transport

Applying the transforms, Eqs. (4.44) and (4.45) to the solute transport, Eq. (4.26), and noting the definition of  $e'$ , Eq. (4.53) will yield

$$\theta \frac{\partial C_s}{\partial T} + F \frac{D_1}{D_t} \frac{\partial C_s}{\partial X} + e' C_s = \frac{\partial}{\partial X} \left( D_s \frac{\partial C_s}{\partial X} \right) . \quad (4.54)$$

The boundary conditions will be

$$\begin{aligned} C_s(X,0) &= C_{sn} , \\ C_s(\infty,T) &= C_{sn} , \quad \text{and} \\ F_s(0,T) &= F_{so} \neq F_{so}(T) , \end{aligned} \quad (4.55)$$

where  $F_{so}$  is the solute mass influx.

Equation (4.54) can be simplified further by applying the chain rule with respect to  $\theta$  or  $\theta$  and making substitutions obtained from the total flow analysis. Those procedures produce second order partial differential equations that contain functions of  $\theta$  and  $\theta$ . These equations will yield to approximations. Another procedure available is to separate variables by assuming  $F=g(\theta)/h(t)$ , such as  $F=\theta=(\theta-\theta_n)/(\theta_o-\theta_n)$ . While separation is possible, the separation constants cannot be evaluated easily.

The problem with these methods is the inlet boundary condition. Remember for the constant content boundary, care has to be taken in defining the inlet concentration. Even though a liquid source can have a constant concentration as the liquid enters the medium, the flow will dictate that a portion of the inflow will evaporate and actually enter the porous media as vapor leaving the liquid phase at a higher solute concentration. With the constant flux boundary the inlet boundary content and the liquid flux changes with time.

Neglecting solute dispersion at  $x=0$ , the mass flux of solute is equal to the convective transport

$$F_{so} = q_{1o} C_s(0,T) = C_{ss} q_{to} , \quad (4.56)$$

where  $C_{ss}$  is the source solute concentration. Applying Eq. (4.50) and solving for  $C_s$  shows,

$$C_s(0,T) = C_{ss} \frac{D_t(\theta_o)}{D_l(\theta_o)} \quad (4.57)$$

The quantity  $D_l/D_t$  is a function of  $\theta_o$ . It has a minimum at the liquid content of the vapor diffusivity maximum, and approaches unity at saturation. Likewise,  $\theta_o$  is a complex function increasing with  $T$ , from 0 to saturation. Therefore,  $C_s(0,T)$  will increase from  $T=0$ , to a maximum at  $T>0$ , and will then fall to 1 at large  $T$ .

Considering the complexity of the inlet concentration it is doubtful that an analytical solution of any sort can be obtained. As in the previous case it will still be beneficial to examine even a simplified solution of Eq. (4.54). To do so, it will be necessary evaluate the solute concentration by numerical methods.

#### Numerical Particle Tracking

A unique particle tracking method will be used to calculate the solute transport. The method makes the maximum use of the approximate analytic solution to the liquid-vapor flow. The method will track a set of particles and calculate solute concentration based on their positions at given times. As with the constant solution content analysis, this method only considers the convective transport of solute. Dispersion is neglected.

Consider a solute particle in the liquid phase. The particle does not have mass. The velocity of the particle will equal the seepage velocity,  $q_1/\theta$ . Using Eq. (4.50) for  $q_1$  and dividing by  $\theta$  yields

$$v_s = \frac{D_1}{D_t} \frac{F}{\theta} q_{t_0} \quad , \quad (4.58)$$

where  $v_s$  is the seepage velocity. During a given time increment,  $\Delta t$ , the particle will move the distance  $\Delta x$ , or

$$\Delta x = v_s \Delta t = \frac{D_1}{D_t} \frac{F}{\theta} q_{t_0} \Delta t \quad . \quad (4.59)$$

Multiplying by  $q_{t_0}$  and applying the definitions of  $X$  and  $T$  yields

$$\Delta X_{ji} = \frac{D_1}{D_t} \frac{F}{\theta} \Delta T_i \quad , \quad (4.60)$$

where  $\Delta X_{ji}$  is a transformed incremental step of particle  $j$  during the transformed time step  $\Delta T_i$ . The position of a particle at time  $i+1$ , then will be given by the forward finite difference,

$$X_{j,i+1} = X_{j,i} + \Delta X_{j,i} \quad . \quad (4.61)$$

Given Eq. (4.61) and the known liquid content profile the position of any solute particle at any time can be calculated if its initial position is known.

When a set of particles are tracked, the concentration profile can be calculated. While particles are considered massless, the solution between particles will have a specified mass of solute based on the initial and boundary conditions. For an invading solute several particles which enter the porous media at varying times are tracked. The mass of solute between particles will be equal to the product of

solute mass flux (Eq. (4.56)) and the differential time. In terms of transformed time the solute mass is

$$M_{s_j} = \frac{C_{ss}}{q_{to}} \left( T_{o_{j+1}} - T_{o_j} \right) , \quad (4.62)$$

where  $M_{s_j}$  is the mass between particles  $j$  and  $j+1$  and  $T_{o_{j+1}}$  and  $T_{o_j}$  are the release times of the particles. The average concentration between particles is calculated by dividing by the volume of solution between the particles. The solution volume can be calculated using the trapazoidal rule between the particles. In terms of transformed length the volume will be

$$V_{j,i} = \frac{1}{2q_{to}} (\theta_{j,i} + \theta_{j+1,i})(X_{j,i} - X_{j+1,i}) , \quad (4.63)$$

where  $V_{j,i}$  is the total volume of solute between the particles and  $\theta_{j,i}$  and  $\theta_{j+1,i}$  are the liquid content at the respective particle position. Dividing Eq. (4.62) by both Eq. (4.63) and  $C_{ss}$  provides the average relative solute concentration between invading solute particles

$$\frac{C_{s_{j,i}}}{C_{ss}} = \frac{2(T_{o_{j+1}} - T_{o_j})}{(\theta_{j,i} + \theta_{j+1,i})(X_{j,i} - X_{j+1,i})} . \quad (4.64)$$

For resident solutes the mass of solute between particles is calculated from the initial conditions

$$M_{s_{j,i}} = C_{sn} \theta_n (X_{j,o} - X_{j+1,o}) / q_{to} \quad (4.65)$$

where  $X_{j,o}$  and  $X_{j+1,o}$  are the initial position of the particles.

Dividing Eq. (4.65) by Eq. (4.63) and  $C_n$  provides the average relative solute particles

$$\frac{C_{s_{j,i}}}{C_{sn}} = \frac{2 \theta_n (X_{j,o} - X_{j+1,o})}{(\theta_{j,i} + \theta_{j+1,i}) (X_{j,i} - X_{j+1,i})} \quad (4.66)$$

The strength of this numerical method can now be seen. While the method is roughly analogous to other particle tracking methods, (such as Reddell and Sunada, 1970), this method takes maximum advantage of the approximate analytical solution of the combined liquid-vapor flow. Equations (4.64) and (4.66) show that the solute concentration profiles, like the liquid content profiles, can be normalized by the transformed variables  $T$  and  $X$ . Likewise, this method allows the calculation of solute concentrations directly from the approximate analytical solution of solvent transport.

## Chapter 5

### EXPERIMENTAL PROCEDURES AND RESULTS

This chapter presents the experimental procedures and results obtained during the course of the research. The tests performed determined the physical properties, water characteristic, total diffusivity, hydraulic conductivity, and transient solute transport. Each test and its results are presented in the following sections.

#### MATERIAL AND PREPARATION

All experiments were performed on Lurgi retorted oil shale. The material was produced by a pilot Lurgi plant operated by Gulf Research and Development Co., Gulf Corporation, at Harmarville, Pennsylvania. The material designation was 10/31/83-2100-Run 108.C. In the Lurgi pilot plant the raw shale was crushed to about minus 3 mm and retorted to extract the kerogen. It is then combusted or decarbonized to remove residual carbon compounds. The process produces a fine textured, gray solid residue. Rio Blanco (1976, 1977 and 1981) present details of the Lurgi process and proposed operation.

Lurgi retorted shale is a chemically active material due to the high process temperatures to which it is exposed. Upon the addition of water, the material hydrates, similar to a cement. McWhorter and Brown (1985) carried out experiments which investigated the hydrating properties. They concluded the cementing was basically a surface reaction and that only a small portion of the material reacted. This

property has been reported by others (Pilz, 1982; Marcus, Sangrey and Miller, 1984).

When the material is wet to about 50 percent water content by weight, a paste is formed. If the paste is allowed to cure, it forms a rock-like mass with some strength. This property caused considerable concern for the manner in which the material is prepared for hydraulic testing. There are no known similar cases in the literature. Therefore, the sample preparation method was designed to replicate, to the extent possible, the field conditions.

Since the principal area of concern was the long-term properties of the material, it was decided to test only hydrated samples. The disposal pile will probably have 10 to 20 percent water by weight added at placement and it is believed, based on the results of the wetting tests reported by McWhorter and Brown, that hydration should be essentially complete within a month.

Packing columns with wet material and allowing it to hydrate in place was considered as a means of creating a column of hydrated material. This was rejected due to the difficulty of completely drying the column and keeping cracks from forming. Likewise, it was considered impractical to drill a core of the material since its strength is relatively low. Therefore, it was decided to grind the hydrated material to a particle size distribution which replicated the initial. It is believed that this procedure results in packed columns with a pore structure reasonably similar to that expected in the field. The following is a description of the sample preparation.

A sample of Lurgi retorted shale was wet with distilled water to 30 percent by weight. The sample was allowed to hydrate in a closed container at 100 percent relative humidity and approximately 22°C.

After 28 days, the sample was removed and oven dried at 105°C. The entire sample was then ground by hand with an iron mortar and pestle. A portion of the sample was placed in a disk mill and ground to obtain a size distribution which replicated the initial size distribution. Finally, the sample was redried at 105°C to remove any moisture it may have gained in processing. Samples processed in this manner were used in all subsequent hydraulic tests.

#### PARTICLE SIZE AND DENSITY

A particle size analysis of the fresh material was performed by dry sieving. Dry sieving was performed because it was considered inappropriate to use wet sieving and hydrometer analysis as called for by ASTM-D422 on a reactive material such as the Lurgi retorted shale. The result of the sieve analysis is presented in Figure 5.1. Thirty-five percent of the material by weight was smaller than 0.045 mm. A large portion, 31 percent, was between 1 and 2 mm. The largest particles were 5 mm.

The apparent specific gravity, or particle density of the material was determined by ASTM-D854. A total of four tests were performed on unsorted and sieved samples. The average density obtained was 2.74. The difference between fine and course samples were insignificant.

#### WATER CHARACTERISTIC

##### Procedures

The water characteristic was developed using two methods. The methods used were vapor sorption, and pressure cells. Each of these methods has its own range of capillary potentials and the combination

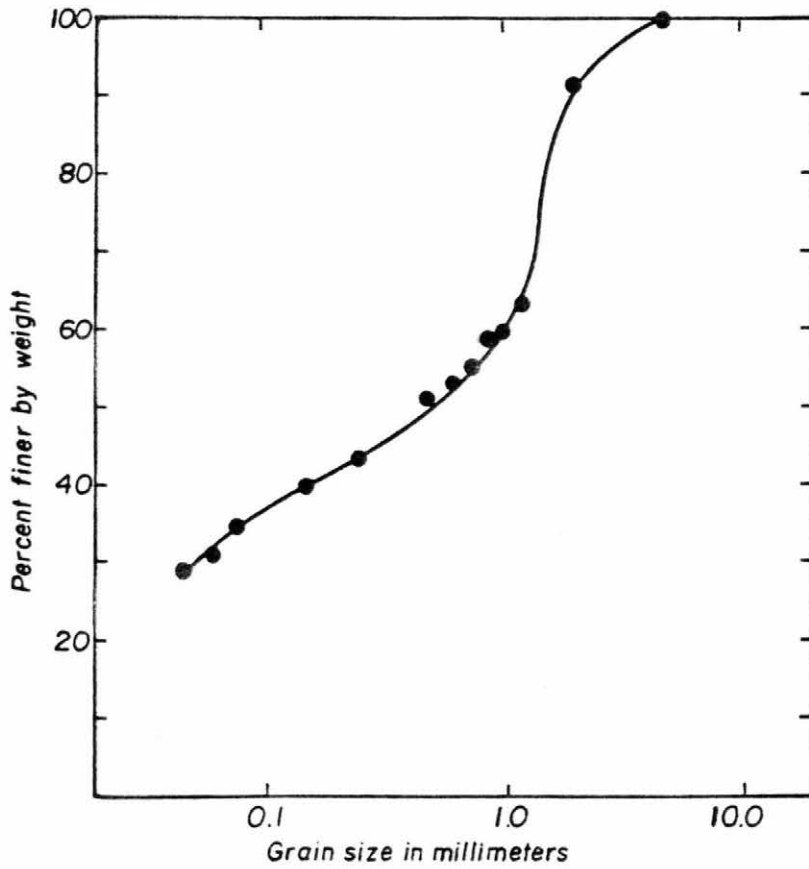


Figure 5.1. Grain size distribution of Lurgi retorted oil shale.

of the data from both provides a water characteristic over the range from 0 to less than  $-10^6$  cm. of water.

Pressure Cells. The wetting and drainage characteristics over the range of 0 to  $-15,000$  cm of water were determined by pressure cell apparatus. The procedures were consistent with ASTM-D2325, except a modification was made to the pressure plates to allow for measurement of the wetting characteristic. Following Klute (1986) a second tap was placed in each pressure plate as shown in Figure 5.2. This second tap allowed the circulation of  $0.01$  N  $\text{CaSO}_4$  solution behind the sample which provided a source of water for sample wetting. The reservoir height is adjusted to maintain a slow drip at the drain.

In operation, samples were dry packed to a constant bulk density of  $1.4$  g/cm<sup>3</sup> in aluminum rings  $4.9$  cm I.D. by  $2.54$  cm high. Half of the samples were then saturated by standing overnight in wetting solution and the remaining half kept dry. Triplicate, dry and wet samples were placed in the cells on top of the plates and  $500$  g lead weights placed on top of each sample to provide a small normal load. The cells were closed and pressurized. After three (for low pressures) to seven days (for high pressures), the cells were opened and the samples removed. Water contents were determined gravimetrically. Samples were used for only a single measurement. Finally, the data was critically reviewed and several measurements repeated to insure accuracy.

Vapor Sorption. Vapor adsorption and desorption were used to determine the water characteristic in the range  $-10^4$  to  $-3 \times 10^6$  cm. Vapor sorption samples are placed in chambers in which the humidity and temperature are maintained at constant values. Samples will adsorb or desorb water from the liquid phase until the thermodynamic potential of

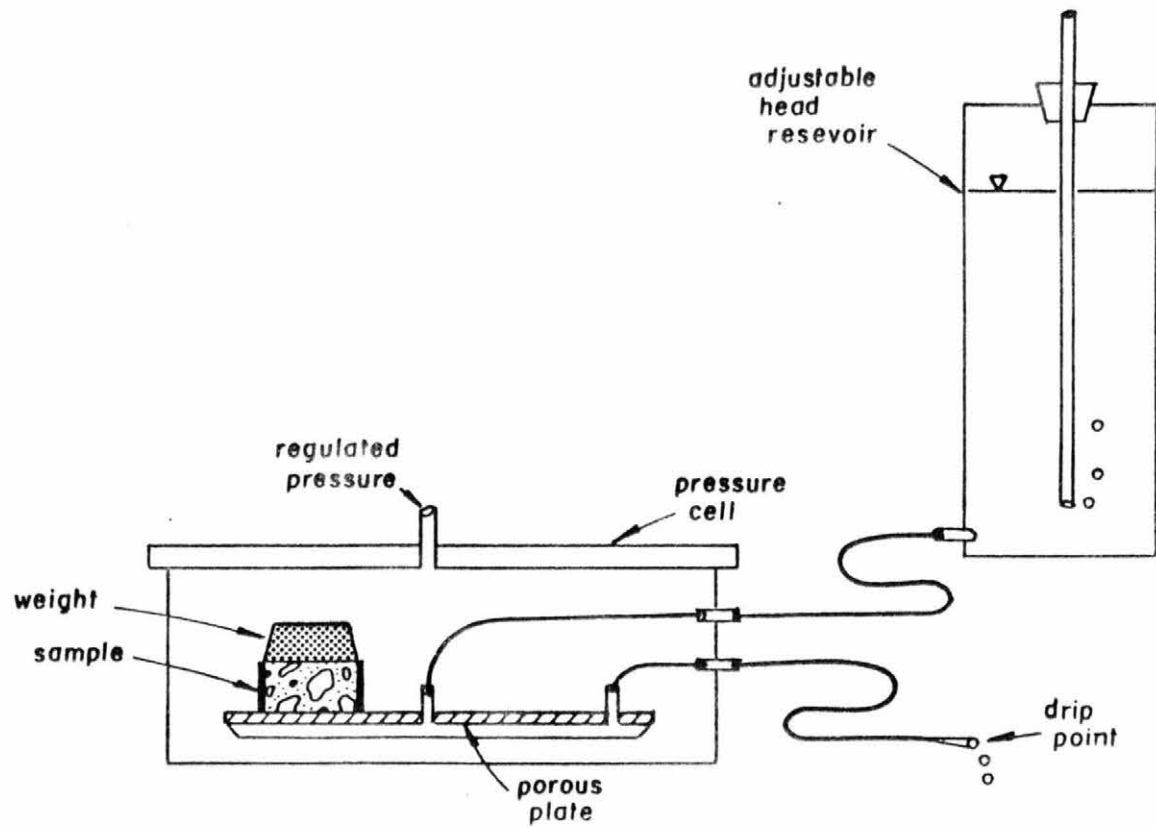


Figure 5.2. Pressure cell apparatus.

the soil solution is at equilibrium with the potential of the vapor. At equilibrium the thermodynamic potential is given by

$$h_t = \frac{R'T'}{M_w g} \ln \left( \frac{C_v}{C_{vs}} \right) , \quad (5.1)$$

while  $R'$  is the ideal gas constant,  $T'$  is the absolute temperature,  $M_w$  is the gram molar weight of water,  $g$  is the acceleration of gravity,  $C_v$  is the vapor density, and  $C_{vs}$  is the saturated vapor density. Under isothermal conditions the thermodynamic potential can be related to the pressure head by

$$h = h_t + h_o , \quad (5.2)$$

where  $h_o$  is the osmotic potential which arises from salts in the soil water solution. The osmotic potential is always positive. Thus it decreases the magnitude of the pressure potential.

If a sample of the equilibrium soil water can be obtained, the osmotic potential can be measured by the freezing point depression or estimated from the electrical conductivity (Richards, 1954). Obtaining a representative sample of undisturbed solution at low solution contents is difficult. The E.S.M. column leach test developed by Nazareth (1984) can obtain a solution sample from soils at moderate water contents. But, at the very low water contents obtained in vapor sorption experiments, typically around 0.05 by weight, even the E.S.M. test fails.

The osmotic potential can be estimated by curve matching the vapor sorption data to the pressure cell data if the water contents overlap

as is normal. In that case, at a constant solution content,  $\theta$ , the osmotic potential is estimated by

$$h_o = h + h_t \quad , \quad (5.3)$$

where  $h$  is obtained from the pressure plate data at  $\theta$ , and  $h_t$  is obtained from the vapor sorption data at  $\theta$ . From a single curve match, the remaining vapor sorption data can be corrected by Eq. (5.2).

The measurements were made with 5 g samples contained in aluminum cans. Duplicate samples were placed in a multiple chamber cell. A different saturated salt solution was placed in the bottom of each chamber. The cell was placed in a constant temperature bath set at  $22.5^\circ\text{C} \pm 0.1$ . Measurements were made by opening the cell, quickly covering the cans with lids, and weighing the samples to  $\pm 0.0001$  g. The samples were then quickly uncovered, and replaced in the cell. Equilibrium took considerable time to obtain. Equilibrium was assumed to be achieved if two measurements at least one day apart were within  $\pm 0.001$  g. Equilibrium took roughly two weeks to achieve, but small changes could be measured for over two months. The solutions used in the measurements are listed in Table 5.1.

## Results

The results of the water characteristic measurements are shown in Figure 5.3. The Lurgi retorted shale packed at a dry bulk density of  $1.4 \text{ g/cm}^3$  had a displacement pressure of approximately 300 cm. The pressure plate data provides the bulk of the solution content change, while the vapor sorption data provides the majority of the range in  $h_c$ .

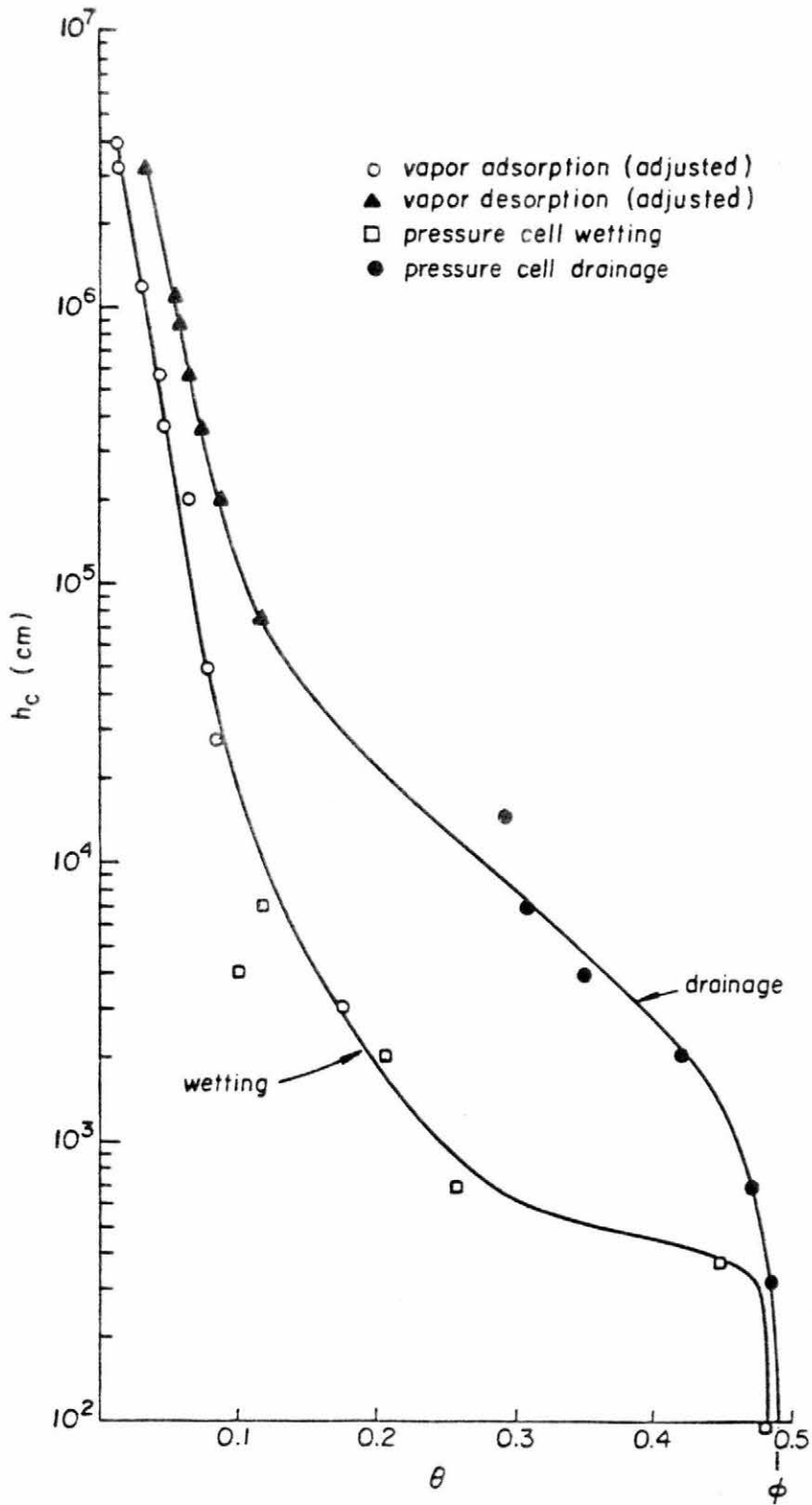


Figure 5.3. Water characteristic for Lurgi retorted oil shale.

Table 5.1. Saturated salt solutions used in vapor sorption.<sup>1</sup>

Salt	$C_v/C_{vs}$ @22.5°C	$h_t$ (cm)
NaOH	0.061	-3.89 x 10 <sup>6</sup>
ZnCl <sub>2</sub>	0.100	-3.20 x 10 <sup>6</sup>
MgCl <sub>2</sub>	0.328	-1.55 x 10 <sup>6</sup>
K <sub>2</sub> CO <sub>3</sub>	0.436	-1.15 x 10 <sup>6</sup>
Mg(NO <sub>3</sub> ) <sub>2</sub>	0.542	-8.51 x 10 <sup>5</sup>
NaNO <sub>2</sub>	0.649	-6.00 x 10 <sup>5</sup>
NaCl	0.758	-3.85 x 10 <sup>5</sup>
KCl	0.850	-2.26 x 10 <sup>5</sup>
KNO <sub>3</sub>	0.931	-9.93 x 10 <sup>4</sup>
Ca(H <sub>2</sub> PO <sub>4</sub> ) <sub>2</sub>	0.948	-7.42 x 10 <sup>4</sup>
K(H <sub>2</sub> PO <sub>4</sub> ) <sub>2</sub>	0.963	-5.24 x 10 <sup>4</sup>
K <sub>2</sub> Cr <sub>2</sub> O <sub>7</sub>	0.980	-2.82 x 10 <sup>4</sup>

<sup>1</sup>From: Ecology 41:233 (1960) Saturated solutions for the control of humidity in biological research.

The values of  $h_c$  (negative  $h$ ), for the vapor sorption samples have been adjusted by  $2.5 \times 10^4$  cm to account for the osmotic potential. This value was arrived at by matching the 98 percent relative humidity solution content to the pressure plate data. In any event, the curves shown in Figure 5.3 are insensitive to the estimated osmotic potential.

Figure 5.4 presents the vapor sorption isotherms obtained from the experiments. It has a classical B.E.T. Type III shape. The shape indicates that the first monolayer is strongly adsorbed, additional coverage forms uniform layers, and that capillary effects occur at higher humidities. The data is also listed in the appendix.

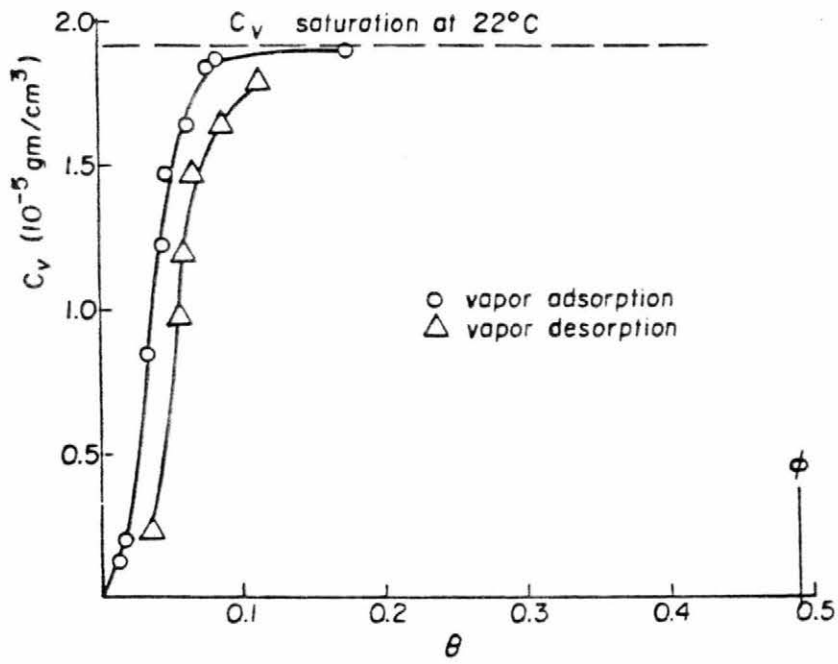


Figure 5.4. Water vapor sorption isotherms for Lurgi retorted oil shale.

## SPECIFIC SURFACE

The B.E.T. equation (Brunauer, et al., 1938) can be used with the water vapor adsorption data to relate the volume of adsorbed vapor to the vapor density and the specific surface of the porous media. The B.E.T. equation was developed with the assumption that at a given vapor density there will be a uniform, constant depth of adsorbed vapor on all surfaces. This assumption limits the range of application of the equation to humidities, generally less than 50 percent, where capillarity is not significant. The B.E.T. equation states

$$\frac{C_v/C_{vs}}{\theta(1-C_v/C_{vs})} = \frac{1}{\theta_m c} + \frac{(c-1)C_v/C_{vs}}{\theta_m c} \quad (5.4)$$

where  $\theta_m$  is the volume of adsorbed gas for one monolayer, and  $c$  is an adsorption constant. The monolayer volume and  $c$  are determined by plotting the left-hand side of Eq. (5.4) versus  $C_v/C_{vs}$  and drawing a straight line through the data as shown in Figure 5.5. With the slope,  $s$  and vertical axis intercept,  $i$ ,  $\theta_m$  and  $c$  can be calculated from

$$\theta_m = 1/(s+i) \quad (5.5)$$

$$c = s/i+1 \quad (5.6)$$

A least squares regression using the lowest four data points yields the  $i$  and  $s$  values shown and a regression coefficient of 1.0000. The calculated monolayer volume is  $0.0175 \text{ cm}^3/\text{cm}^3$  at a dry bulk density of  $1.4 \text{ g/cm}^3$ . With the monolayer volume the specific surface can be calculated by

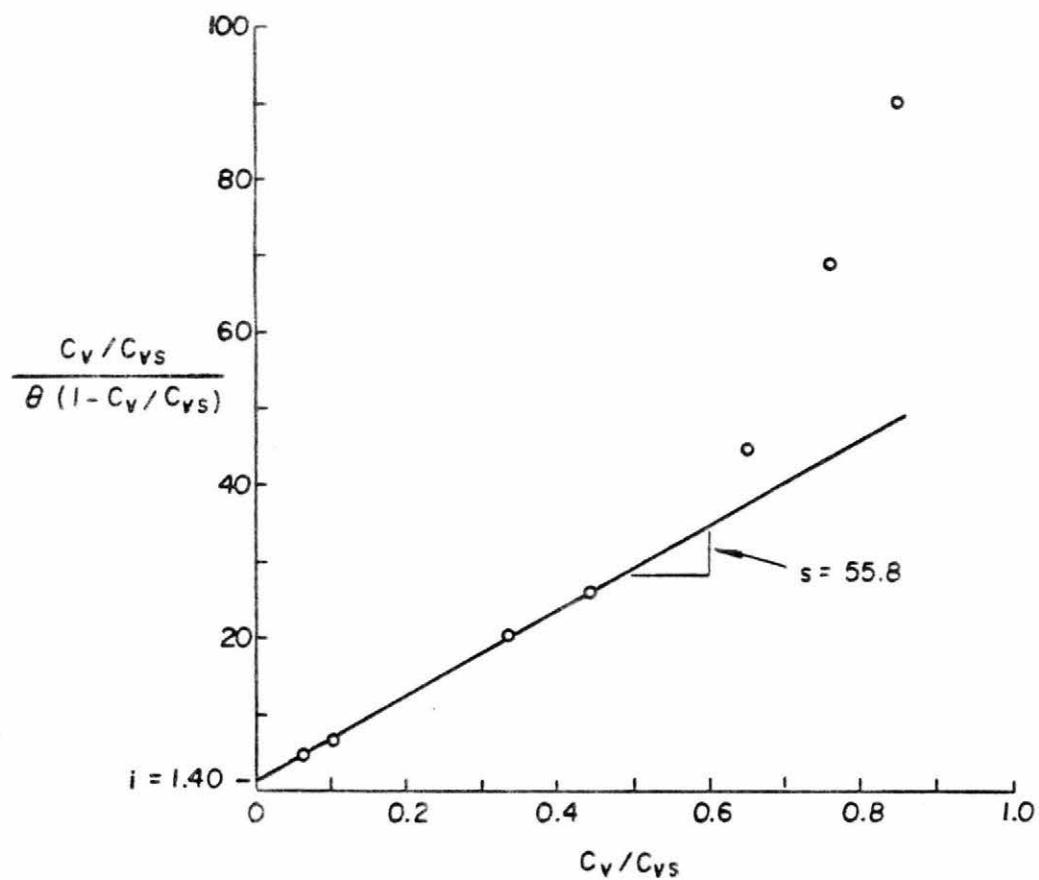


Figure 5.5. B.E.T. plot of vapor adsorption data.

$$SS = \theta_m / \rho_b h_m \quad (5.7)$$

where  $SS$  is the specific surface, and  $h_m$  is the monolayer height that is assumed to be  $3.1 \times 10^{-8}$  cm. Equation (5.7) yields a specific surface for the Lurgi of  $40 \text{ m}^2/\text{g}$ . This is a relatively large value for a nonclay material. The plot also shows that at around 50 percent relative humidity the adsorption deviates from the straight line. This would indicate the start of capillary effects.

#### SATURATED CONDUCTIVITY

The saturated hydraulic conductivity of the processed Lurgi retorted oil shale was determined by a falling head permeameter. A single column, 6.95 cm in diameter and with a test section 33 cm long was packed to a dry bulk density of  $1.37 \text{ g}/\text{cm}^3$ . The column was allowed to saturate overnight by filling with a solution from the bottom. The same  $\text{CaSO}_4$  solution used in the water characteristic tests was used for both saturation and testing here. After saturation, the permeameter was connected to a glass, (2.2 cm I.D.), tubing reservoir. The reservoir level was then read periodically for 3 days. The hydraulic gradient ranged from 6.6 to 3.5. The conductivity of the sample can be calculated by (McWhorter and Sunada, 1977)

$$K_s = aL/At \ln(H_o/H_t) \quad (5.8)$$

where  $K_s$  is the saturated conductivity,  $a$  the area of the reservoir,  $A$  the area of the permeameter,  $L$  is the sample length,  $t$  is the time from the start of flow, and  $H_o$  and  $H_t$  are the reservoir height above the outlet at times zero and  $t$ . The

conductivity can be calculated between any two data points, which will give a series of estimates. A better analysis is provided by plotting  $\ln(H_o/H_t)$  versus  $At/aL$ . The plot should be a straight line with a slope of  $1/K_s$ .

Figure 5.6 presents a plot of the falling head data. The plot is linear as required, and indicates a saturated conductivity of  $9.1 \times 10^{-6}$  cm/s.

#### SOLUTE TRANSPORT BY LIQUID-VAPOR FLOW

##### Theory

The dual source gamma ray attenuation method of monitoring water and salt movement developed by Grismer (1984) was used. The method simultaneously measures volumetric solution content and salt concentration, by the attenuation of gamma rays of two different energies. If the sample is a mixture of materials its mass adsorption coefficient,  $\mu$ , can be approximated (Grismer et al., 1986a) by the weighted average

$$\mu = \sum_i w_i \mu_i \quad (5.9)$$

where  $w_i$  is the mass fraction of component  $i$  that has an absorption coefficient  $\mu_i$ . The attenuation coefficient  $\beta$ , is the product of  $\mu$  and solution density,  $\rho_1$ . Multiplying Eq. (5.9) by  $\rho_1$  yields

$$\beta = \sum_i w_i \rho_1 = \sum_i \mu_i C_i \quad (5.10)$$

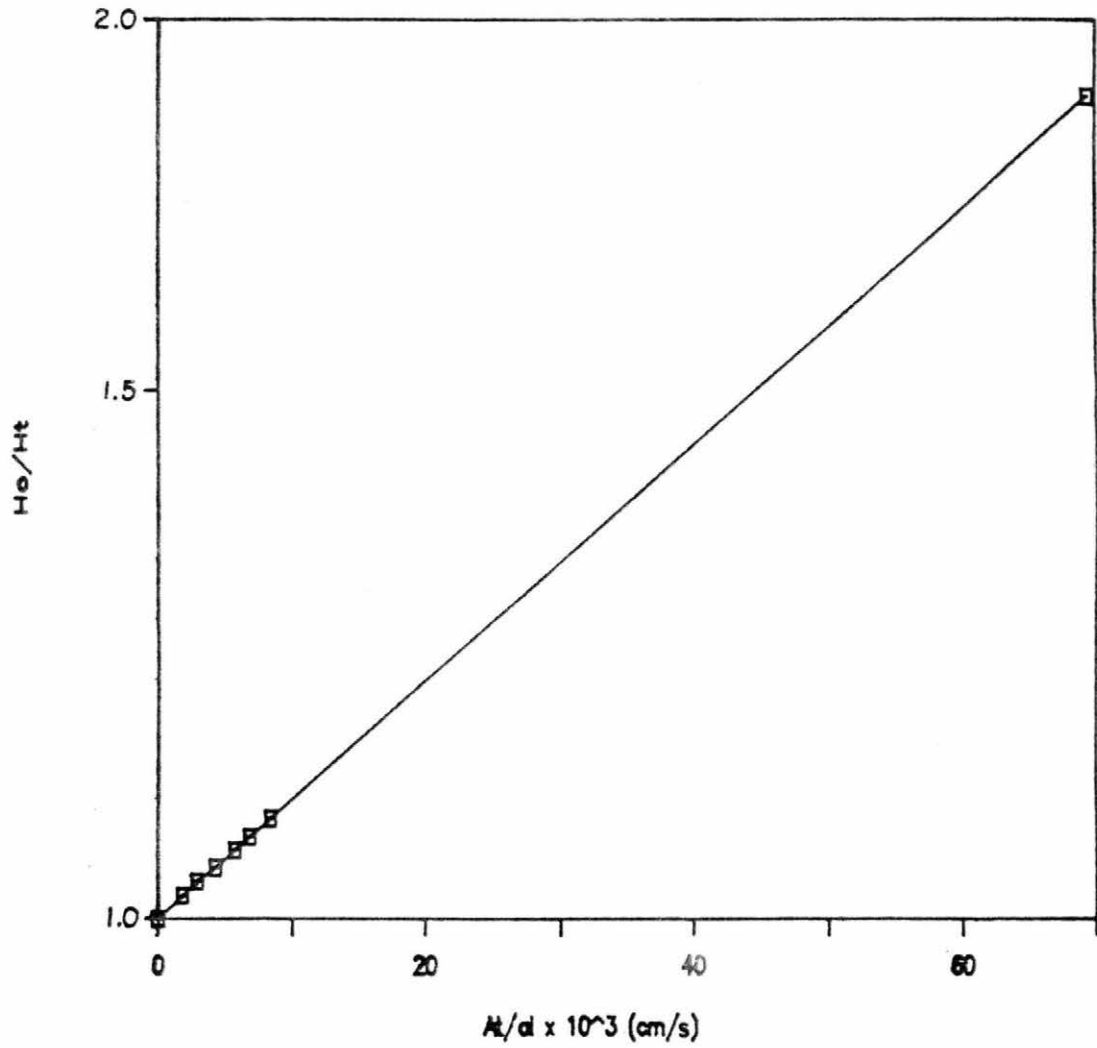


Figure 5.6. Falling head permeameter analysis.

where  $C_i$  is the concentration of component  $i$ . For a single salt solution the summation of Eq. (5.10) contains only two terms, one for the salt, the other for the water

$$\beta = \mu_w C_w + \mu_s C_s \quad (5.11)$$

It is impractical to measure the mass absorption coefficient of a pure salt, but it is easy to measure the attenuation of varying solution concentrations. This suggests the transformation of Eq. (5.11) to

$$\beta = \beta_w + bm \quad (5.12)$$

where  $\beta_w$  is the attenuation coefficient for pure water,  $m$  is the molality based concentration unit equal to  $C_s/C_w$ , and  $b$  is an attenuation coefficient measured using a series of solutions. The molality base is used since it is easy to accurately mix solutions by mass.

If a column of rigid porous media and solution is placed between a gamma source and a detector, the count rate,  $I$ , is given by

$$I = I_0 e^{-\beta L} \quad (5.13)$$

where  $I_0$  is the count rate obtained with only the container and oven dried porous media, and  $L$  is the radiation path length through the sample. Two different sources, americium and cesium, would have separate count rates,  $I_a$ ,  $I_{oa}$ ,  $I_c$  and  $I_{oc}$ , and attenuation coefficients

$\beta_a$ ,  $\beta_c$ ,  $b_a$  and  $b_c$ . Simultaneous counts at a single position provide two equations and two unknowns

$$I_a = I_{oa} \exp[-(\beta_a + b_a m)\theta L] \quad , \text{ and} \quad (5.14)$$

$$I_c = I_{oc} \exp[-(\beta_c + b_c m)\theta L] \quad . \quad (5.15)$$

Solving for  $\theta$  and  $m$  yields

$$\theta = \frac{\left( \frac{b_c}{b_a} \ln \frac{I_a}{I_{oa}} - \ln \frac{I_c}{I_{oc}} \right)}{L \left( \beta_c - \frac{b_c}{b_a} \beta_a \right)} \quad , \text{ and} \quad (5.16)$$

$$m = \frac{\left( \beta_c \ln \frac{I_c}{I_{oc}} - \beta_a \ln \frac{I_a}{I_{oa}} \right)}{\left( b_a \ln \frac{I_c}{I_{oc}} - b_c \ln \frac{I_a}{I_{oa}} \right)} \quad . \quad (5.17)$$

If Eq. (5.16) indicates no salt is present the solution content can be determined more accurately with the single americium count. Solution of Eq. (5.12) for single energy counts shows

$$\theta = - \frac{1}{\beta_a L} \ln(I_a/I_{oa}) \quad . \quad (5.18)$$

The accuracy of gamma ray attenuation is limited by characteristics of the equipment and the random nature of emissions from the sources. A large amount of the equipment error is caused by electronic drift. That is, the equipment counting characteristics change between the time of the dry count,  $I_o$ , and the wet counts,  $I$ .

This error is minimized by counting at a standard absorber,  $I_s$ , before and after each measurement. The actual count  $I'$  is then adjusted by the ratio of standard counts

$$I = I' I_{so}/I_s \quad , \quad (5.19)$$

where  $I_{so}$  is the standard count when the dry measurement is made.

The random nature of emissions, attenuation, and detection produce count rates that have a binomial distribution. The distribution is approximated by a normal distribution with a standard deviation equal to the square root of the mean. Grismer (1984) presents a detailed error analysis based on this assumption. He shows that errors in solution content and solute concentration are a complex function of the magnitude of  $\theta$ ,  $m$ , the count magnitude, and the salt used. While his conclusions are somewhat system dependent, they can be summarized as follows:

1. Total count number should exceed 600,000. For 3-4 cm I.D. columns, this requires count times of 3 minutes for americium and one minute for cesium.
2. The relative probable error in salt concentration increases with decreasing solution content. The probable error generally exceeds the actual value for volumetric solution contents less than 0.03.
3. Salts with the least relative error are NaI,  $SrCl_2$ , and  $Pb(NO_3)_2$ . In all of these salts the heavy element provides the majority of the attenuation effect. The most conservative of the salts is NaI.

Additional errors are produced by coincident beam interference if both beams are exposed at once. When counts are simultaneously taken, interference from the high energy source is produced in the lower energy count. While this interference can be corrected, the correction may equal one-half of the actual count. Correction of such magnitude result in relatively meaningless data. The need for correction is eliminated when only one source is exposed at a time and the counts are performed sequentially. For the slow flow process examined here, there is no significant change in  $\theta$  or  $m$  during the brief time interval required to scan the column with each source exposed.

#### Apparatus

The apparatus used is the same used by Grismer (1984), and Grismer et al. (1986a and b). A schematic of the system is shown in Figure 5.7. The sources used were 200 mCi of  $^{241}\text{Am}$  with a 0.476 cm active diameter, and 33 mCi of  $^{137}\text{Cs}$  with a 0.35 cm active diameter. The sources were held in a container which allowed each source to be quickly aligned with the collimator hole. The collimator hole was 0.476 cm in diameter and provided 1.7 cm of lead for the Am and 7.1 cm of lead for the Cs. When exposing the Am source alone, there was enough shielding of the Cs source to render its contribution to the total count insignificant.

In operation, a single gamma source is passed through the sample at a know location. The gamma radiation is detected by a NaI(Tl) crystal and generates a signal from the photomultiplier tube. The signal is passed through the ORTEC system elements and counted for a specific time period. The count information is then passed to a HP-9825 computer for computation of  $\theta$  and  $m$ .

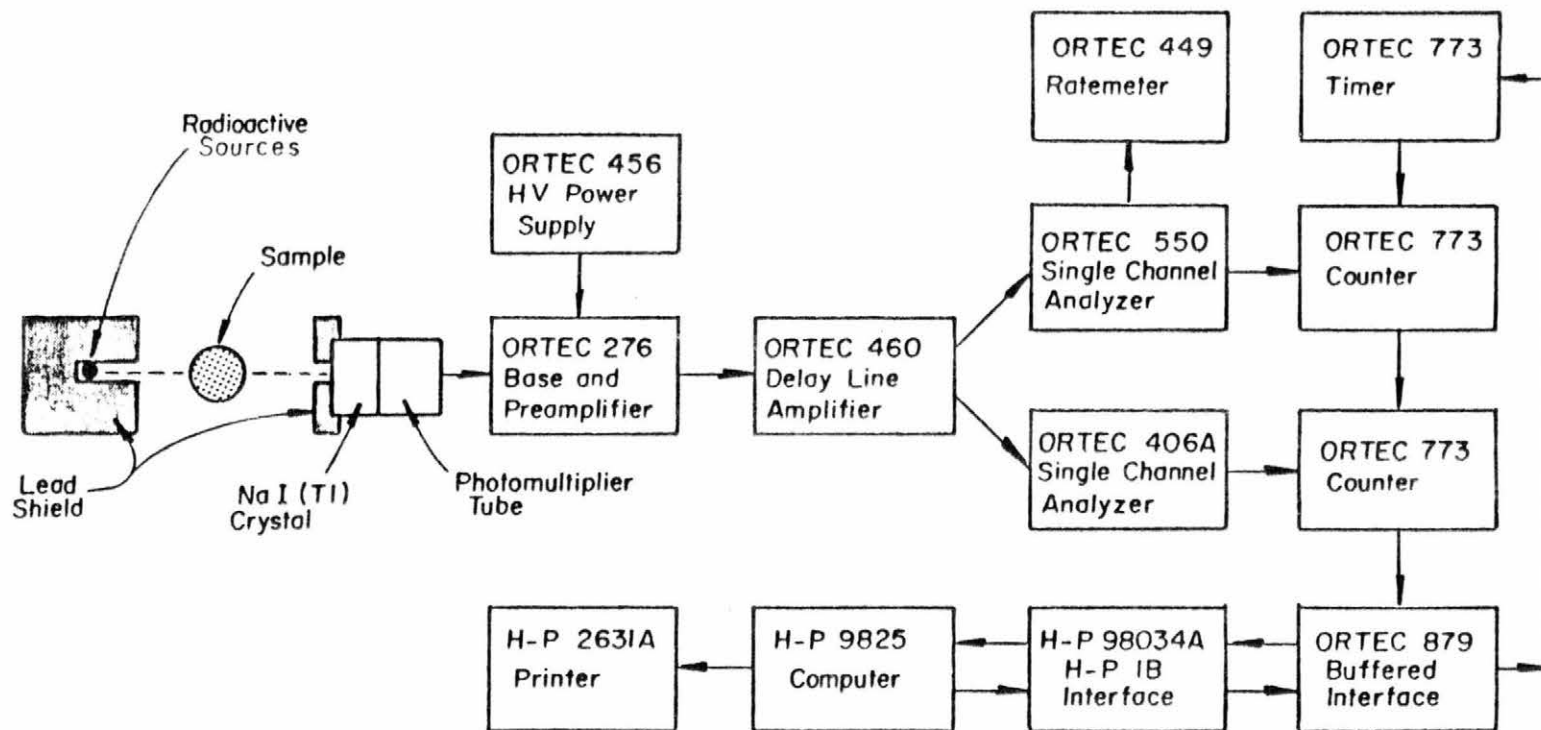


Figure 5.7. Dual source gamma system.

## Procedures

A 0.10 molar, NaI solution was injected at one end of a column by a Sage 355 syringe pump. The column was lucite with a 3.5 cm I.D. and 15 cm long. The column was sealed except for a needle septum at the inlet and a small vent at the far end. The injection mass was determined by periodically removing the entire column and weighing it. The weighing required stopping injection for less than five minutes. The column was scanned periodically by the dual source system at positions 0.5 cm on center. Between scans the injection rate was held constant, but was adjusted at the end of scans if necessary to produce adequate profiles.

Two separate tests were performed. In each test the column was packed with the Lurgi retorted shale. Care was taken during packing to insure the material did not separate by sizes or into layers. The compacted bulk density obtained in the columns was  $1.4 \text{ g/cm}^3$ . The total column porosity was 0.49.

Run 1. In the first test a total of 6.05 g of solution was injected over a seven-day period. Due to an equipment operation error no solution was injected during a period from hours 48 to 96. This failure did not affect results from the latter part of the test. The injection rate was held constant at about  $1.5 \times 10^{-5} \text{ g/s}$ . The inlet mass flux of solution was  $1.3 \times 10^{-6} \text{ g/cm}^2\text{s}$ . After the injection was terminated the solution redistribution was measured. The redistribution was monitored for a total of 97 days.

Run 2. In the second run the column was injected with 34.75 g of solution at varying rates of  $2.9 \times 10^{-5}$  to  $3.7 \times 10^{-4} \text{ g/s}$ . The mass flux of NaI was  $2.6 \times 10^{-6}$  to  $3.4 \times 10^{-5} \text{ g/cm}^2\text{s}$ . This range of injection rates was used to induce solution content profiles adequate

for estimation of the total diffusivity over the entire saturation range. Injection was stopped after 8 days. No redistribution was measured since the final water contents were well above the range of interest.

### Interpretation and Results

Interpretation. Before the test data are detailed it will be instructive to describe in general terms the expected results. Figure 5.8 presents an idealized depiction of a soil's properties and a single scan on an initially dry column. Figure 5.8a shows a typical vapor adsorption isotherm similar to Figure 5.4. Notice that the slope,  $dC_v/d\theta$ , is large at small solution contents and decreases to zero well before saturation. Figure 5.8b shows a typical graph of combined liquid-vapor diffusivity for a fine-grained material, similar to Figure 2.1. Notice the local maximum that occurs at low solution contents. In Figure 5.8c the horizontal axis is the column position from the inlet. The vertical axis is both the volumetric solution content, and the solution salt concentration. The profiles shown would be typical of conditions after injecting solution for a day or more. When examining the solution content profile it is necessary to remember that the flow is unsteady and the profile is only valid for an instant in time. At a later moment the profile would lie above the one shown.

The solution content profile shows that at the injection end, the solution content has been raised to a relatively large but less than saturated value. Since the material's diffusivity increases with increasing solution content, the gradient,  $dC_v/d\theta$ , is practically zero and therefore vapor transport is practically zero. All flow is by liquid convection.

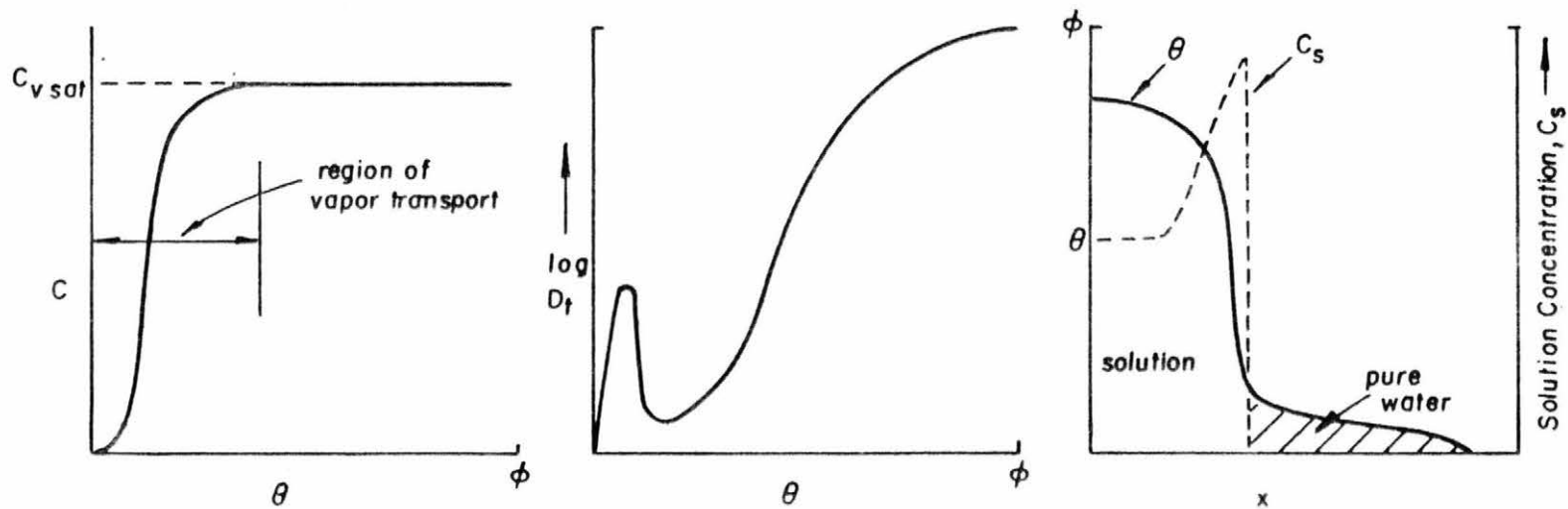


Figure 5.8. Idealized depiction of dry column behavior.

Further into the column the solution content decreases rapidly. In this region, the diffusivity becomes small, and the gradient,  $\partial\theta/\partial x$ , increases in order to maintain the flow. At these intermediate solution contents, vapor transport becomes significant relative to liquid convection.

Still further into the column, the solution contents reach very small values. At these values of solution content the slope of the vapor adsorption isotherm,  $(dC_v/d\theta)$ , is quite large. Thus, vapor transport is responsible for the increased  $D_t$ . Notice in Figure 5.8c that due to the larger value of  $D_t$ , the water content gradient,  $(\partial\theta/\partial x)$ , can be reduced to almost zero and is still adequate to drive the small mass flux that occurs.

The salt concentration in Figure 5.8c is equal to the injection concentration at  $x=0$ . Further into the column, the salt concentration increases significantly. The increase is due to the initiation of vapor transport. As water evaporates from the solution phase the remaining solution must contain the same mass of salt in less solution volume. As the salt concentration increases, back diffusion toward the inlet of the column occurs. At some point in the column the concentration decreases to zero in a sharp front.

In most instances, the limited spatial resolution of the experimental data, coupled with the steep gradients of salt concentration and solution content, make it impossible to identify the solution content at the salt front from a single measurement of the profiles. Instead, a series of measurements provide a range of solution contents within which the salt front lies. The range is progressively narrowed by measuring several salt and solution content profiles.

Profiles. In Run 1, a total of seven scans were performed during injection and an additional 14 during redistribution. Figure 5.9 shows three of the solution content and NaI concentration profiles obtained during injection. The profiles are quite similar to the ideal profiles in Figure 5.8c. Notice that a significant zone of salt free water developed ahead of the salt front. Figure 5.10 shows typical liquid and solute profiles for the redistribution. The graphs show that while the water content profile adjusted toward a more uniform distribution, the salt concentration profile continued to exhibit a sharp front and the concentration behind the front continued to increase as water moved forward in the column.

In Run 2, a total of 17 scans were performed. Figure 5.11 shows typical solution and salt profiles for the run. The early profiles at 120.5 hrs., which corresponds to the lower injection rates, is similar to Run 1. The profiles resulting from high injection rates show a much steeper solution content front. This is to be expected, since the diffusivity increases greatly with solution content, and the wetter contents will sweep over the early profiles. The sharpness of the salt front is reduced due to increasing injection rate.

Solution Content at Salt Front. Figure 5.12 presents the range of solution contents at the front in Run 1 for each scan. Scans 13 to 21 are unsuitable for analysis due to the redistribution to solution contents below previous values. The top of each bar represents the lowest solution content at which salt was observed while the bottom of the bars represents the highest water content with pure water. The shaded water content range, 0.063 to 0.083, is common to all but one observation.

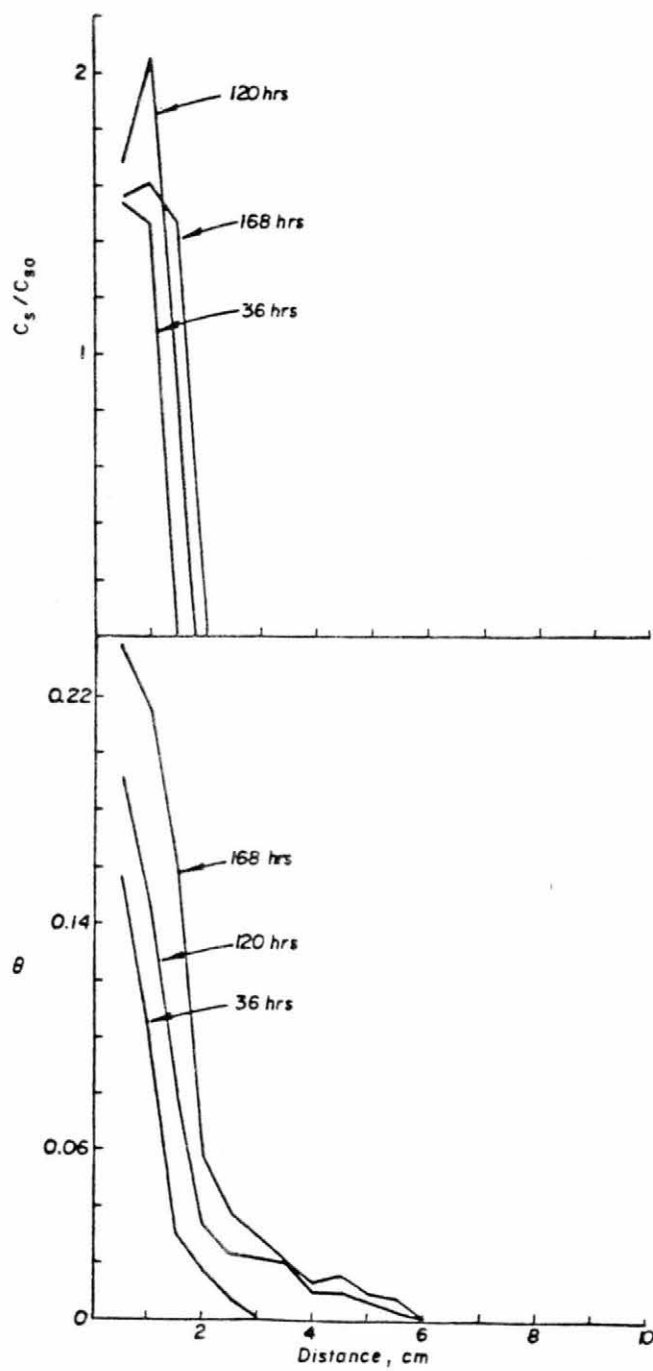


Figure 5.9. Solution and solute profiles for wetting in Run 1.

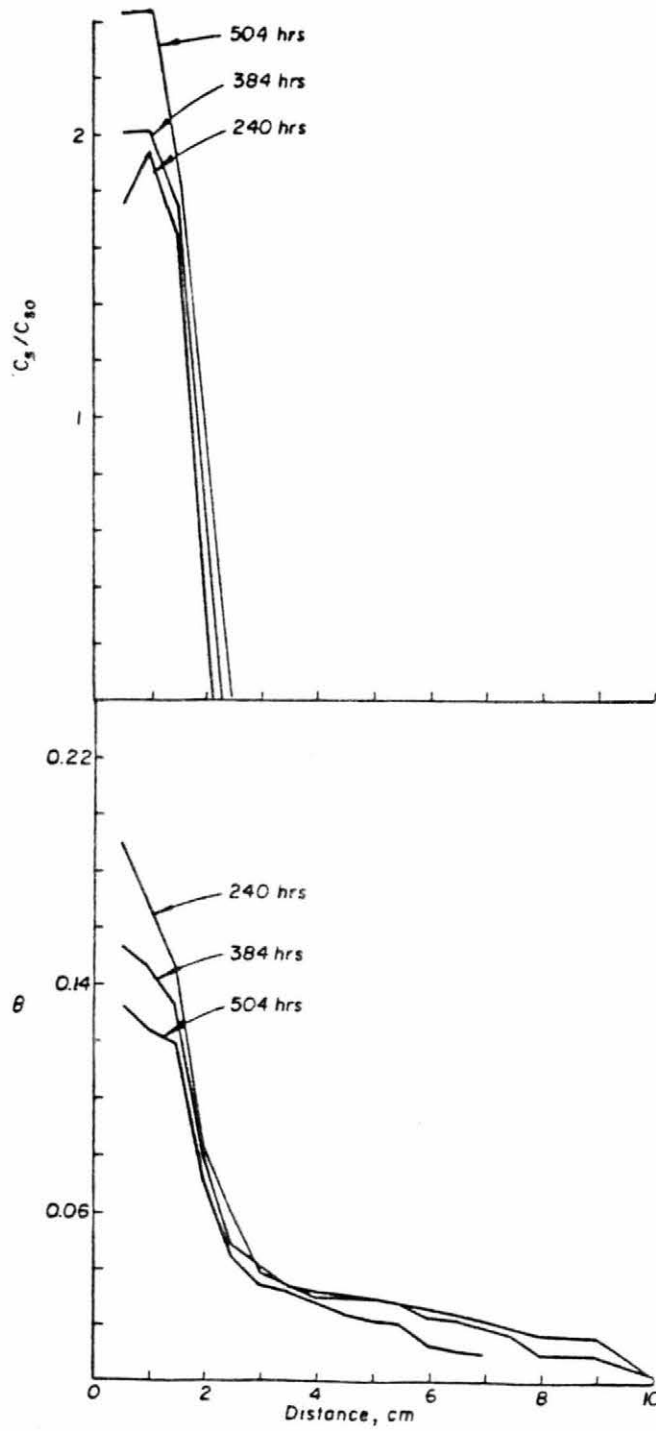


Figure 5.10. Solution and solute profiles for redistribution in Run 1.

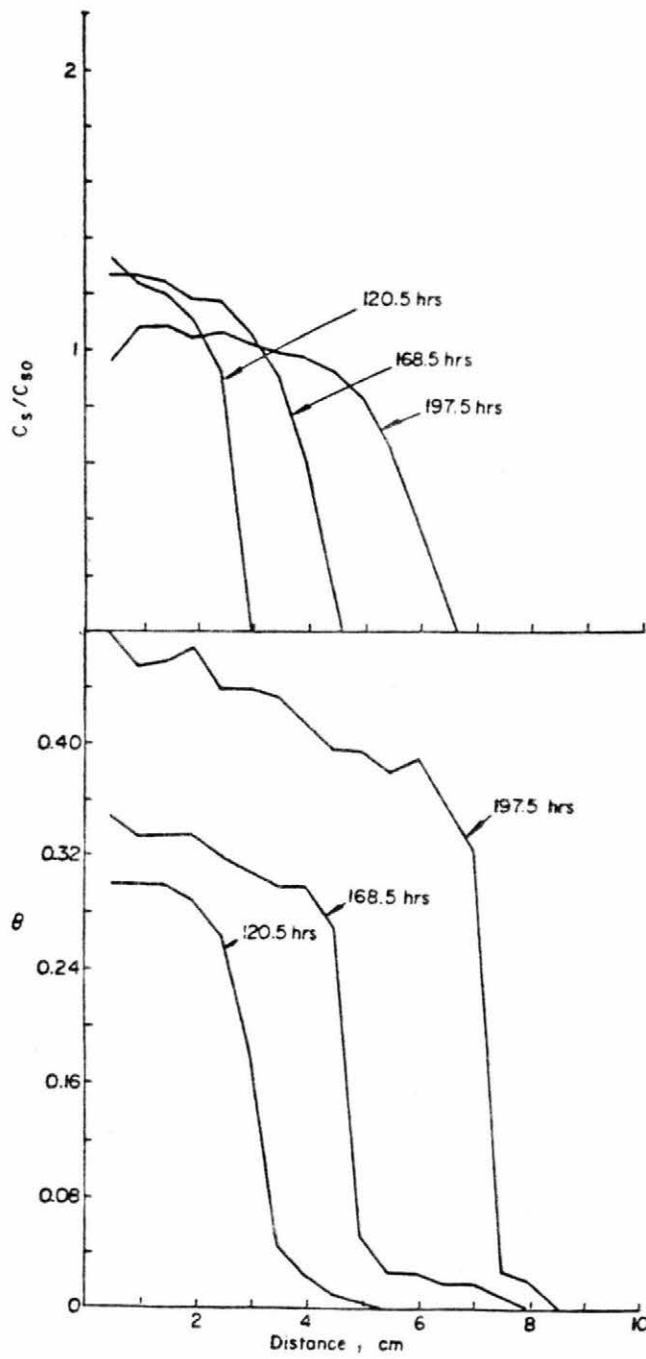


Figure 5.11. Solution and solute profiles for wetting in Run 2.

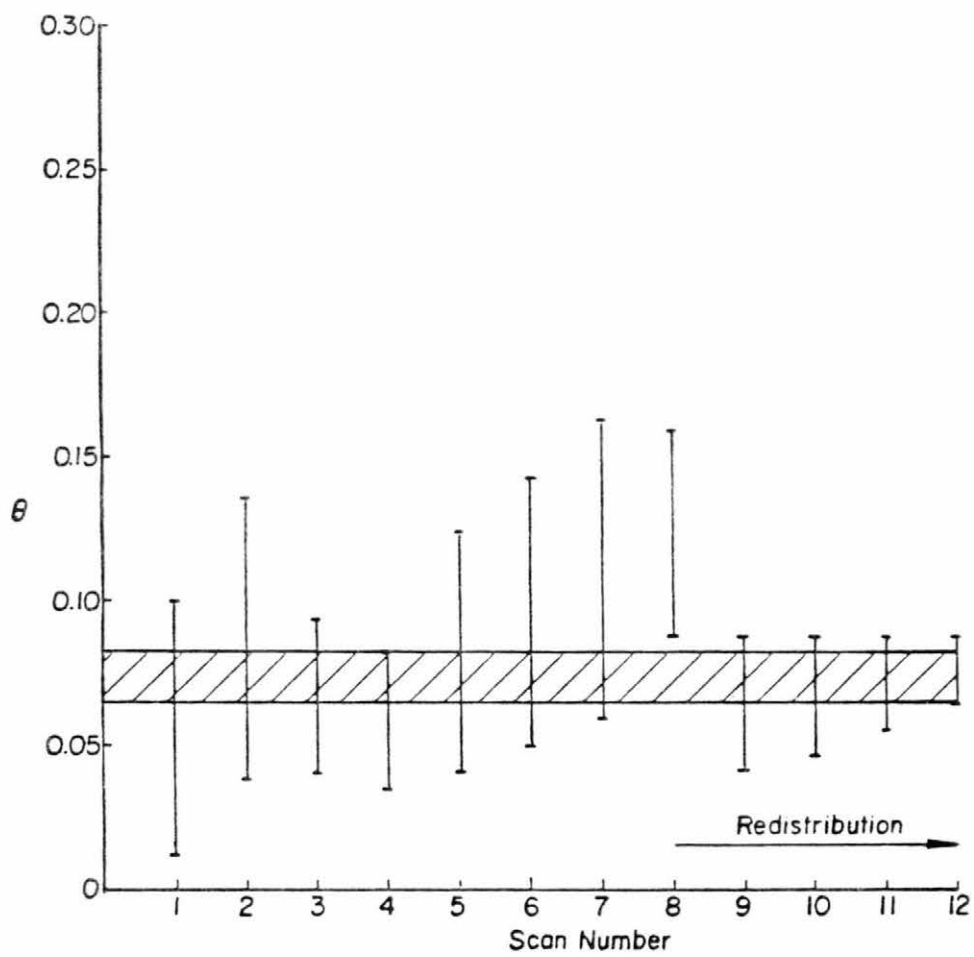


Figure 5.12. Range of solution contents at salt front in Run 1.

Figure 5.13 shows the range of solutions contents at the salt front in Run 2. Scans 15, 16, and 17 are unsuitable due to the increasing injection rate. Due to the steep solution content profiles caused by the high injection rates, the ranges tend to be much larger than in Run 1. Two scans, 1 and 13, show dashed regions. In these scans the position of the salt front was uncertain. The shaded common area from 0.053 to 0.066 solution content is common to 12 of the 14 scans. Comparison of Figures 5.16 and 5.17 indicates a common overlap of solution contents between 0.063 and 0.066 by volume.

Hydraulic Properties. Using Eq. (2.9) the diffusivity for each position and between each scan was calculated using the HP-9825 computer. Figure 5.14 presents a graph of  $D_t$  versus  $\theta$  for the results of both runs. As can be seen the function exhibits the expected local maximum in the range where vapor transport dominates. The results of the two runs are quite comparable. Using Eq. 3.11 and data from the water characteristic curve, Figure 5.3, the hydraulic conductivity as a function of water content can be calculated. Figure 5.15 presents the relationship. As the figure shows, the conductivity varies over eight orders of magnitude from  $10^{-5}$  cm/s at saturation, to  $10^{-13}$  cm/s at 0.06 solution content. Insofar as the majority of transport below this solution content is by vapor flow, the hydraulic conductivity curve is ended there. This does not imply liquid conduction does not occur, it only reflects that the uselessness of defining hydraulic conductivity at such low contents. The detailed test results are presented in the appendix.

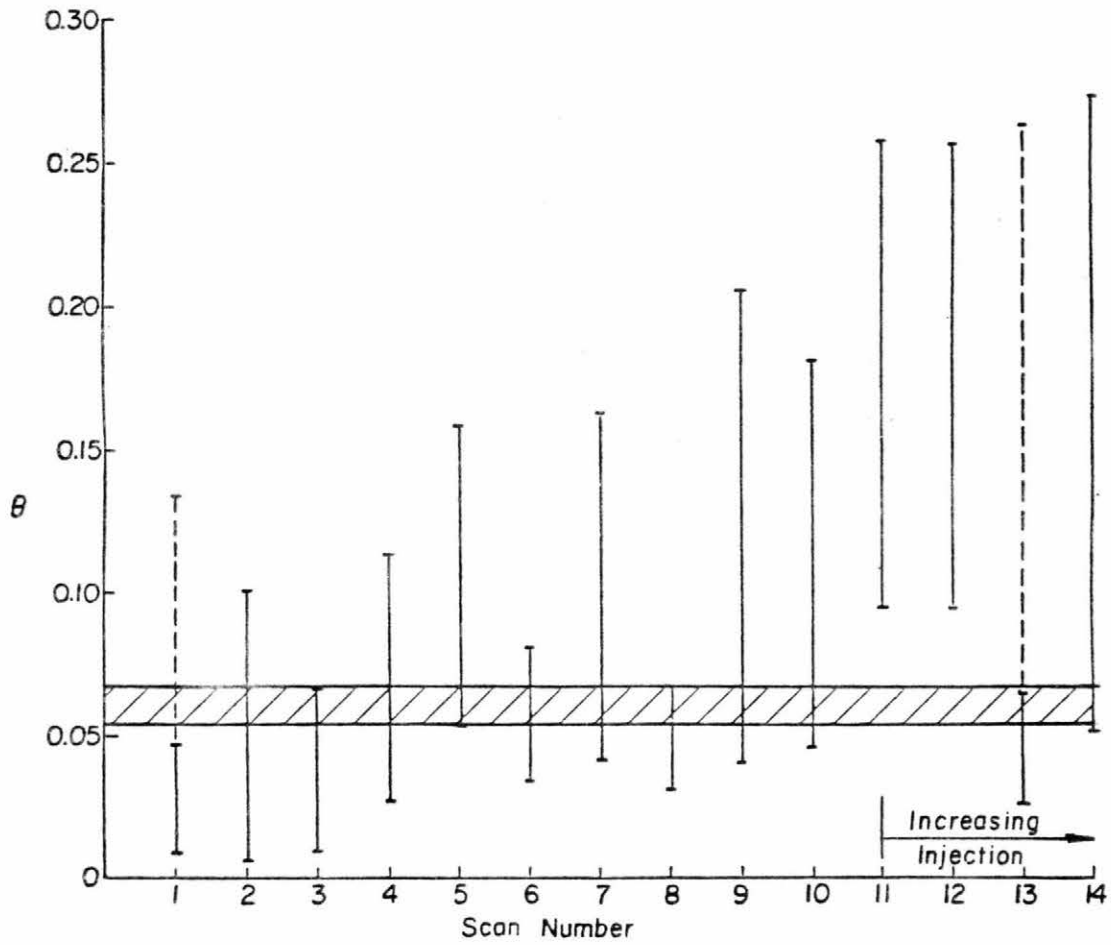


Figure 5.13. Range of solution contents at salt front in Run 2.

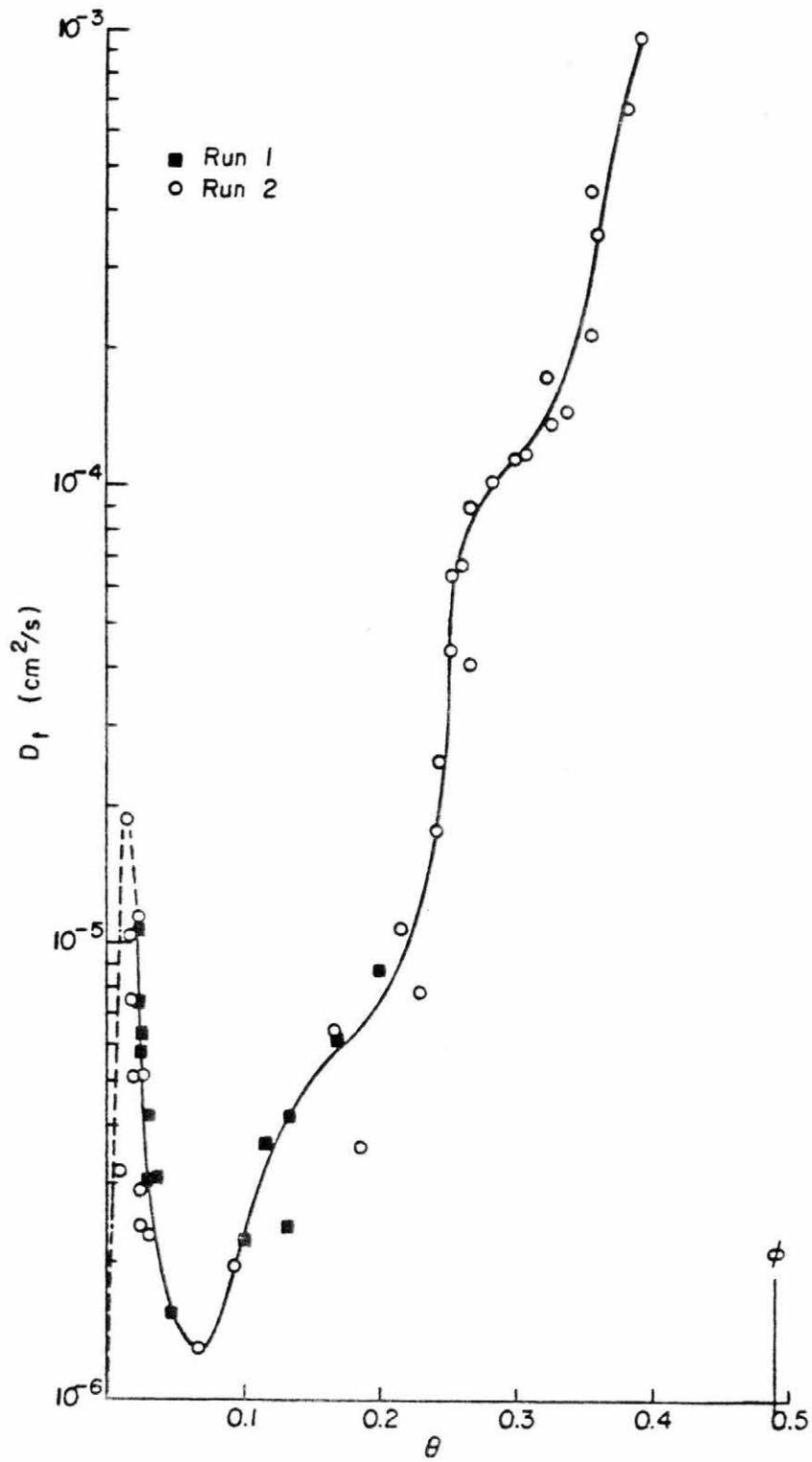


Figure 5.14. Total diffusivity for Lurgi retorted shale.

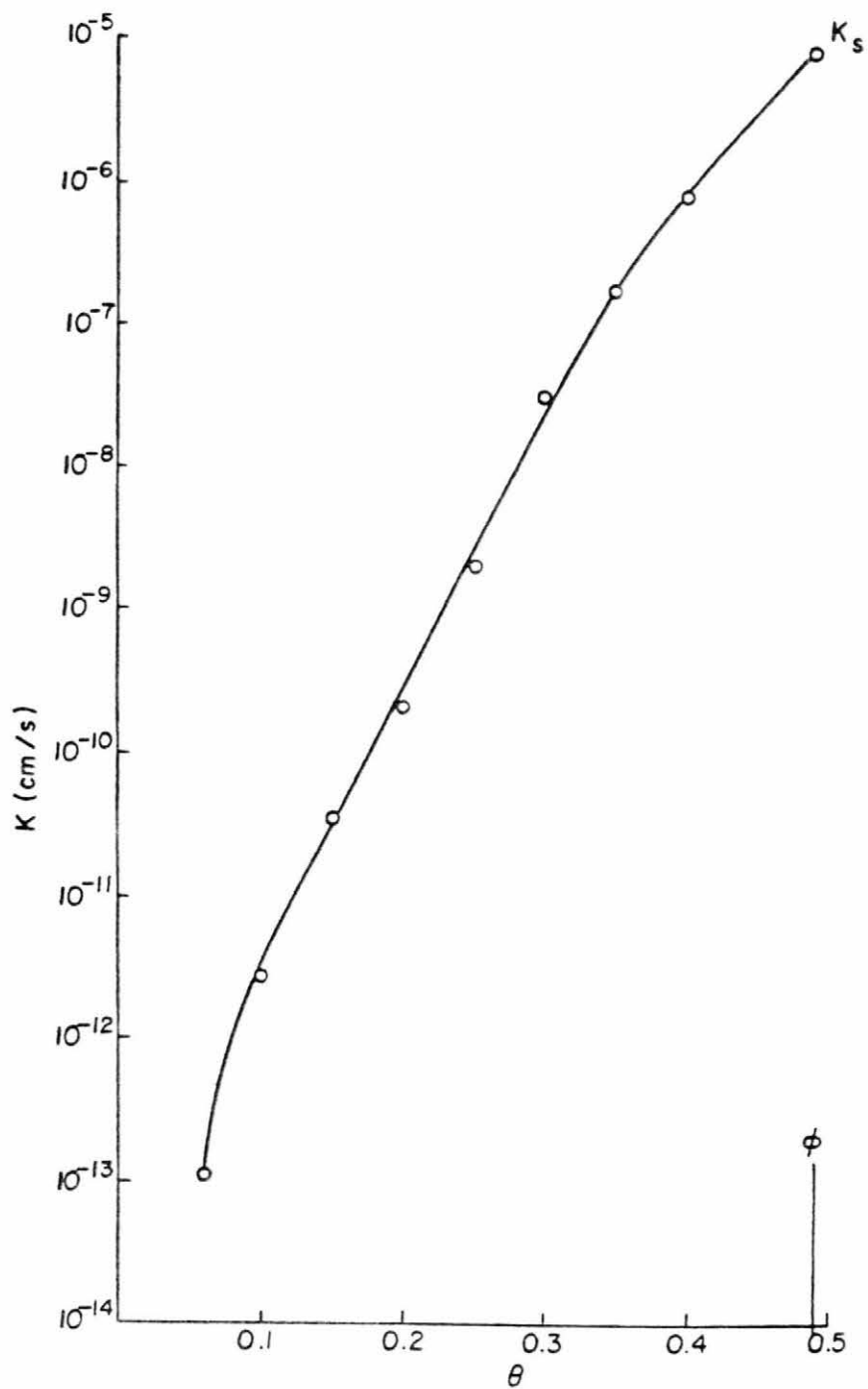


Figure 5.15. Unsaturated conductivity for Lurgi retorted shale.

## Chapter 6

### ANALYSIS

At this point it is possible to compare the theory and mathematical solutions obtained in Chapters 3 and 4 with the experimental results obtained in Chapter 5. If the theory and mathematical solutions are adequate in their description of the flow processes, they should be able to replicate the experimental data. Conversely, if the developed theory can produce flow features seen in the experimental data, there would be no justification to explain the experimental data with any physical process not included in the theoretical development. Thus, we should be able to properly interpret and strongly defend the experimental results, and confidently apply the measured transport coefficients and the developed theory to design problems.

There are two ways this chapter could be presented. The first would just apply the equations for the experimental conditions and present what they yield. Such a presentation would have the significant benefit of being concise, but would leave interpretation to the reader. Instead the chapter will attempt to provide an understanding of the analysis and results, such that the processes will become intuitive. This can only be accomplished at the loss of conciseness. It will be necessary to examine small details, so that each feature's relation to the others' are understood.

In the following sections, several special cases using the properties of Lurgi retorted oil shale will be examined. The cases will differ by boundary and initial conditions, and material properties. As in previous chapters, both the constant content boundary and the constant flux boundary will be examined.

#### DIFFUSIVITIES

In the previous chapter the total liquid-vapor diffusivity for the Lurgi retorted shale was measured. Before the analysis can proceed it will be necessary to make an assumption on how the total diffusivity is divided between liquid and vapor components. As outlined in Chapter 2, there is no direct method available to measure the liquid and vapor transport coefficients separately. Jackson (1965) using an indirect method was able to estimate the liquid diffusivity down to less than a monolayer as shown in Figure 2.1. His measurements showed the liquid diffusivity to continue a general decreasing trend beneath the vapor maximum.

In the spirit of Jackson's results, the Lurgi diffusivities will be fitted and divided by a set of exponential functions. The functions are;

$$D_v \frac{dC_v}{d\theta} = 10^{-7} e^{(212 \times \theta)}, \quad 0 < \theta \leq 0.025; \quad (6.1a)$$

$$D_v \frac{dC_v}{d\theta} = 1.7 \times 10^{-4} e^{(-85.6 \times \theta)}, \quad \theta > 0.025; \quad (6.1b)$$

$$D_l = 3.7 \times 10^{-7} e^{(19.7 \times \theta)}, \quad \theta > 0; \quad \text{and} \quad (6.1c)$$

$$D_l = D_v = 0, \quad \theta = 0. \quad (6.1d)$$

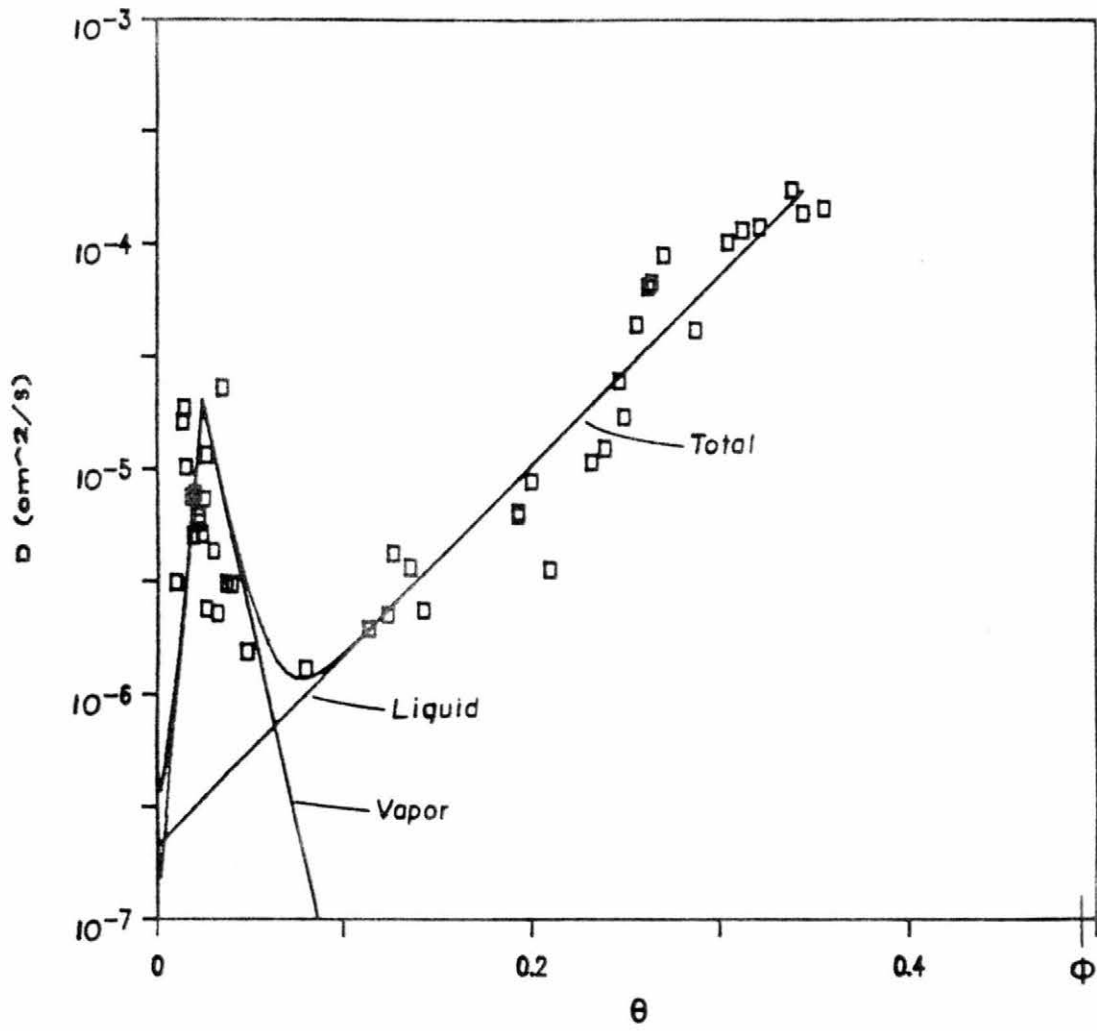


Figure 6.1. Assumed normal divisions of diffusivity.

Figure 6.1 presents a graph of these relations and their fit to the experimental data. Each assumed diffusivity has a nonzero value though the entire range of non-zero liquid contents. Diffusivities are set to zero at zero solution content to be theoretically correct. The relationship for the liquid diffusivity (Eq 6.1c) was obtained by least squares regression on the measured total diffusivity for solution contents above 0.08. The regression coefficient obtained was 0.95. The data for low liquid contents are too noisy for regression fitting. Therefore, the vapor relationships were determined by fitting exponential functions through the point  $\theta = 0.025$ ,  $D_v dC_v/d\theta = 2 \times 10^{-5}$  cm<sup>2</sup>/s. The solution content was chosen since it corresponds to the steepest part of the vapor adsorption isotherm, while the diffusivity value corresponds to about the maximum observed  $D_t$  in the vapor region. As the graph shows, the liquid diffusivity dominates at solution contents greater than 0.08, vapor diffusivity dominates between 0.01 and 0.05, and the two are the same order of magnitude between 0.04 to 0.08 and 0 to 0.01.

The relationships at very low liquid contents are not accidental. Because of its S shaped curve, the slope of the vapor adsorption isotherm is zero at  $\theta=0$ , and increases very slowly until  $\theta \approx 0.01$ . It is reasonable to expect the vapor diffusivity to be quite small at very low liquid contents. Even with the liquid diffusivity decreasing exponentially with  $\theta$ , if liquid diffusivity exists, it could exceed the vapor diffusivity at very low liquid contents.

While it is felt that these approximations are the best interpretation of the experimental data, the significant conclusions of the research are unaffected by the exact values of the assumed

diffusivities. Any assumed set of functions with separate liquid and vapor maximums will provide similar results.

#### CONSTANT SOLUTION CONTENT BOUNDARY

##### Sorption into a Dry Column

The special case of sorption into a completely dry column will be examined in detail. While looking at a single solution would be beneficial, the effects of vapor transport can be shown more clearly by considering three special cases. The cases are;

1. Liquid diffusivity set at its estimated value (Eq. (6.1c)), but no vapor transport,
2. Liquid diffusivity set at its estimated value (Eq. (6.1c)), with vapor diffusivity set at only one-tenth its estimated value (one-tenth Eqs. (6.1a,b)), and
3. Both liquid and vapor diffusivities set at their estimated values (Eqs. (6.1a,b,c)).

These three cases will allow the affects of the vapor flow to be examined and to some extent separated from the liquid flow. Figure 6.2 shows an arithmetic plot of the total diffusivity for each case.

The boundary conditions to be examined for all three cases will be

$$\theta_n = 0, \text{ and}$$

$$\theta_o = 0.20.$$

F(θ). With these boundary conditions F(θ) can be calculated by Eq. (4.18). Figure 6.3 presents F(θ) for each case. The relation F = θ is also shown for reference. The F(θ) for case 1 has a shape typical for monotonically decreasing D<sub>t</sub>. As vapor diffusivity increases, in

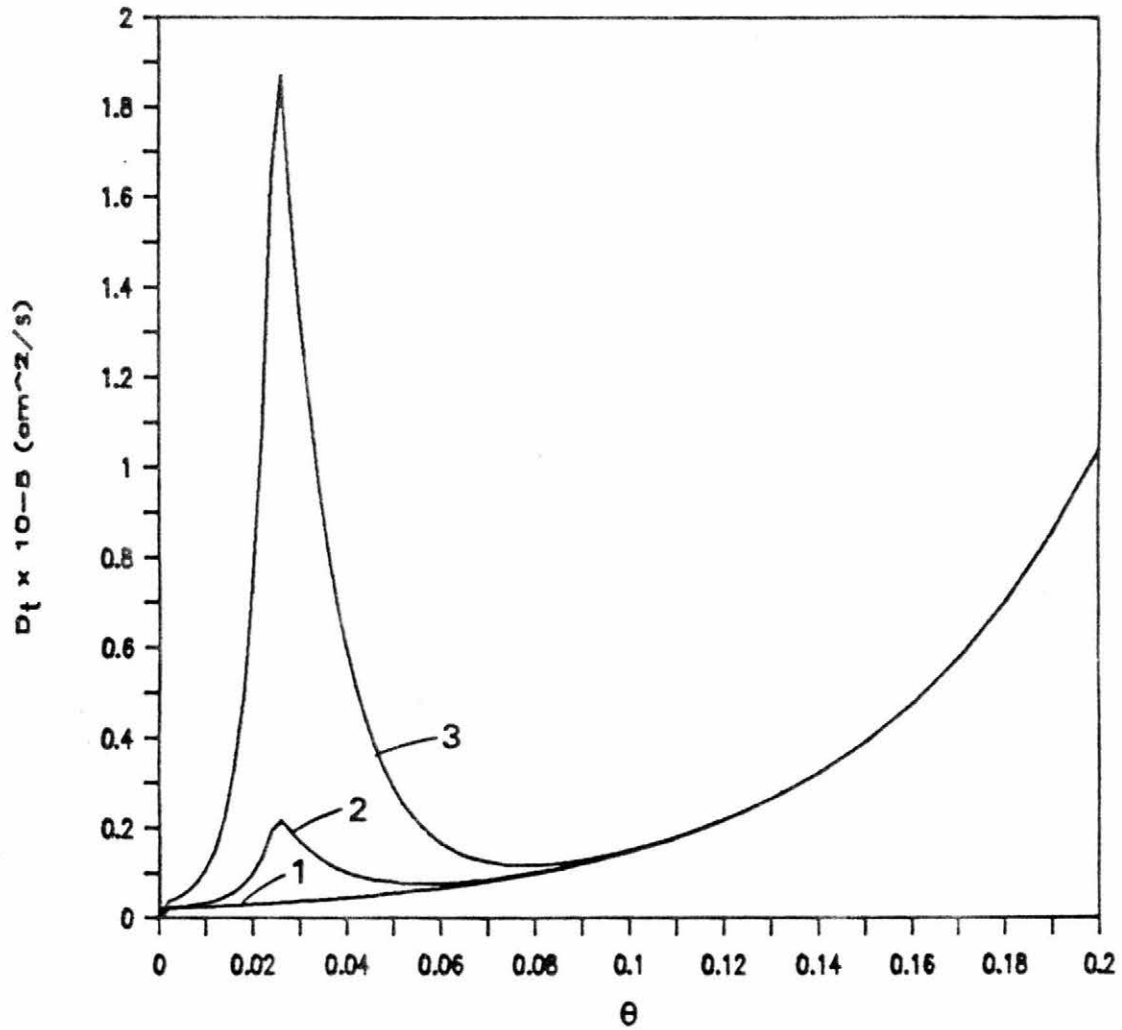


Figure 6.2. Total diffusivity for cases 1, 2, and 3.

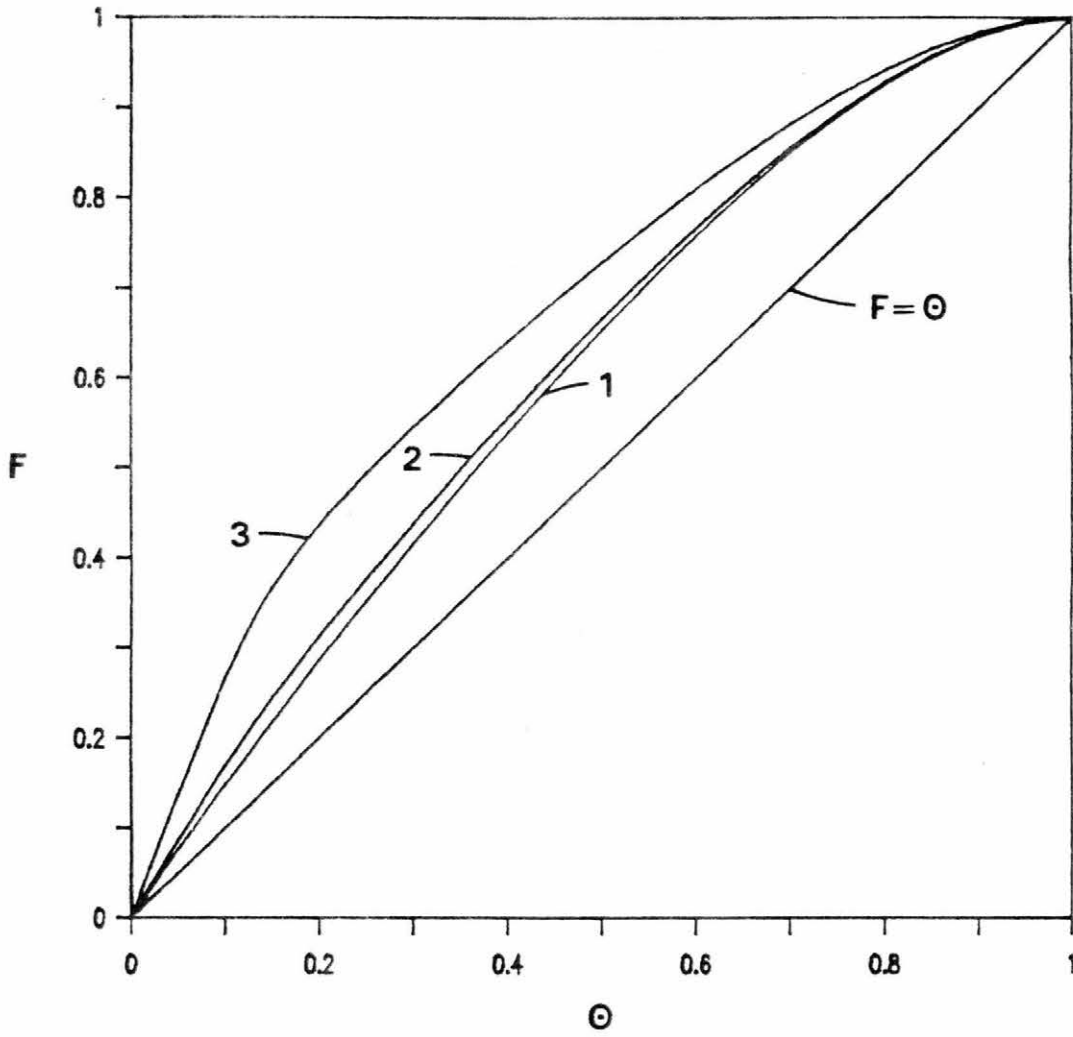


Figure 6.3. Fractional flow function for cases 1, 2, and 3.

cases 2 and 3, the secondary maximum in  $D_t$  tends to increase  $F(\theta)$  at the lower solution contents. This implies greater relative transport at the lower solution contents.

Liquid Content Profile. The effects of vapor transport on the solution profile can be seen in Figure 6.4. As shown in Chapter 4 the Boltzman variable ( $\lambda = x/t^{1/2}$ ), will normalize profiles for various times. As vapor transport increases the solution profile is affected in two ways. A nose of low solution contents develops, and the profile at high solution contents becomes steeper. Both the nose and the steep profile are produced by the high total diffusivity at the lower contents. It is interesting to note that while the profile has elongated, total inflow as measured by the sorptivity  $S$ , increased from case 1 only 1.9 and 12.4%, for cases 2 and 3 respectively. The vapor transport elongated the profile, but since it has almost no effect on the total diffusivity at the inlet, the inflow is only moderately increased.

Seepage Velocity. Figure 6.5 presents the normalized seepage velocity versus  $\lambda$  relations for each case. The normalized seepage velocity,  $v'_s$  is defined as  $v'_s = v_s t^{1/2}$ . With no vapor transport the seepage velocity increases slowly from the inlet to a maximum at the wetting front. With vapor transport the seepage velocity again increases from the inlet, but drops dramatically in the region of the nose. The drop in seepage velocity is due to the reduced solution content gradients in the nose. It is not due to a decrease in liquid conductivity. At the front of the nose the seepage velocity increases, due to the decrease in the vapor diffusivity and the increase in the solution content slope. In as much as the diffusivities at very low

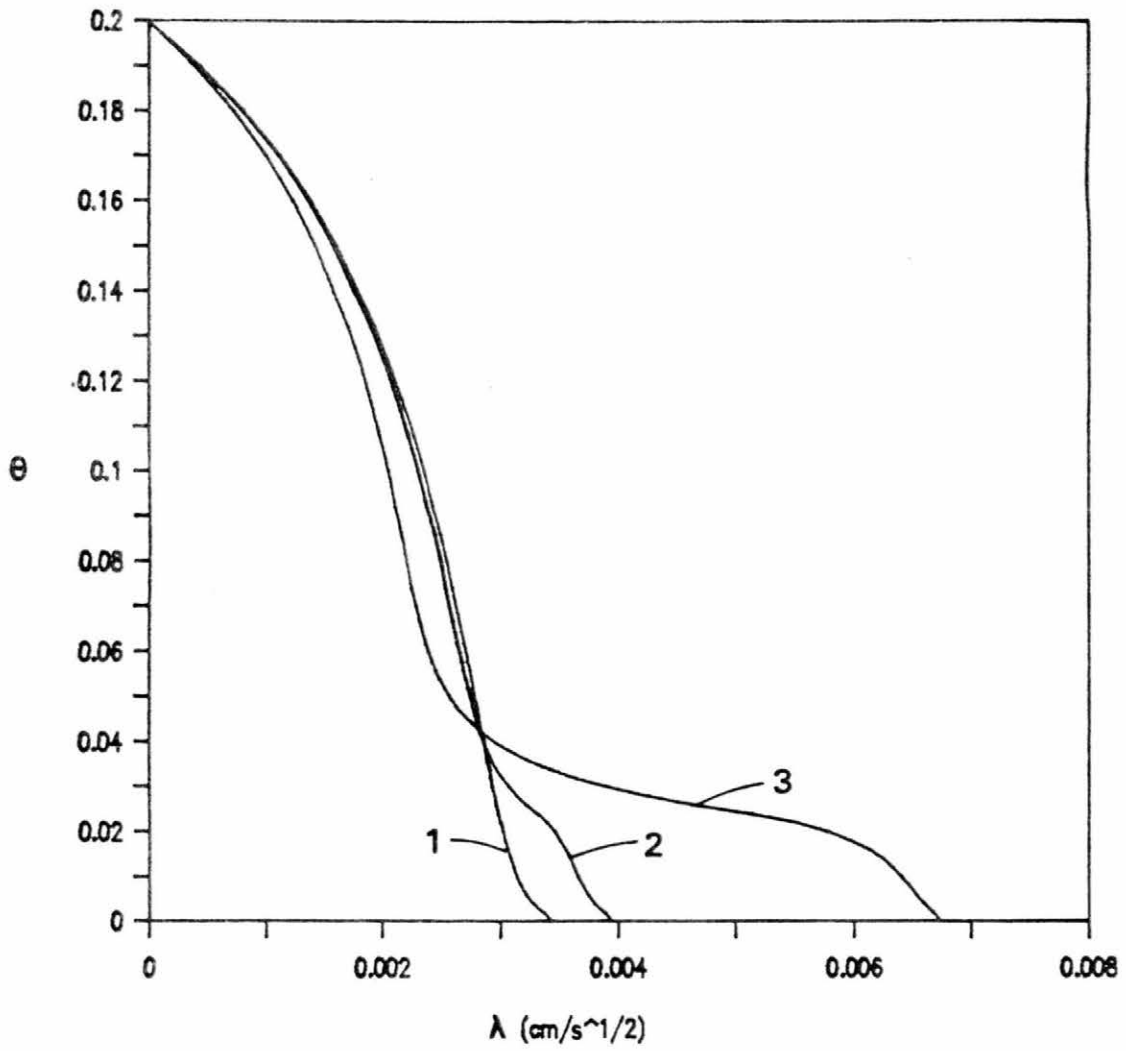


Figure 6.4. Liquid content profiles for cases 1, 2, and 3.

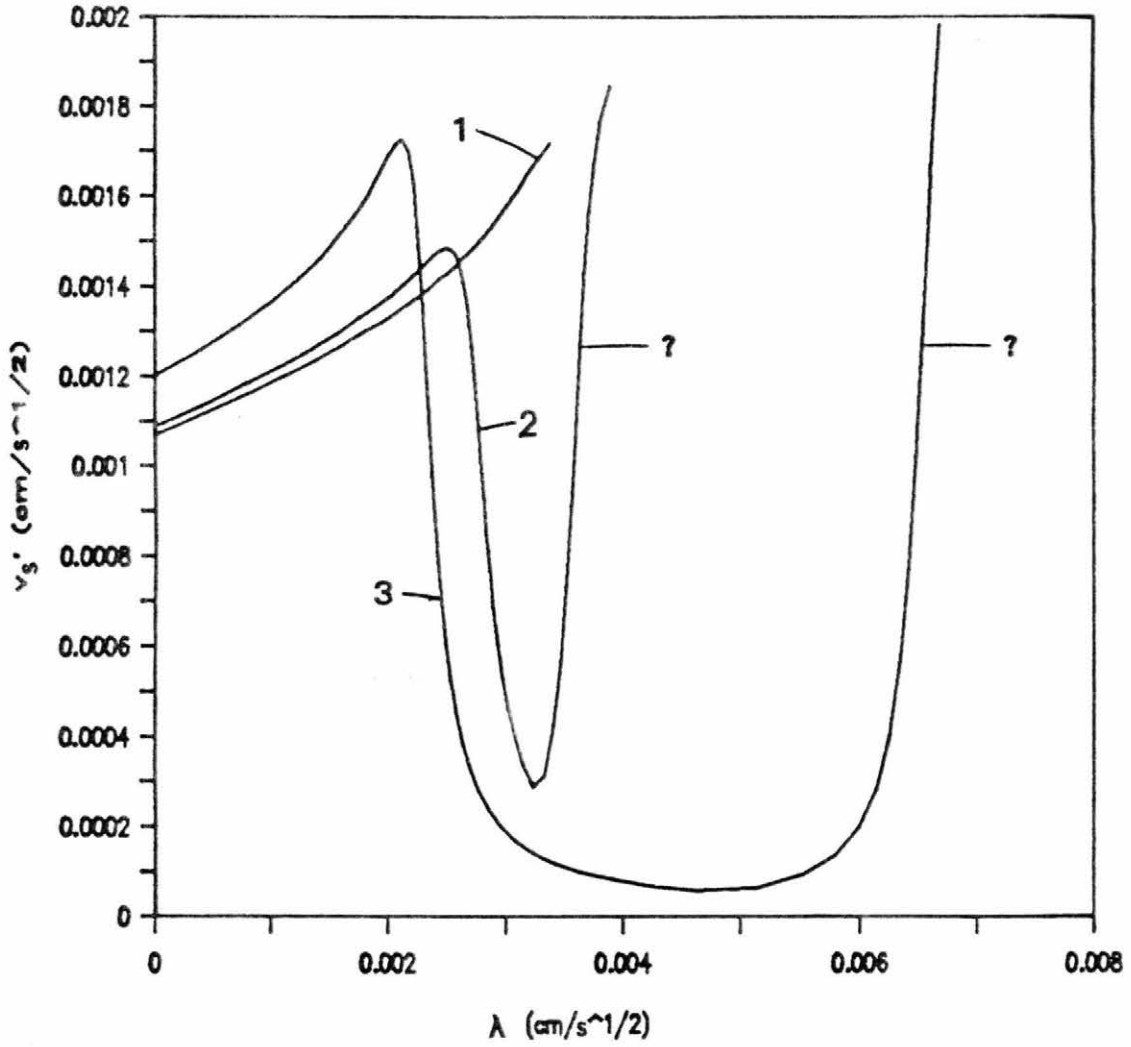


Figure 6.5. Seepage velocity for cases 1, 2, and 3.

solution contents are speculative, the values of seepage velocity at the tip of the nose is conjecture.

Phase Transfer. Figure 6.6 presents the normalized phase transfer. In case 1 the phase transfer is of course zero throughout the flow profile. With vapor transport, evaporation (positive  $e$ ), occurs in a narrow range of liquid contents and condensation (negative  $e$ ), occurs at the tip of the nose. Notice that decreasing the vapor diffusivity by an order of magnitude (case 2 versus case 3), has only decreased the maximum evaporation rate by about one-half, and actually increases the maximum condensation. Plotting the phase transfer versus liquid content in Figure 6.7 brings out an important point. Decreasing the magnitude of vapor diffusivity decreases the solution content of the evaporation maximum, increases the solution content of the condensation maximum, and increases the solution content of the evaporation zero. Thus, reducing the vapor diffusion only reduces the region of water contents of significant phase transfer, it does not significantly reduce the maximum values of phase transfer. The vapor diffusivity maximum occurs at a solution content of 0.025. That is also the liquid content that roughly separate the evaporation and condensation regions.

Solute Transport. Figure 6.8 presents the solute concentration profiles for the three cases. These profiles are for convection only as detailed in Chapter 4. Without vapor transport the relative concentration,  $C_s/C_{s0}$ , remains equal to unity throughout the profile. This is consistent with piston displacement of the invading solution. As vapor transport increases, the solute profile develops a sharp front of increased solute concentration. Comparing Figures 6.4 and 6.8 shows that for the two cases with vapor transport, the solute front moves

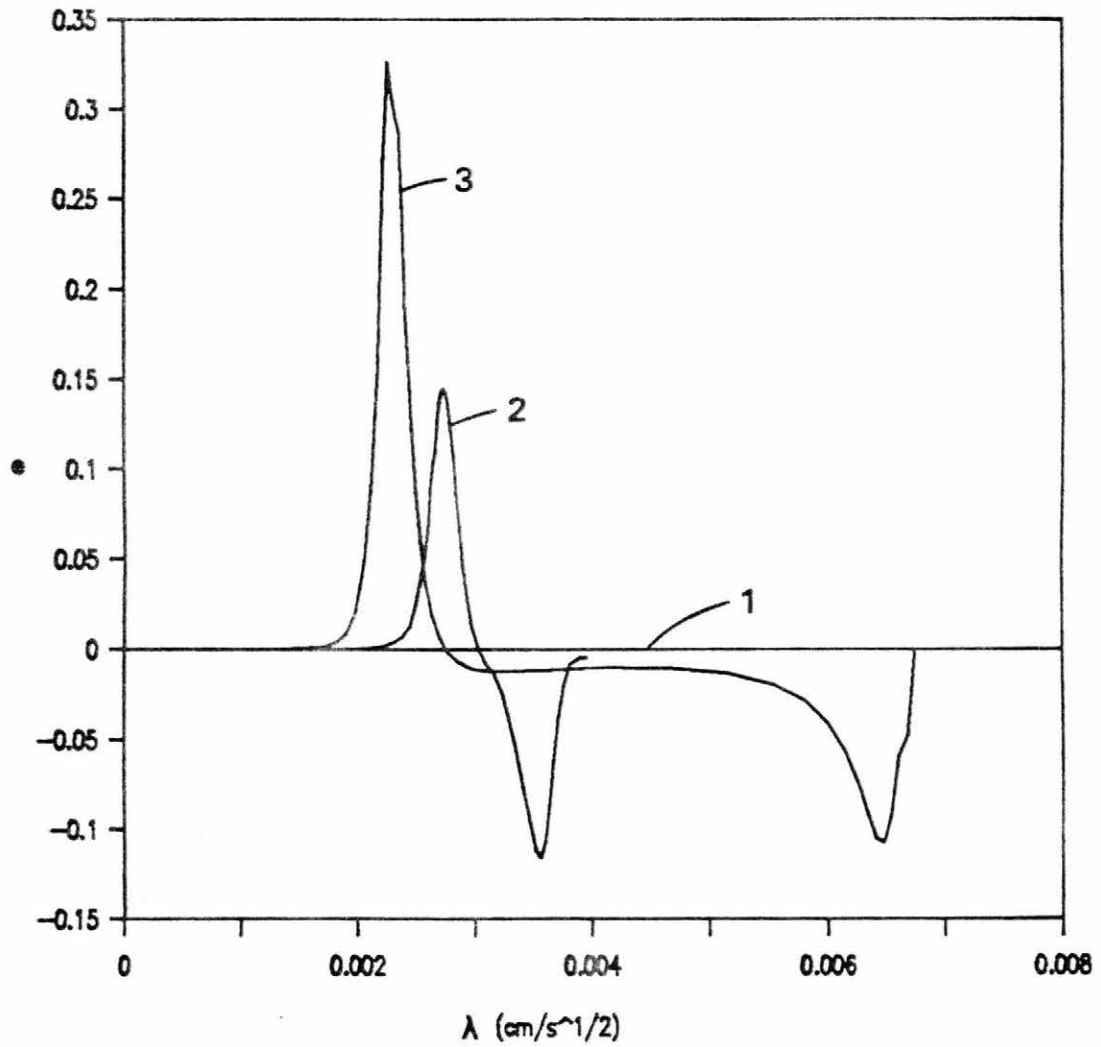


Figure 6.6. Water phase transfer versus  $\lambda$  for cases 1, 2, and 3.

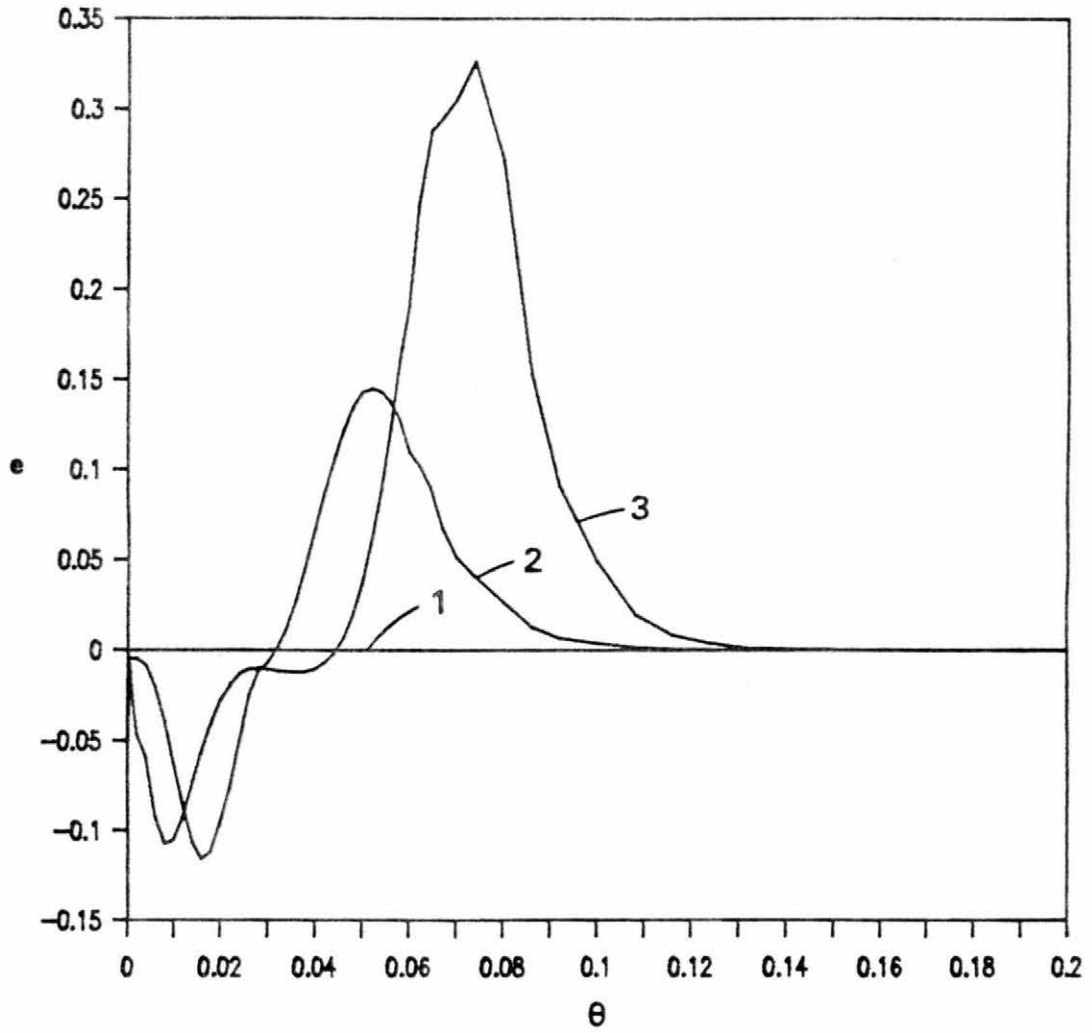


Figure 6.7. Water phase transfer versus  $\theta$  for cases 1, 2, and 3.

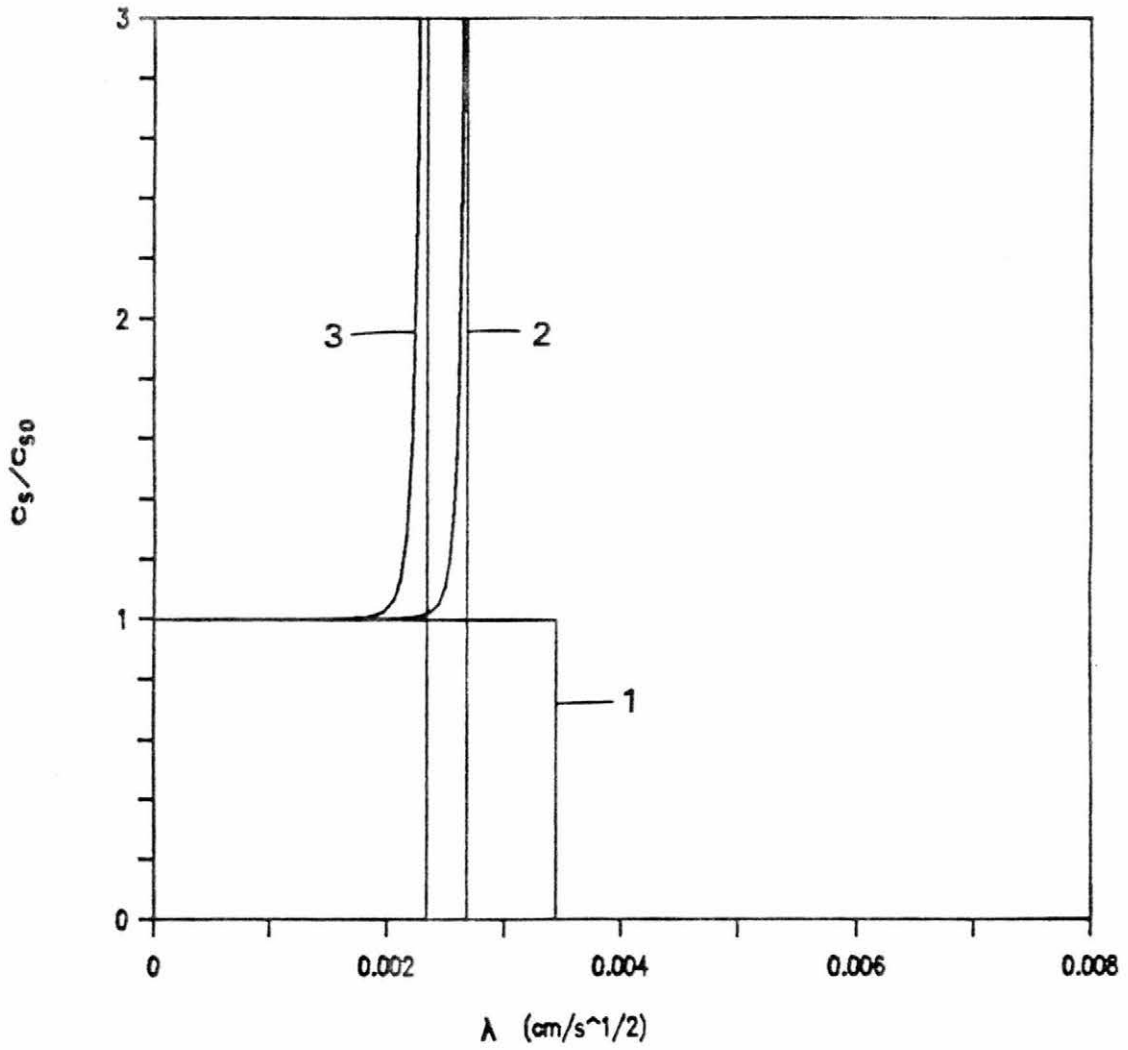


Figure 6.8. Invading solute concentration profiles for cases 1, 2, and 3.

farther back into the liquid profile. This leaves a large region of solute free liquid. While it is difficult to observe in the graph, as the vapor transport increases, the solute concentration near the front increases dramatically.

The solute front at intermediate liquid contents, is exactly what was observed in the experiments presented here and by Grismer (1985). The solute front occurs even though there is a finite seepage velocity throughout the profile. The front occurs at these intermediate liquid contents due to the transient flow processes. Not only are the water and salt transported, but the flow profile itself moves forward in space. Recalling Eq. (4.41), the ratio of the seepage velocity to the velocity of a liquid content can be computed. This ratio,  $B$ , indicates if a solute is moving faster ( $B > 1$ ), slower ( $B < 1$ ), or at the same speed ( $B=1$ ), as the liquid content that it is currently at. Figure 6.9 presents a plot of  $B$  versus  $\theta$  for each case. For case 1 with no vapor flow,  $B > 1$  throughout the flow profile, and equals unity at the wetting front, ( $\theta=\theta_n=0$ ). With vapor transport,  $B$  increases slightly for the high liquid contents and decreases greatly for the lower values. There is a nonzero liquid content at which  $B=1$ , which is the position of the solute front. If a solute particle entered the flow field at  $x=0$  at  $t=0$ , the farthest it could be transported by convection is the position where  $B(\theta)=1$ . The position or liquid content of the solute front, is not a unique value. The two vapor cases have slightly different values. Likewise changing boundary conditions would change the solution content of  $B(\theta)=1$ .

At the risk of belaboring the point, two additional graphs will be examined. These graphs show how vapor transport reduces liquid convection. In Figures 6.10 and 6.11 the relative liquid volume flux

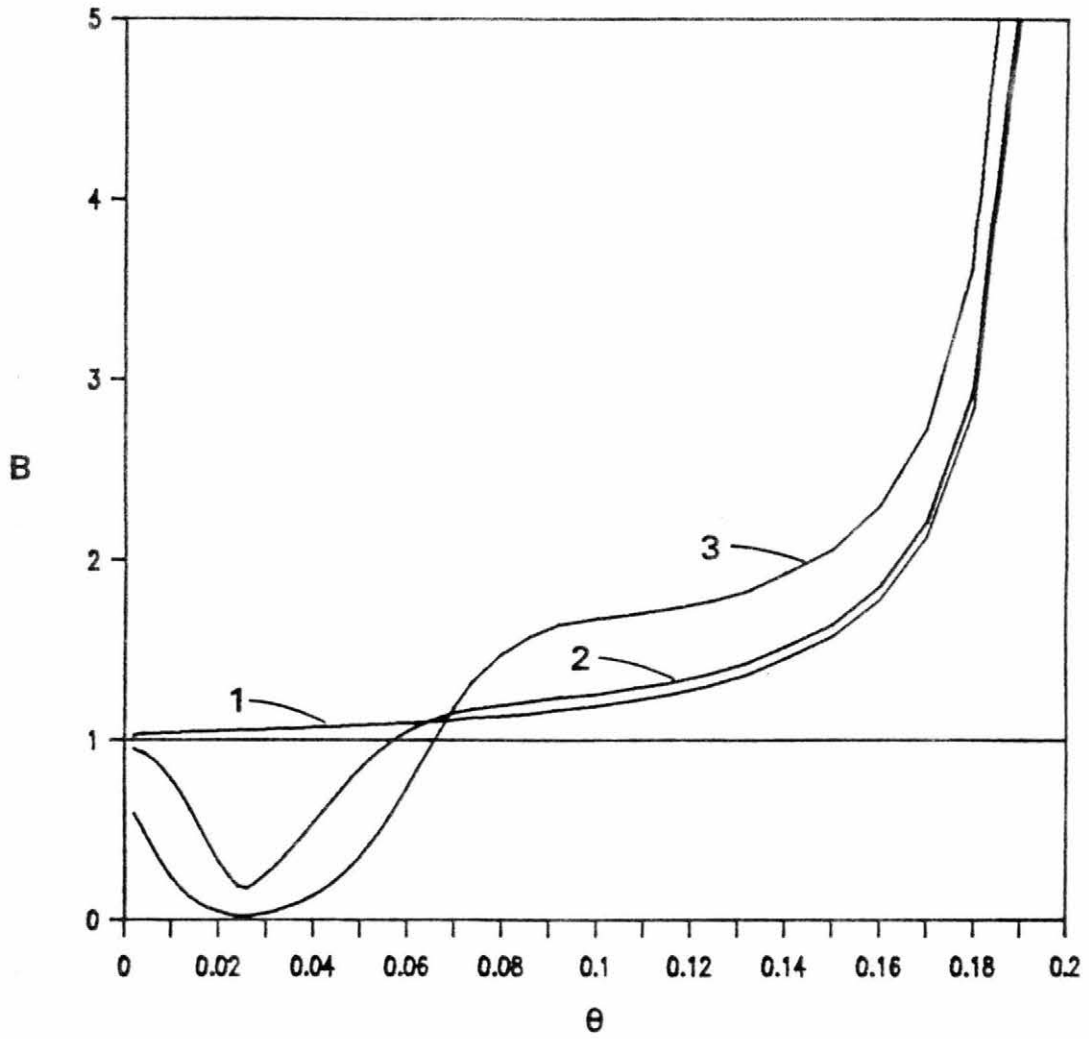


Figure 6.9. Velocity ratio,  $B$  versus  $\theta$  for cases 1, 2, and 3.

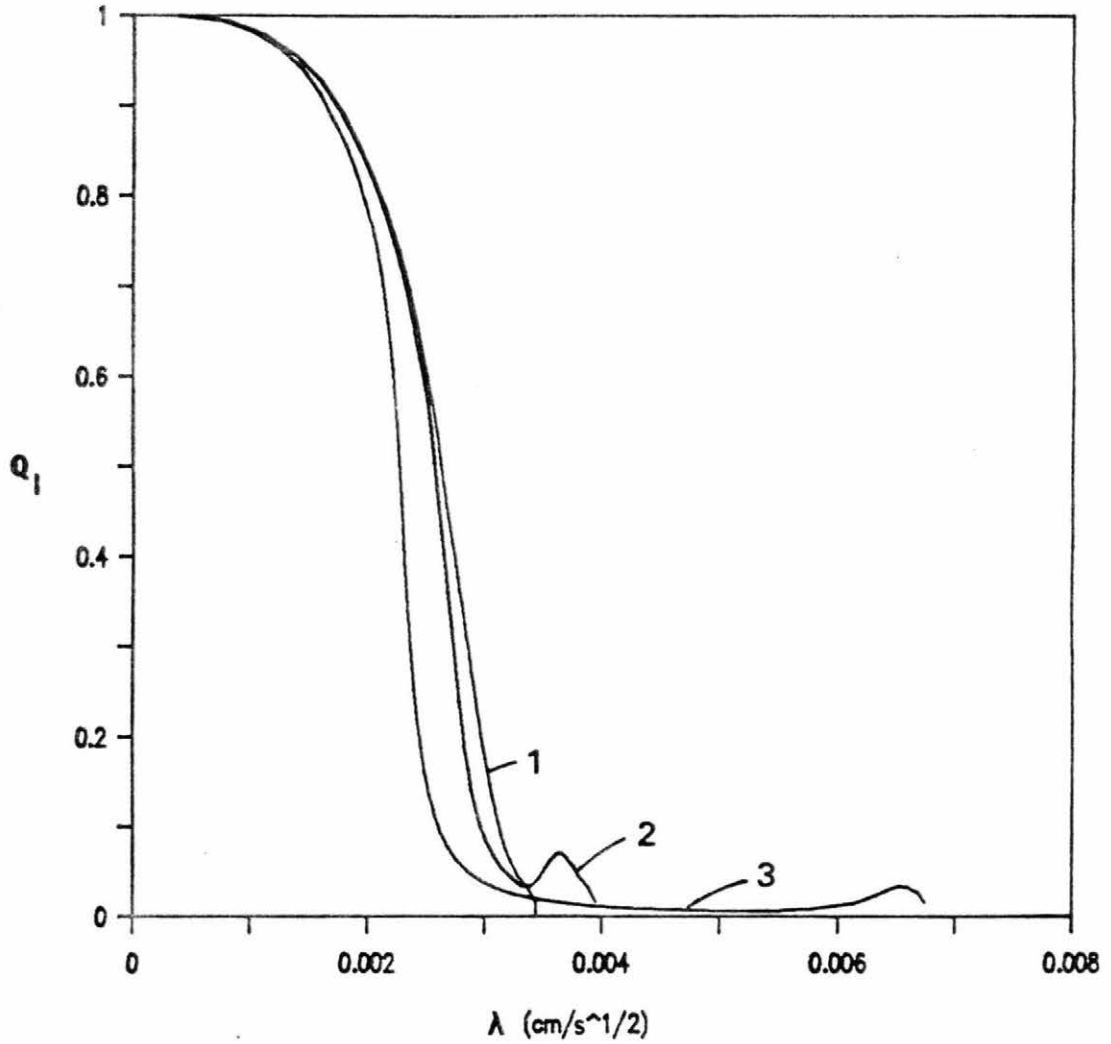


Figure 6.10. Relative liquid flux versus  $\lambda$ , for cases 1, 2, and 3.

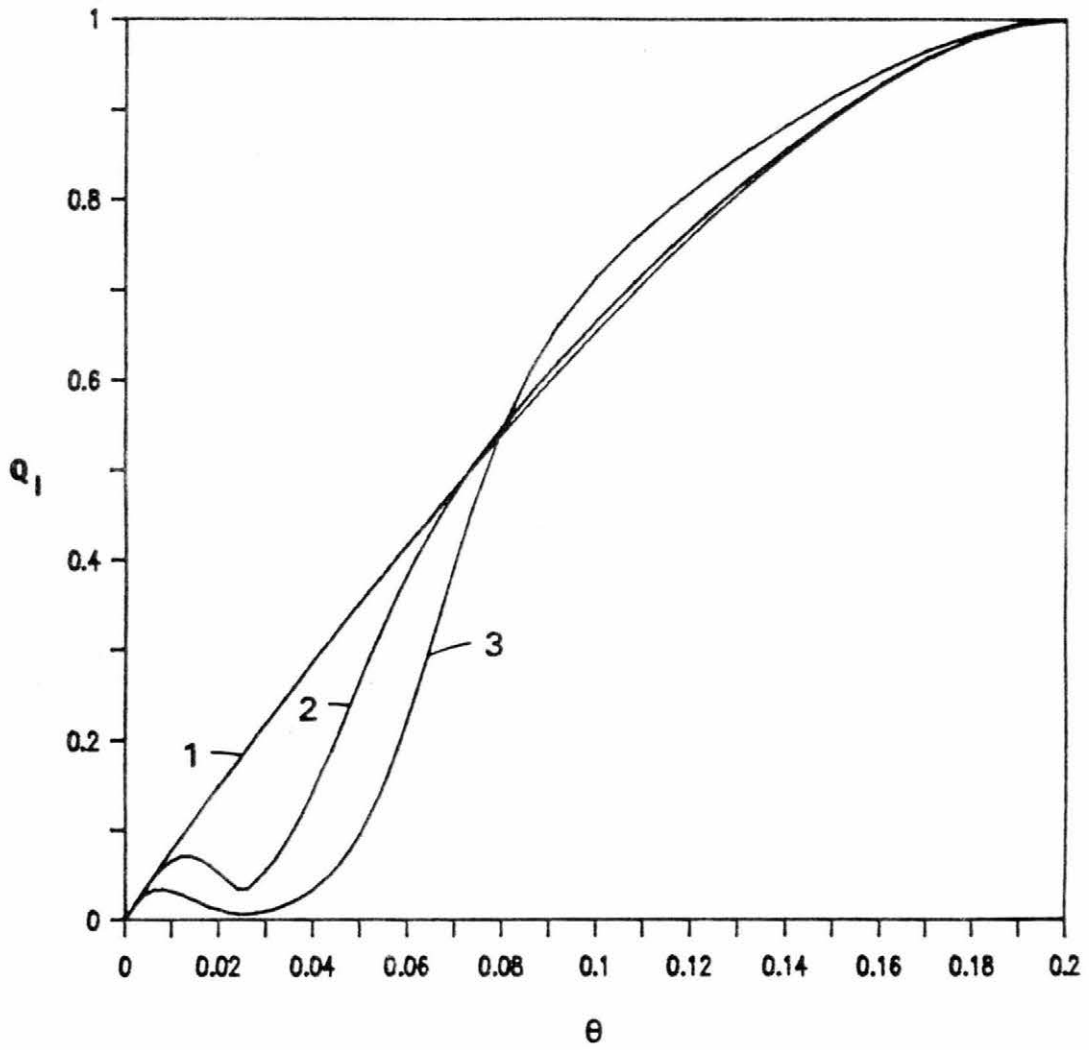


Figure 6.11. Relative liquid flux versus  $\theta$ , for cases 1, 2, and 3.

for each case is plotted versus  $\lambda$  and  $\theta$  respectively. The relative liquid flux,  $Q_1$  is defined as the ratio of the liquid water flux at a position to the total water flux at  $x=0$ , and is given by

$$Q_1 = q_1/q_{t0} = FD_1/D_t \quad (6.2)$$

Figure 6.10 shows that, with no vapor transport, the liquid volume flux drops uniformly from the inlet to the wetting front. As vapor transport increases,  $Q_1$  decreases rapidly at the lower liquid contents. This relation is shown clearly by Figure 6.11. Through the range  $0 < \theta < 0.05$ ,  $Q_1$  with normal vapor transport is an order of magnitude less than the case with no vapor transport. Thus even though both cases have the same value for liquid diffusivity, the ability to transport vapor at the lower liquid contents reduces the ability of the media to transport liquid.

Before leaving these three cases and proceeding to other questions it is worthwhile to emphasize one additional point. Examination of Figures 6.3 to 6.11 shows that the vapor effects in each are almost as strong for case 2 as for case 3. This occurs even though vapor diffusivity in case 2 is only one-tenth the value of case 3. This relation implies that the effects shown here are not significantly dependent on the actual value of vapor diffusion. Any case where vapor diffusion is nonzero will display the features seen here.

#### Gas Convection Effects

In Chapter 3 it was shown that vapor diffusion, phase transfer and gradients of liquid flow produce vapor phase convection. At that time, with only general knowledge of the flow system, it was impossible to

evaluate the magnitude of convective water vapor transport. Now that a specific flow condition has been defined, the gas convection can be quantified.

Solving Eq. (3.33) for the case with  $\theta_n=0$ ,  $\theta_o=0.20$  and normal vapor diffusivities will provide the gas phase convection. As before for this boundary, a normalized gas bulk flow,  $q'_g$  is defined as,  $q'_g = q_g/t^{1/2}$ . Figure 6.12 presents the normalized bulk flow. The bulk flow is negligible near the inlet of the column, increases with the start of evaporation and gradually decreases to a small value at the front. The maximum value is about 500 times the inlet liquid volumetric flux. This is consistent with the approximation made in Chapter 3.

While gas convection is large, it doesn't mean water vapor convection is significant. In Chapter 3 it was shown two conditions must be met for convective effects to be neglected. These conditions are

$$|C_v q_g / C_w q_l| \ll 1, \text{ and} \quad (3.48)$$

$$\left| q_t \frac{\partial}{\partial x} \left( \frac{C_v q_g}{C_w q_t} \right) / \frac{\partial}{\partial x} (q_t) \right| \quad (3.49)$$

These two ratios are plotted in Figures 6.13 and 6.14, respectively. The maximum of the first ratio is only 0.012 while the second has a maximum magnitude of about 0.06. It is concluded that both conditions are met. Figure 6.13 shows that the convection ratio is always positive which indicates an increase in the water transport, mostly in the nose. Figure 6.14 shows that the convection derivative is negative in the region of the solute front and positive in the nose, indicating

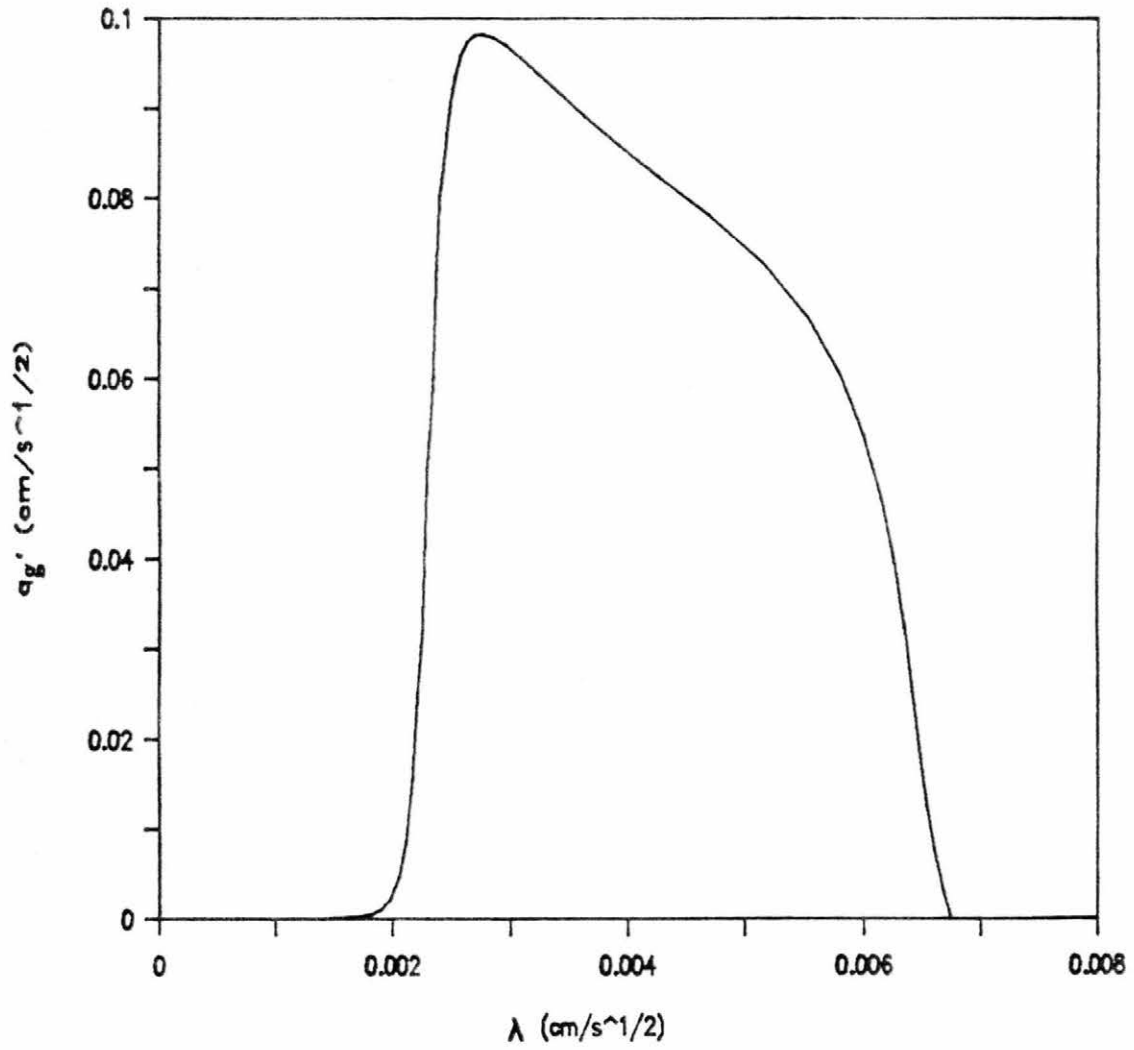


Figure 6.12. Gas convection for case 3.

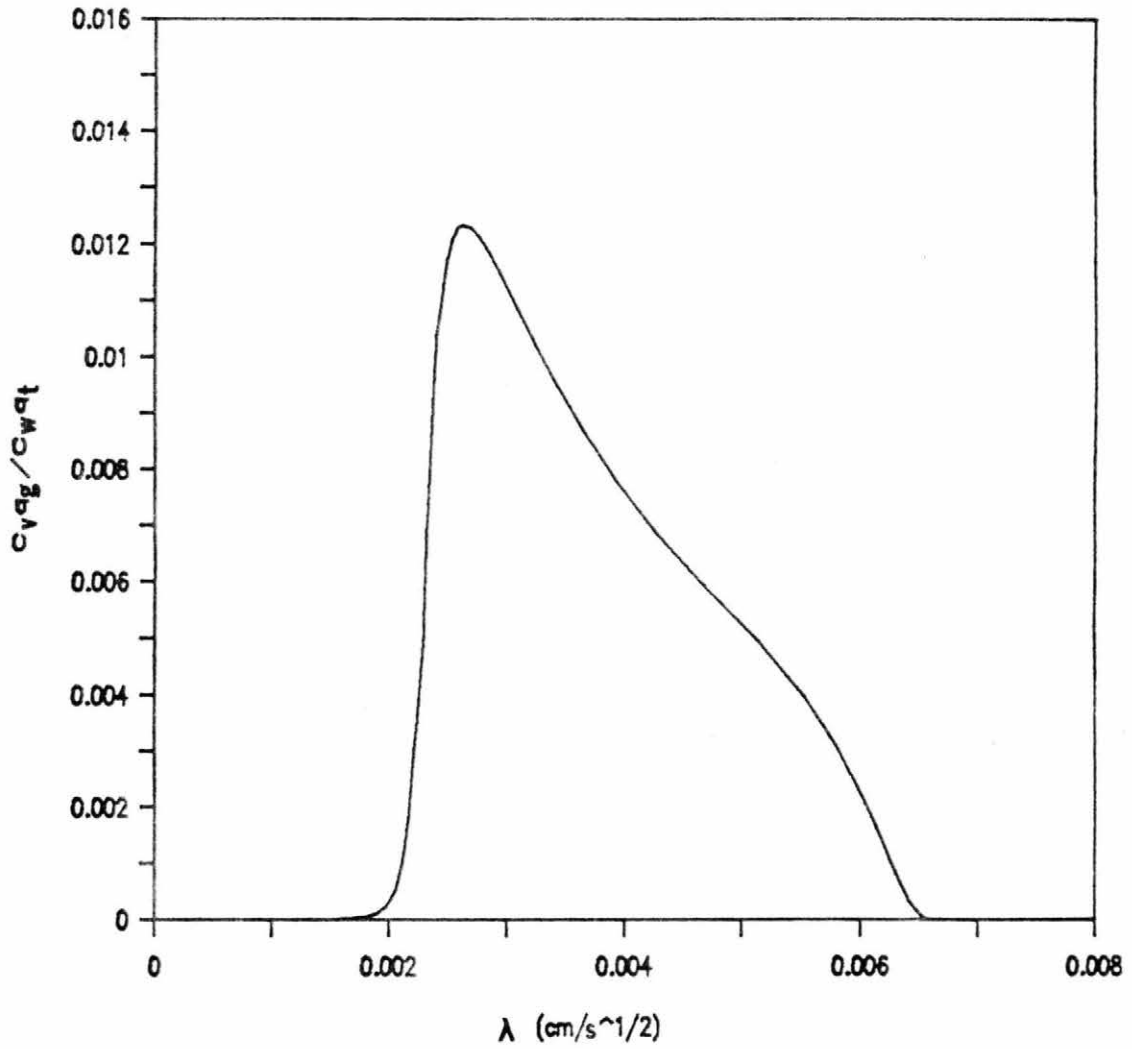


Figure 6.13. Gas convection ratio for case 3.

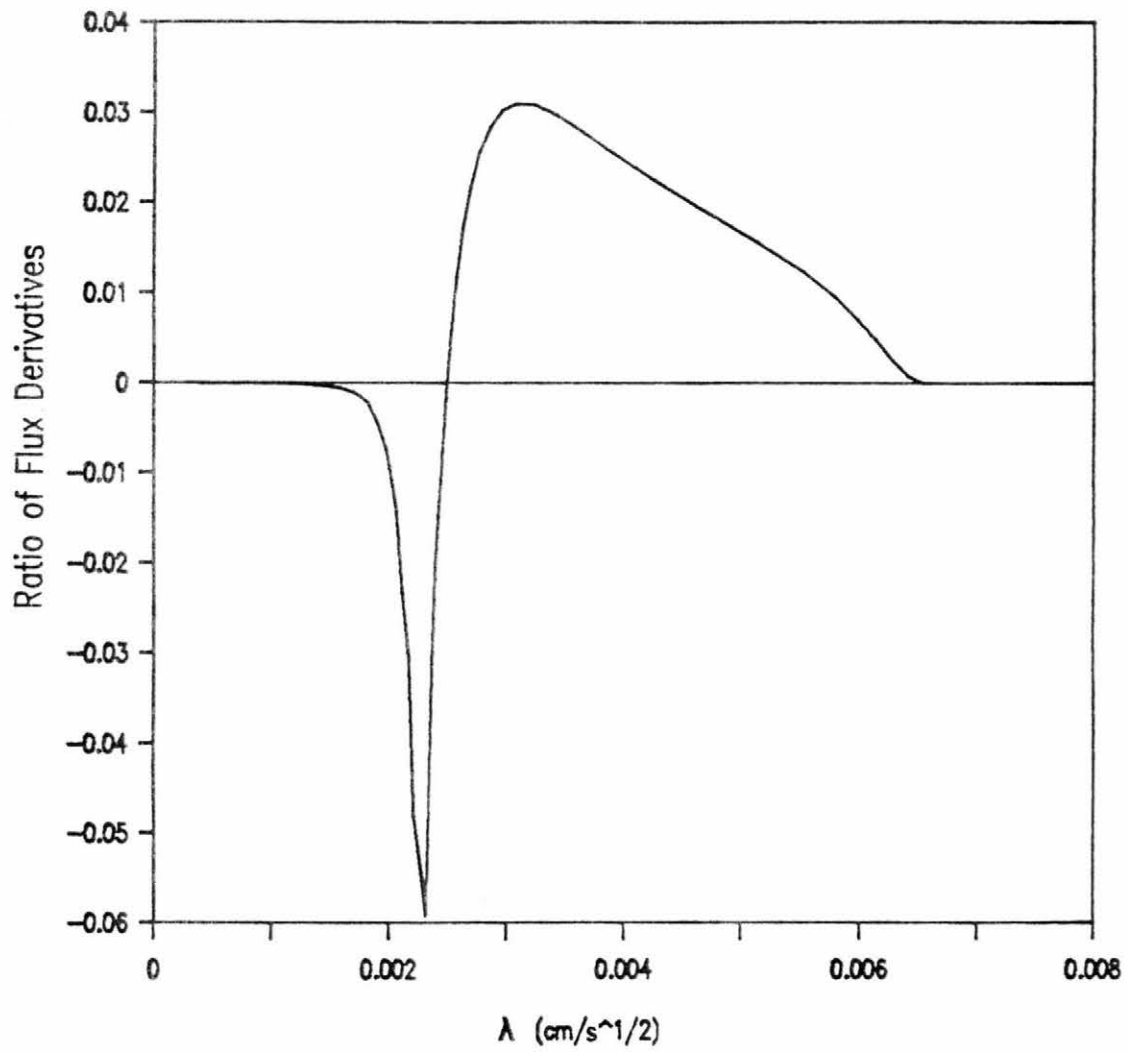


Figure 6.14. Gas convection derivative for case 3.

both an initial decrease and then an increase in water transport over the calculated rates.

#### Sorption with a Resident Solution

This section will examine the special case of constant liquid content sorption into a porous media with a small initial water content and a resident solute. This is the same problem examined by Smiles and Phillip (1979) and Smiles et al. (1978). Two special cases will be compared. The cases are;

4. No vapor transport with normal liquid diffusivity (Eq. (6.1c)), and
5. Normal vapor and liquid diffusivities (Eqs. (6.1a,b,c)).

The boundary and initial conditions used in both cases are  $\theta_n = 0.04$ , and  $\theta_o = 0.20$ . The same diffusivity functions as cases 1 and 3 will be used. Figure 6.2 shows that the initial liquid content occurs at a higher liquid content than the vapor diffusivity maximum.

F( $\theta$ ). As before the fractional flow function, F( $\theta$ ) can be computed and is presented in Figure 6.15. As in the previous cases, the F function with vapor transport lies above the liquid only case, but here the difference is smaller. The difference is small enough that it would be difficult to detect in experimental data.

Liquid Content Profiles. Figure 6.16 shows the computed liquid profiles. While the vapor case has a relatively long nose, the profiles above about 0.06 are almost identical. Indeed the sorptivity of the vapor case is only 2.1% greater. In a practical experimental sense, it would be hard to tell the two curves apart unless the initial solution content was known exactly.

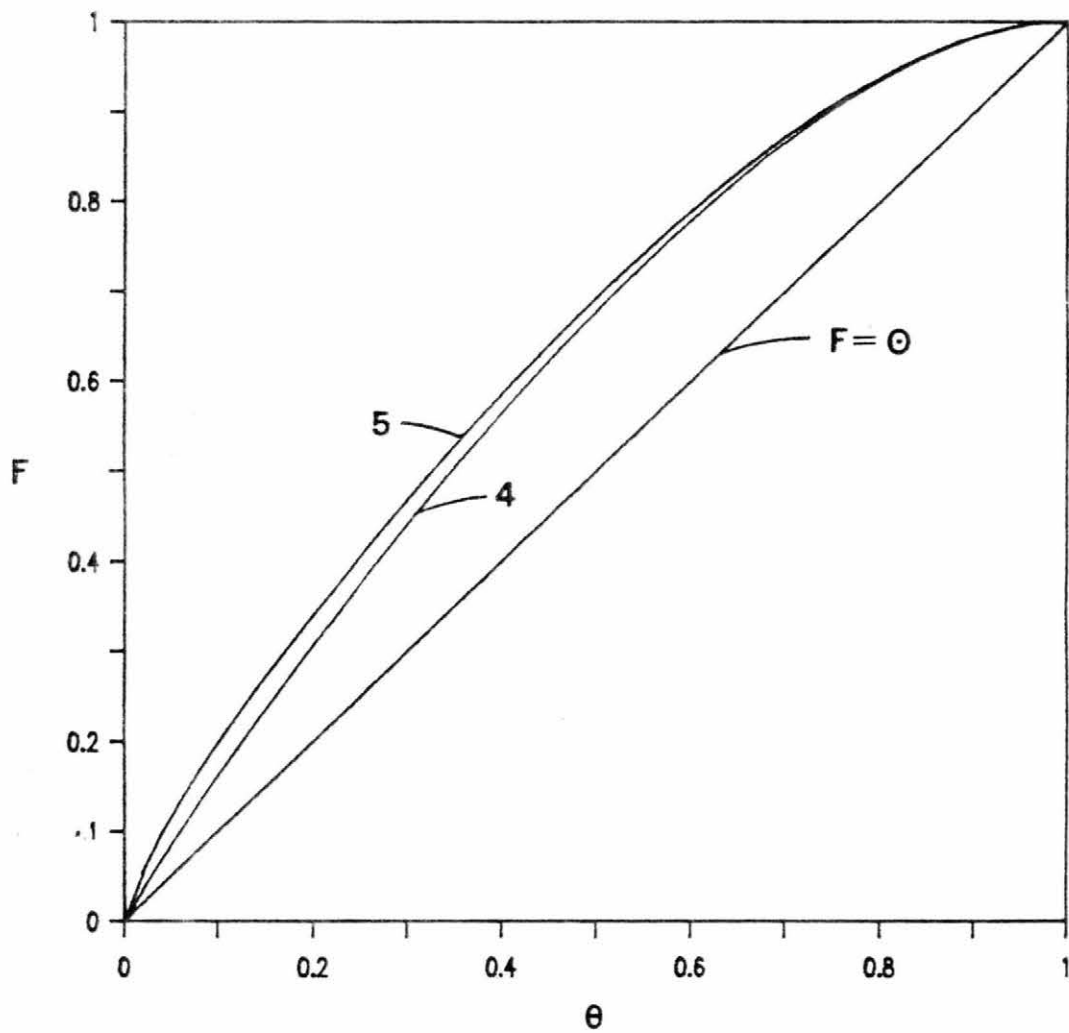


Figure 6.15. Fraction flow function for cases 4 and 5.

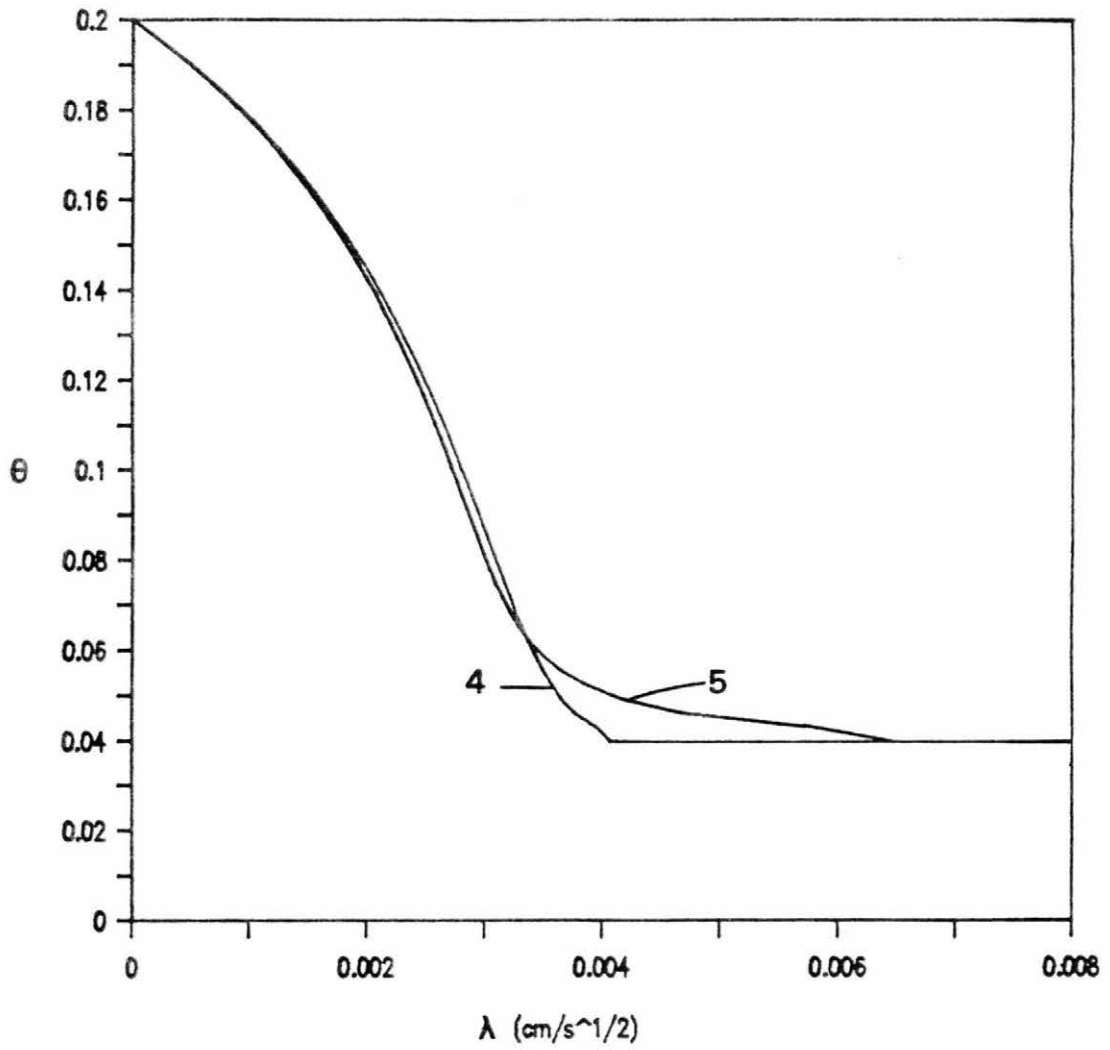


Figure 6.16. Liquid content profiles for cases 4 and 5.

Phase Transfer. Figure 6.17 presents the phase transfer versus  $\lambda$ , and Figure 6.18 the phase transfer versus  $\theta$ . Comparison of case 5 with case 3 in Figures 6.7 and 6.8 shows that the phase transfer has been reduced by an order of magnitude due to the small initial liquid content.

Fluxes and  $B(\theta)$ . The relative liquid flux,  $Q_1 = q_1/q_{t0}$  is plotted in Figure 6.19 and the relative seepage velocity,  $v'_s = v_s t^{1/2}$ , is plotted in Figure 6.20. Again in both of the graphs it is hard to distinguish the two curves, except for the long, thin nose. The velocity ratio  $B(\theta)$  is plotted in Figure 6.21. With initial solution present,  $B$  falls below 1.0 for both cases. For the no vapor case 4, the position of  $B=1$  corresponds to the well known Smiles and Phillip (1979) piston displacement front. With no dispersion all fluid ahead of the front will be the initial resident fluid, while the invading solution will be behind the front. With vapor transport, the position where  $B=1$  separates the invading and resident solute, but not the water. Vapor transport will mix the invading and resident solvent. As Figure 6.21 shows,  $B$  is quite similar for both cases.

Solute Transport. For these conditions the solute concentration profiles of both the resident and invading solute can be computed. Figure 6.22 presents the invading solute concentrations. The profiles for each case are almost identical. While a peak is present for the vapor case, it has a trivial height of about 1.09. Generally, the phase transfer is ahead of the  $B=1$  position, so there is little effect on the invading solute. Such is not the case for the resident solute.

Figure 6.23 shows the concentration profiles of the resident solute. As expected the no vapor case 4 shows a piston displacement with no change in the initial concentration. With vapor transport a

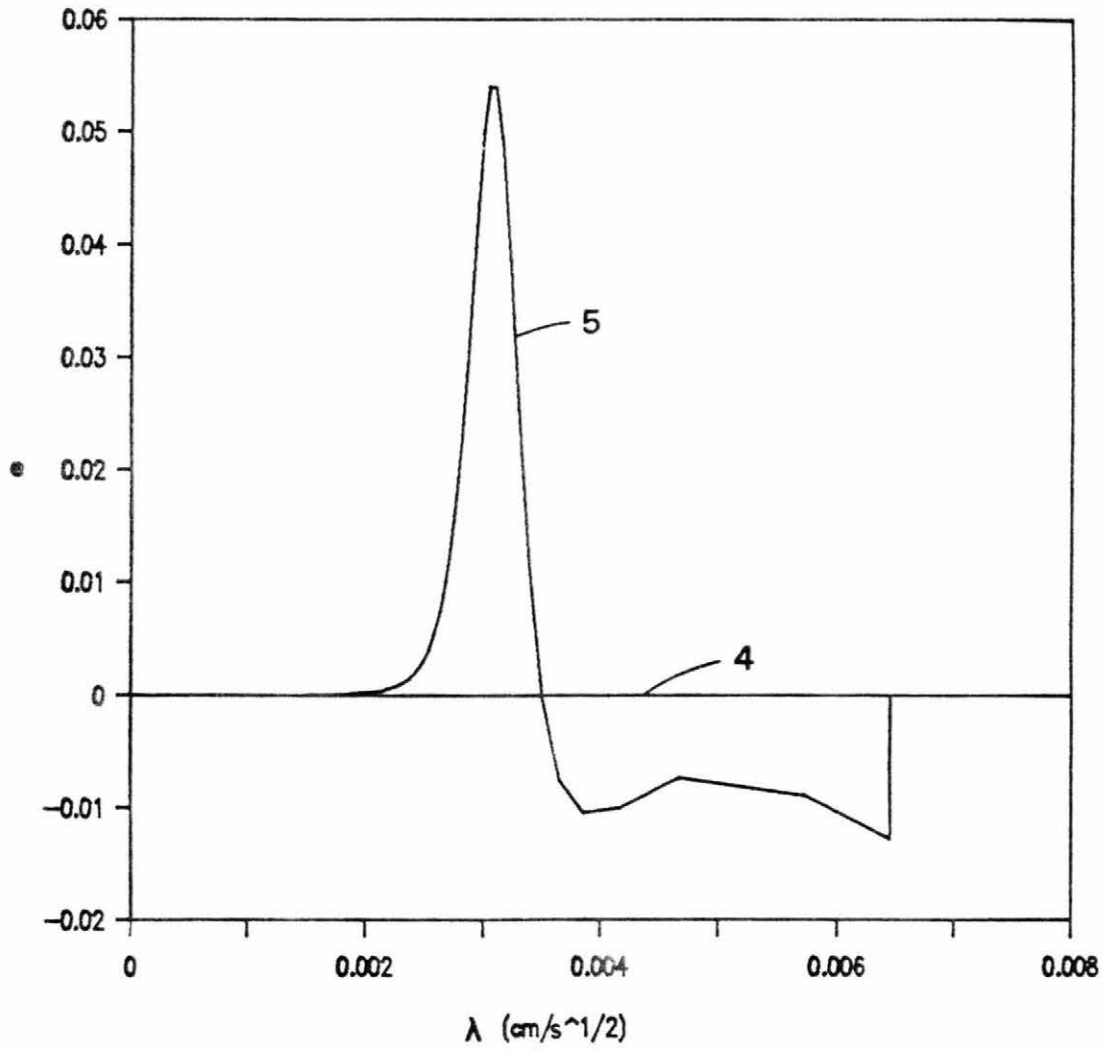


Figure 6.17. Water phase transfer versus  $\lambda$  for cases 4 and 5.

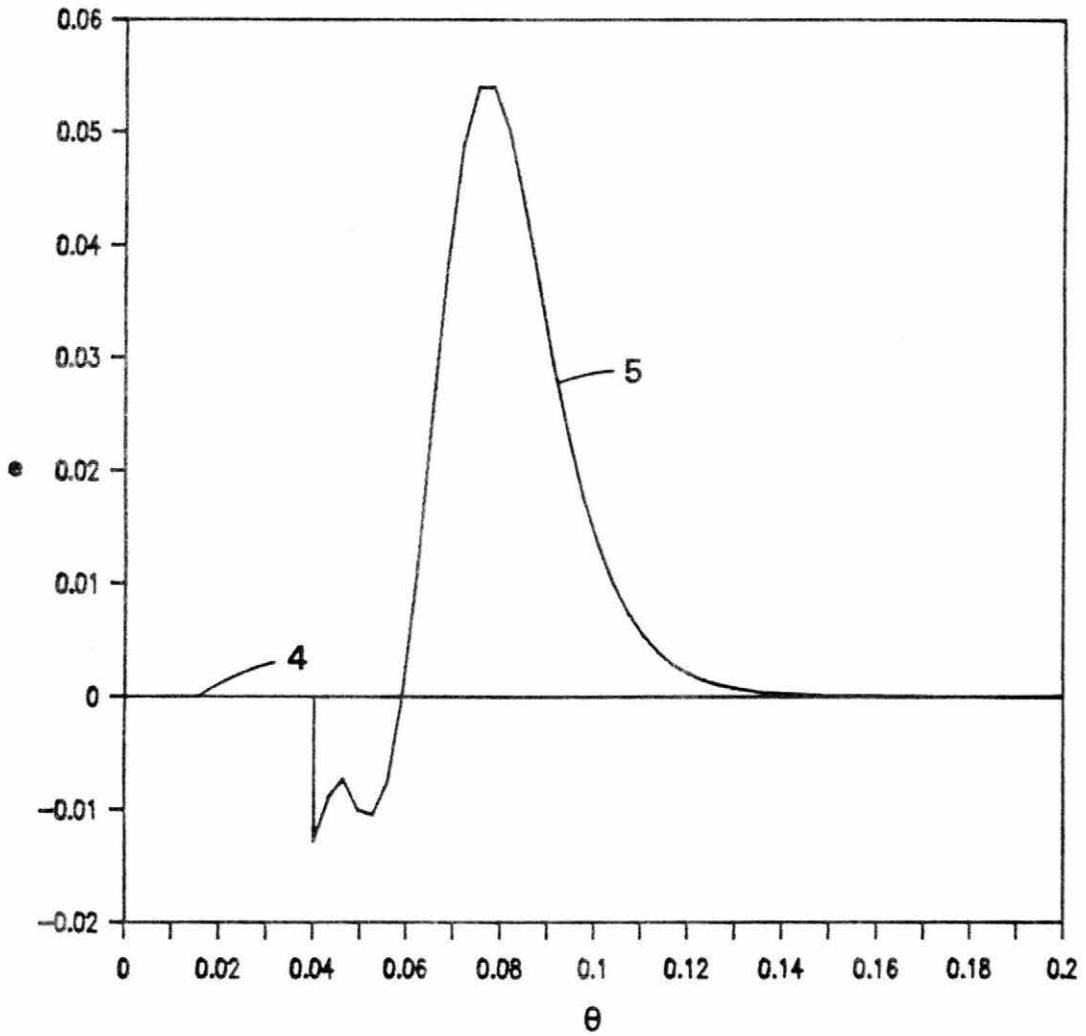


Figure 6.18 Water phase transfer versus  $\theta$  for cases 4 and 5.

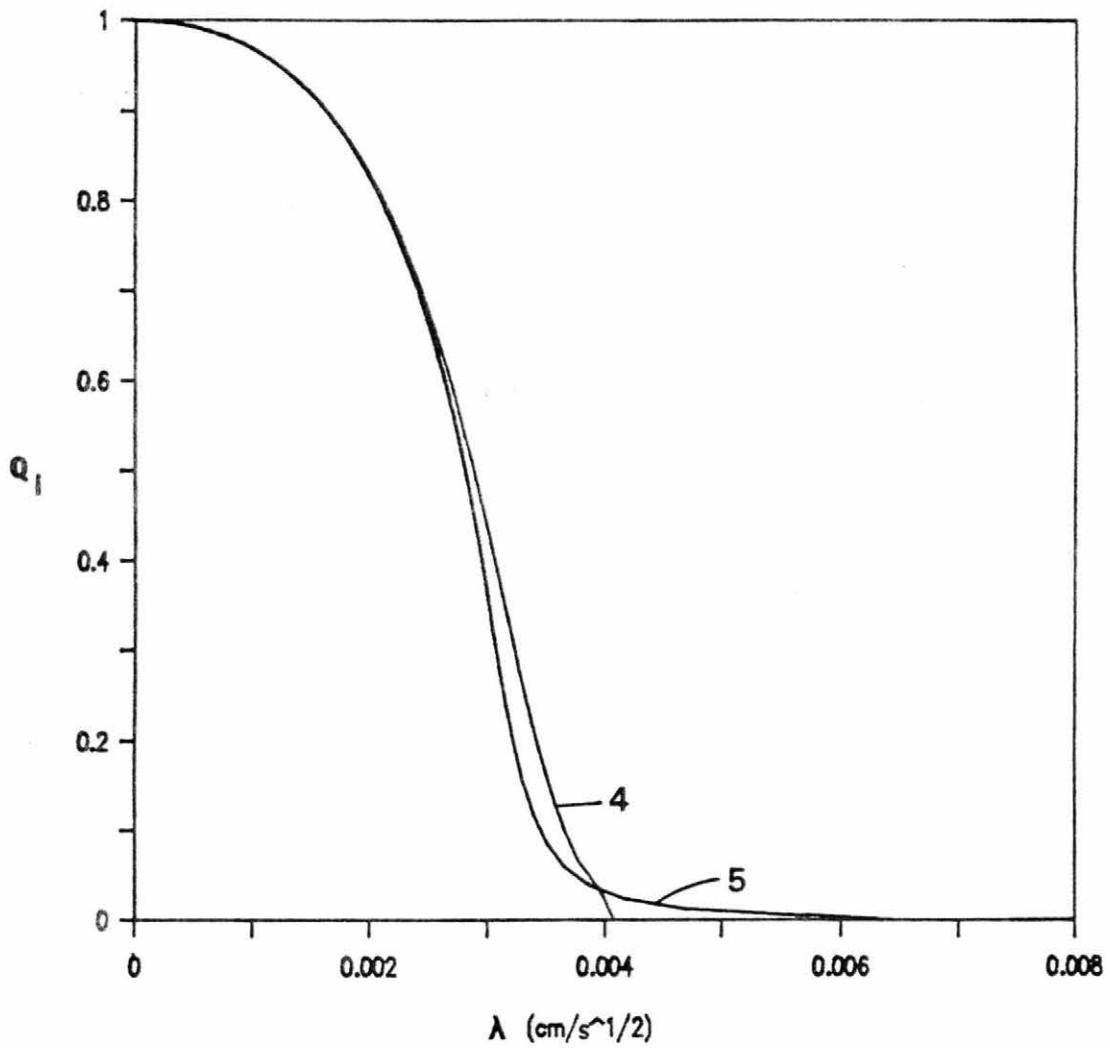


Figure 6.19. Relative liquid flux for cases 4 and 5.

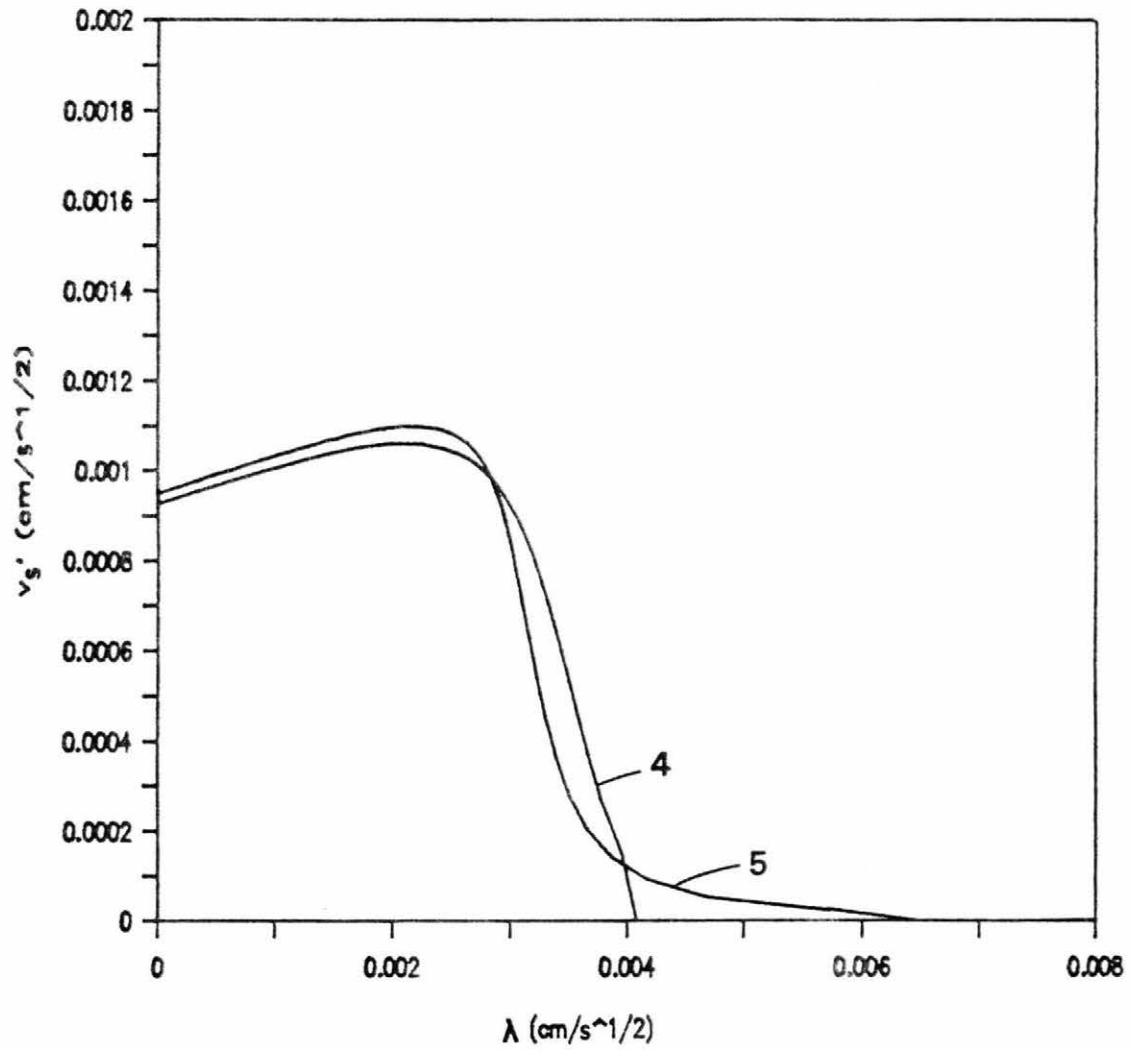


Figure 6.20. Seepage velocity for cases 4 and 5.

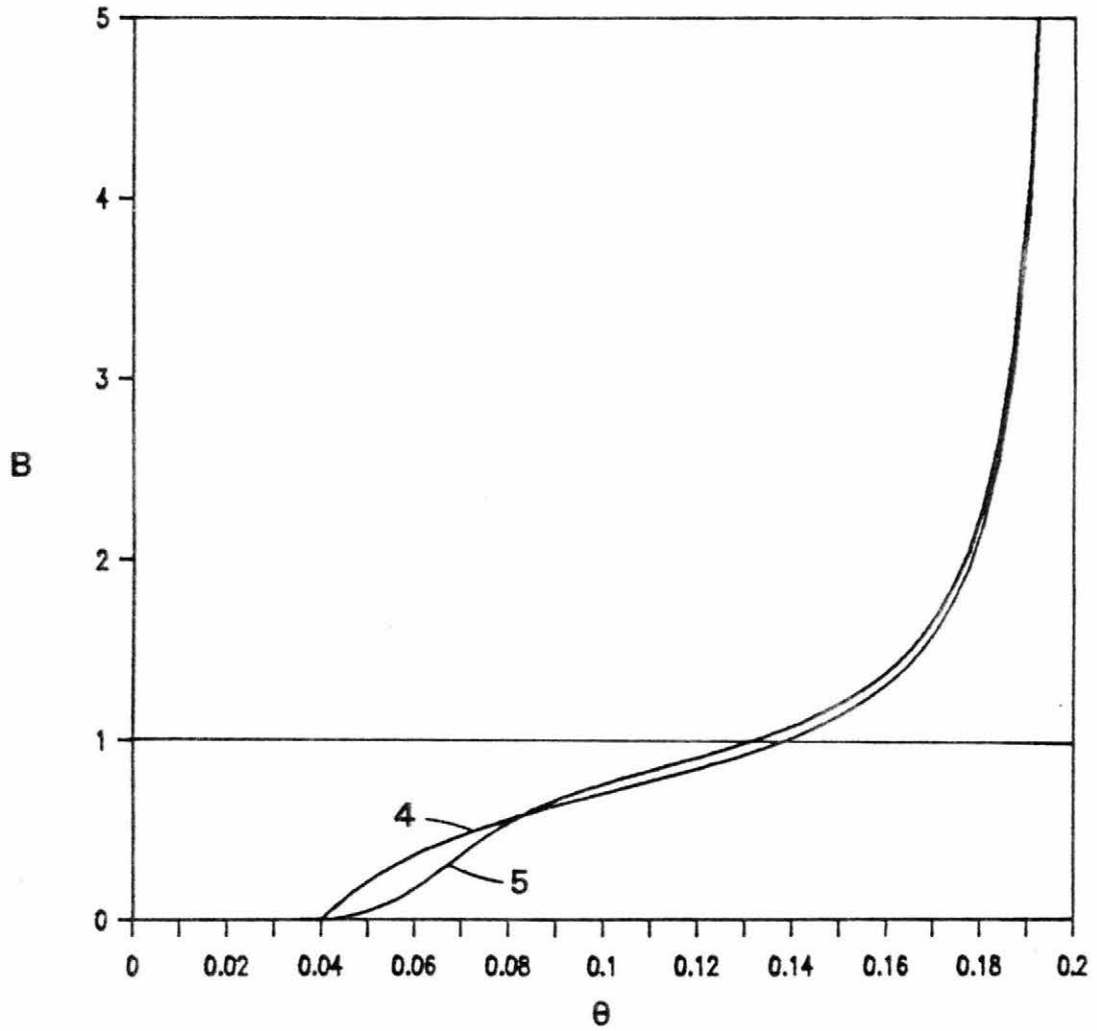


Figure 6.21. Velocity ratio  $B$ , for cases 4 and 5.

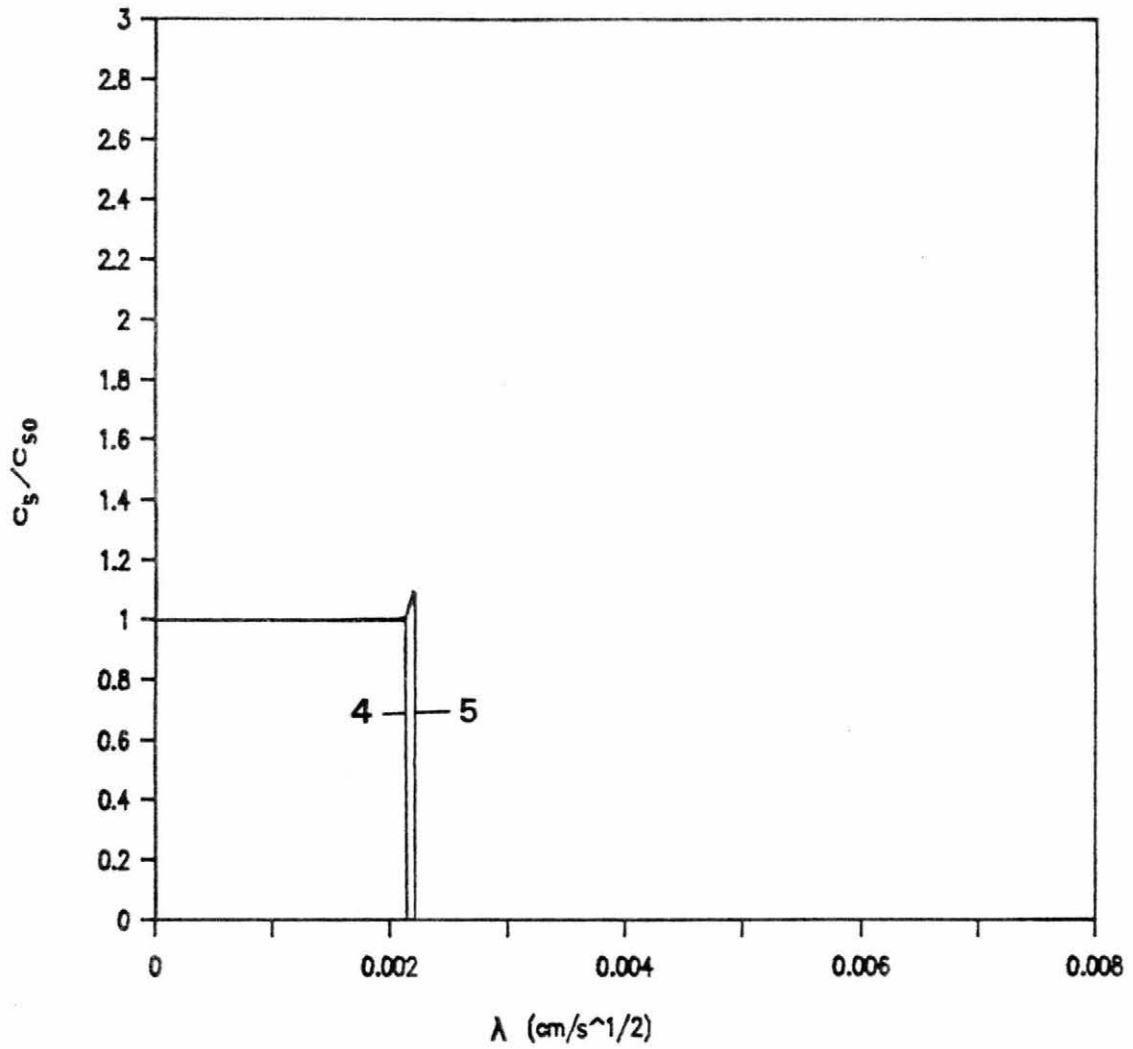


Figure 6.22. Invading solute concentration profiles for cases 4 and 5.

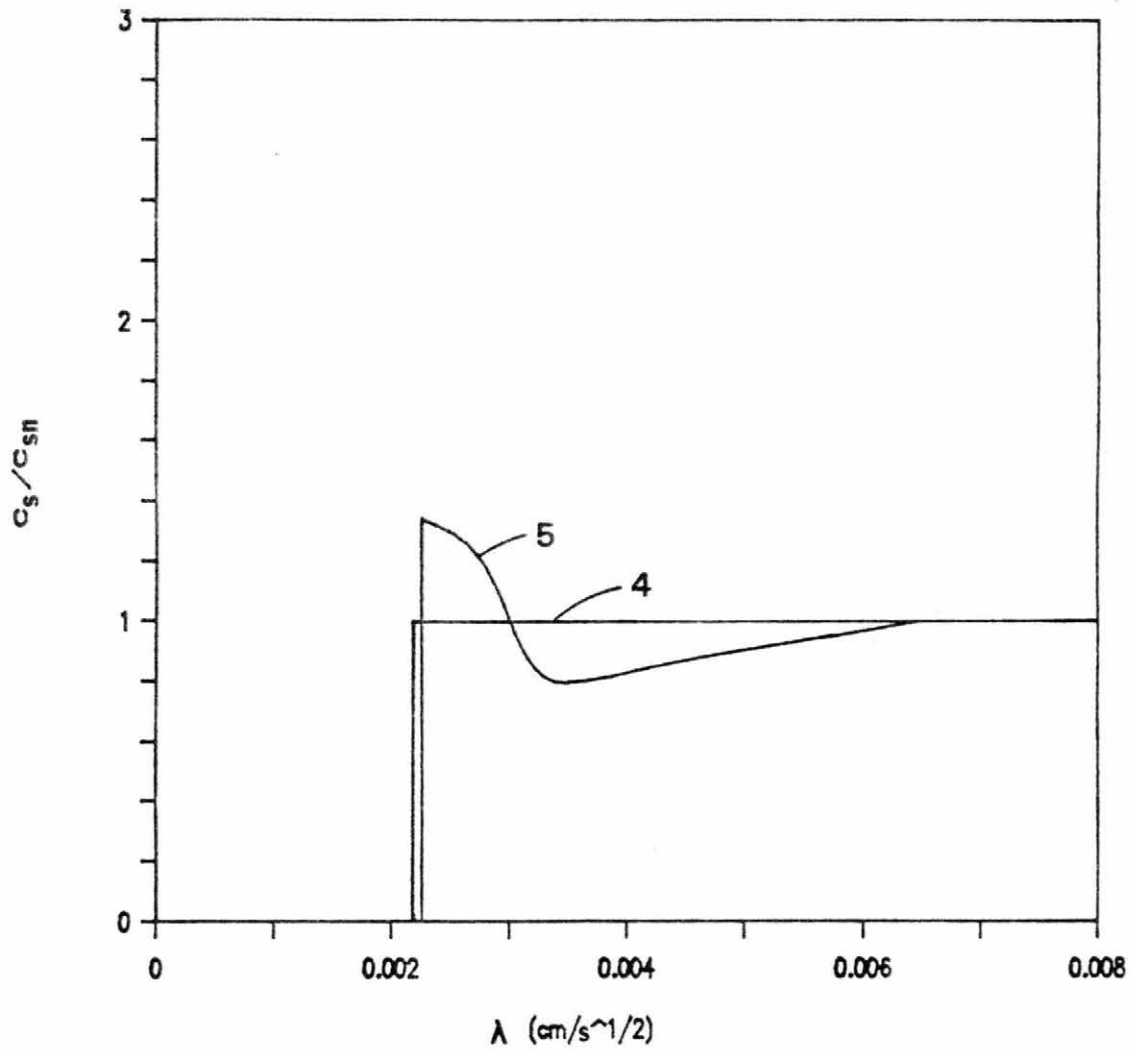


Figure 6.23. Resident solute concentration profiles for cases 4 and 5.

rather strange phenomenon occurs. Out in the nose the resident solute is diluted below the initial value, while near the  $B=1$  position the concentration increases to about 1.3 times the initial value and produces a plateau of elevated concentrations. The concentration profile is a function of both the phase transfer and the convection. The dominant process at the tip of the nose is condensation, thus the initial solute is diluted. Back closer to the solute front, water is evaporating and the resident solute is being concentrated. While phase transfer accounts for much of the concentration, the variation in convection is also playing a part. Comparing the evaporation in Figures 6.19 and 6.23 show that there is not a one to one correspondence between the phase transfer and the concentration. In some evaporating regions the concentration is reduced, and in others concentration is increased. Also notice that with the small initial solution, the vapor transport actually advances the solute front farther into the column. This effect is due to the slight increase in seepage velocity (as shown in Figure 6.20), behind the front.

The elevated concentration of a resident solute is exactly what was reported by Smiles et al (1979). As detailed in Chapter 2 and presented in Figure 2.2, during their experiments, a resident solution was displaced with a constant content boundary. They found elevated concentrations of resident solute ahead of the supposed piston displacement front, (around  $\lambda=1.6 \text{ m/s}^{1/2}$ ). Examination of their data could not explain the results. This analysis explains their difficulty. With the low initial liquid content, the vapor transport of water has only minor effect on the liquid content profile. They could have easily overlooked the vapor nose. Their effect "related to the movement of water" must certainly have been the result of vapor

transport. They did not report the dilution predicted here for the tip of the vapor nose. It is probable that because of its distance from the piston displacement front that they didn't take the data, or that their columns were not long enough.

#### CONSTANT INLET FLUX SORPTION

The constant flux boundary condition (Eq. 4.42), will be examined for two cases. The cases are;

6. Constant flux sorption into a dry material, and
7. Constant flux sorption into a material with a low initial liquid content.

#### Assumed $F(\theta)$

As explained in Chapter 4, the constant flux solution obtained here is only an approximation for the transient flow. A  $F(\theta)$  will be assumed. This assumption is not strictly correct. Examination of the basic equations show that  $F=F(\theta,t)$ , but no method is known to calculate  $F$  as in the constant liquid content boundary condition. It then becomes questionable why a fractional flow formulation should be used. The justification comes in two parts. First, the only alternative is a full numerical simulation of the flow equation, which will have its own assumptions and limitations. Boulrier et al. (1984) have shown that the fractional flow solution even though it is approximate, is as good as numerical solutions in predicting transient, one dimensional flow. It is unjustifiable to use a much more complex numerical model. Second, the fractional flow solution allows an semi-analytical calculation of the phase transfer and seepage velocity, as opposed to finite difference calculations based on the computed liquid profile. These

two points provide ample justification for using a fractional flow solution.

The question of what  $F(\theta)$  to assume can be answered quite readily. Following White (1979), a time averaged  $F(\theta)$  can be calculated from the experimental data using

$$F = \frac{\int_{\theta}^{\theta} x \, d\theta}{\int_{\theta}^{\theta} x \, d\theta} \quad (6.3)$$

Equation 6.3 follows from integrating the equation of motion Eq. (4.6), with respect to  $\theta$ , applying Leibnitz's rule, and integrating with respect to time. The measured  $F$  functions from the two Lurgi runs are presented in Figure 6.24. Also plotted on the graph is the calculated  $F(\theta)$  for case 3 and the relation  $F=\theta$ . As White found, the measured  $F$  for the constant flux boundary is closely approximated by the constant content boundary  $F$  function. It is concluded that a  $F$  relation computed constant for the content boundary will be an accurate approximation for the constant flux boundary condition.

#### Sorption into a Dry Material

Case 6 will examine the constant flux sorption of solution into an initially dry column. The normal diffusivity functions (Eq. (6.1)), for Lurgi retorted oil shale will be used. This is the same condition examined experimentally in Chapter 5.

Liquid Content Profiles. Using Eq. (4.47) the liquid content profiles for inlet liquid contents varying from 0 to 0.3 were calculated and plotted Figure 6.25. The profiles have the expected

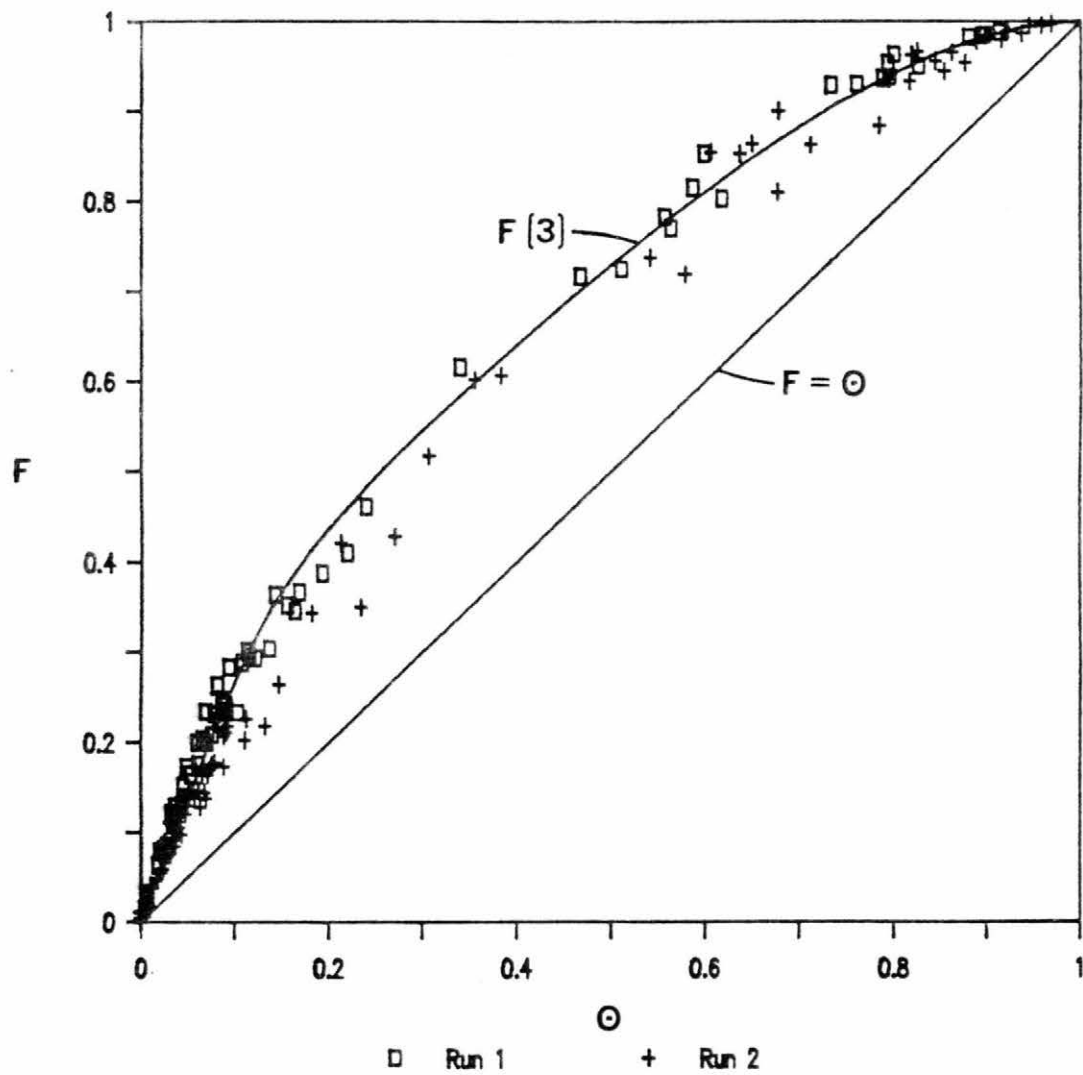


Figure 6.24. Measured constant flux fractional flow functions.

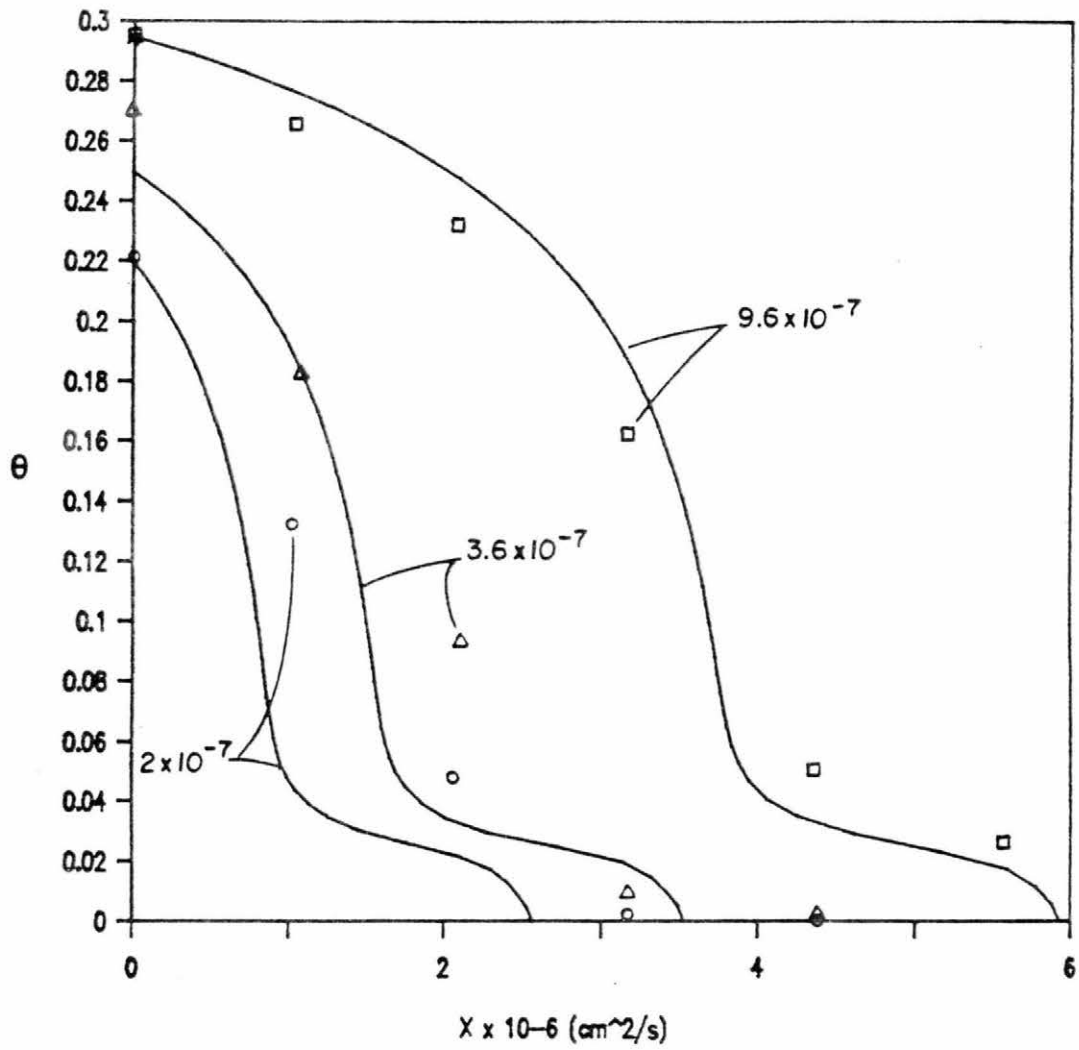


Figure 6.25. Liquid content profiles for case 6.

shape. Also plotted in Figure 6.25 are measured liquid content profiles for the corresponding times. There is a general agreement between measured and calculated profiles. The match between measured and computed profile improves with time.

In Figure 6.26 the calculated time to a given inlet liquid content is plotted along with the measured data. Again there is a general agreement. The differences between the calculated and measured data can be attributed to the noisy nature of the data. Remember these are relatively low solution contents and small measurement errors produce large differences.

Seepage Velocity. The seepage velocity corresponding to the profiles in Figure 6.25 are plotted in Figure 6.27. In this case the seepage velocity reduces with time and also experiences a steep decrease in the nose.

Phase Transfer. The transformed phase transfer  $e'$ , is plotted in Figure 6.28. The phase transfer at early times is all condensation, which indicates a significant fraction of the water mass inflow is vapor. At latter times, the phase transfer takes on the characteristic shape seen in case 3. Like the seepage velocity, the magnitude of the phase transfer reduces with time.

Solute Transport. The solute transport was calculated as described in Chapter 4, using 30 particles and 30 time periods. The solute concentration profile is plotted in Figure 6.29. As expected, the solute is retarded with respect to the water, and develops a sharp maximum at an intermediate liquid content. The liquid content of the solute flux is not a constant, but increases with time. Figure 6.30 shows this relation. The solute front liquid content increases rapidly at early times, and then stabilizes between 0.07 and 0.08. This value

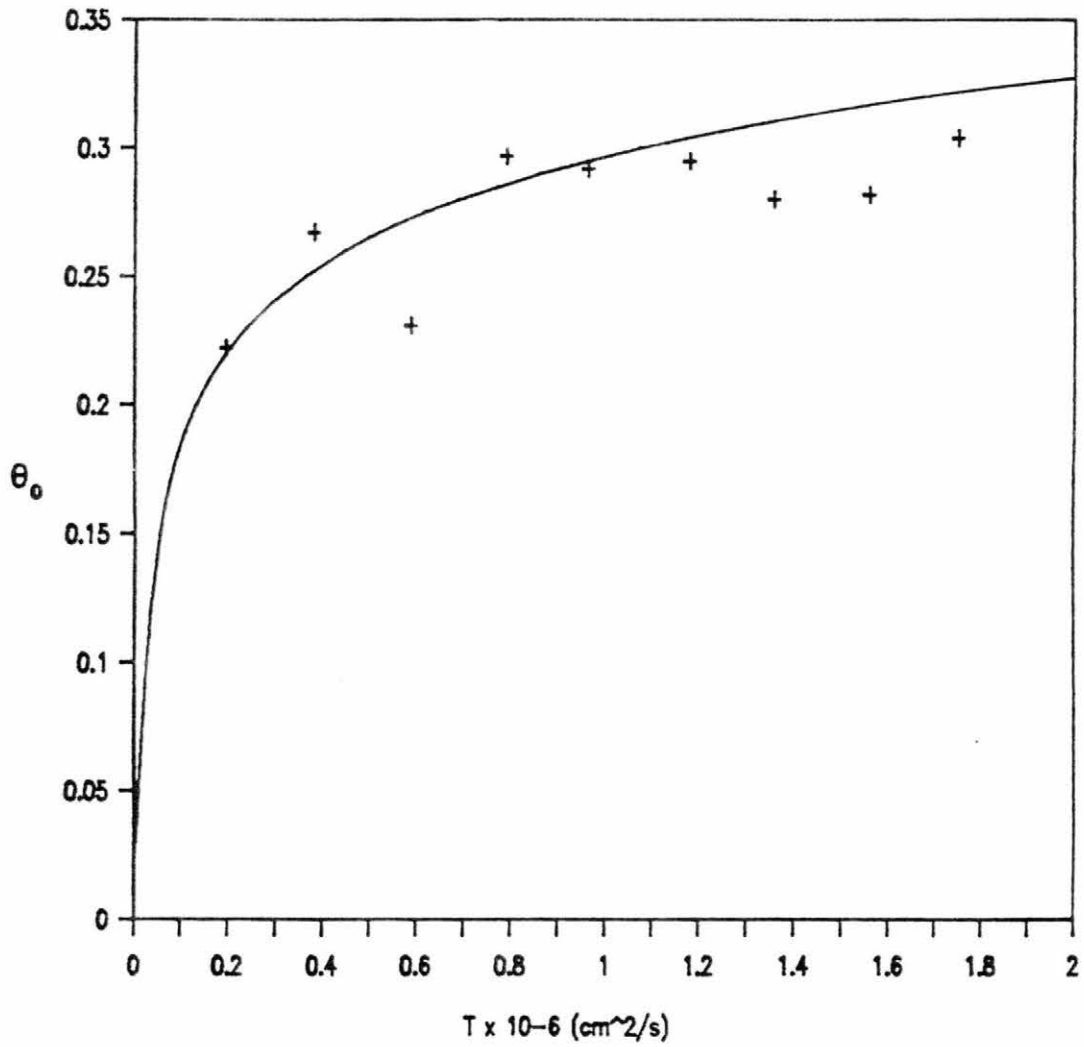


Figure 6.26. Time to inlet liquid content for case 6.

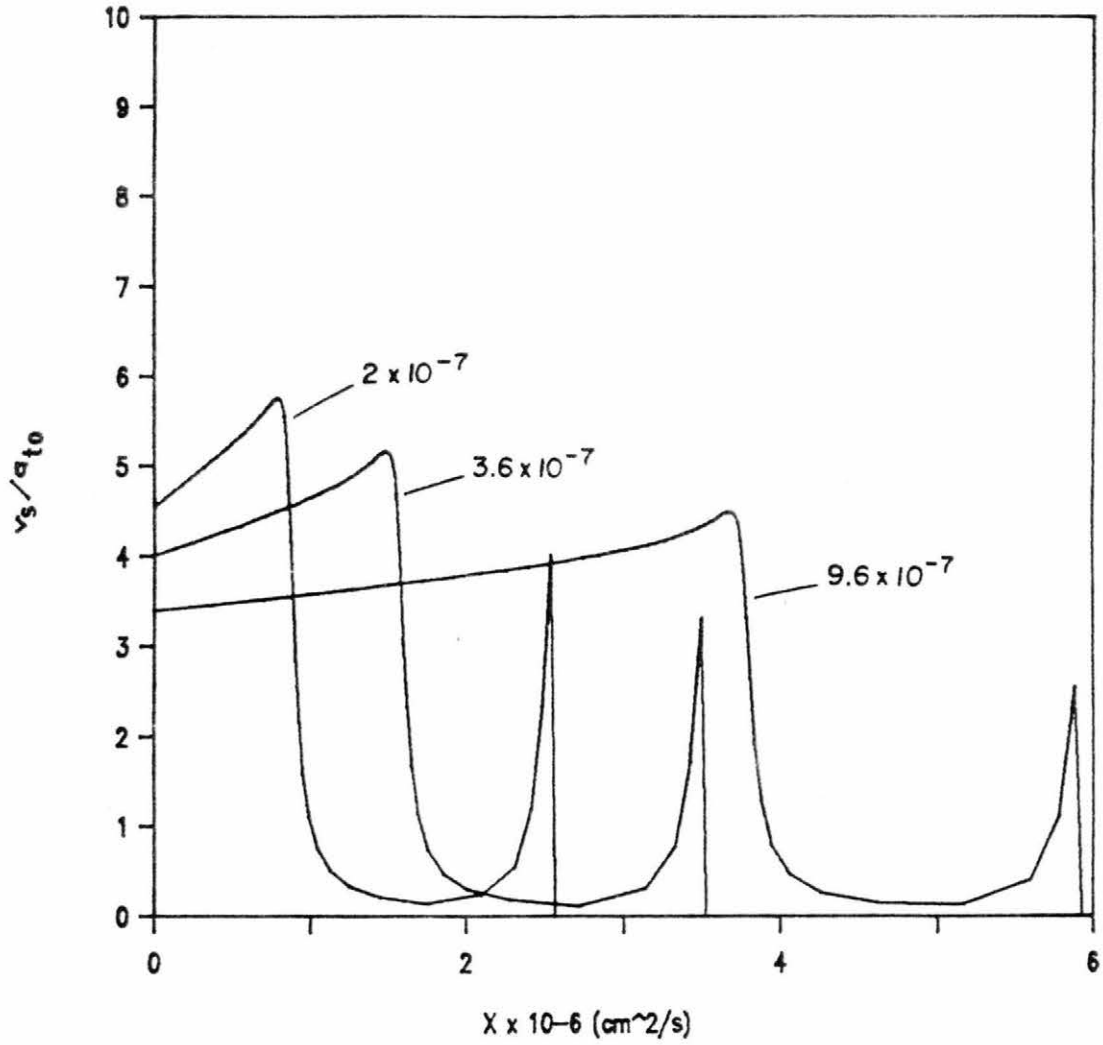


Figure 6.27. Seepage velocity for case 6.

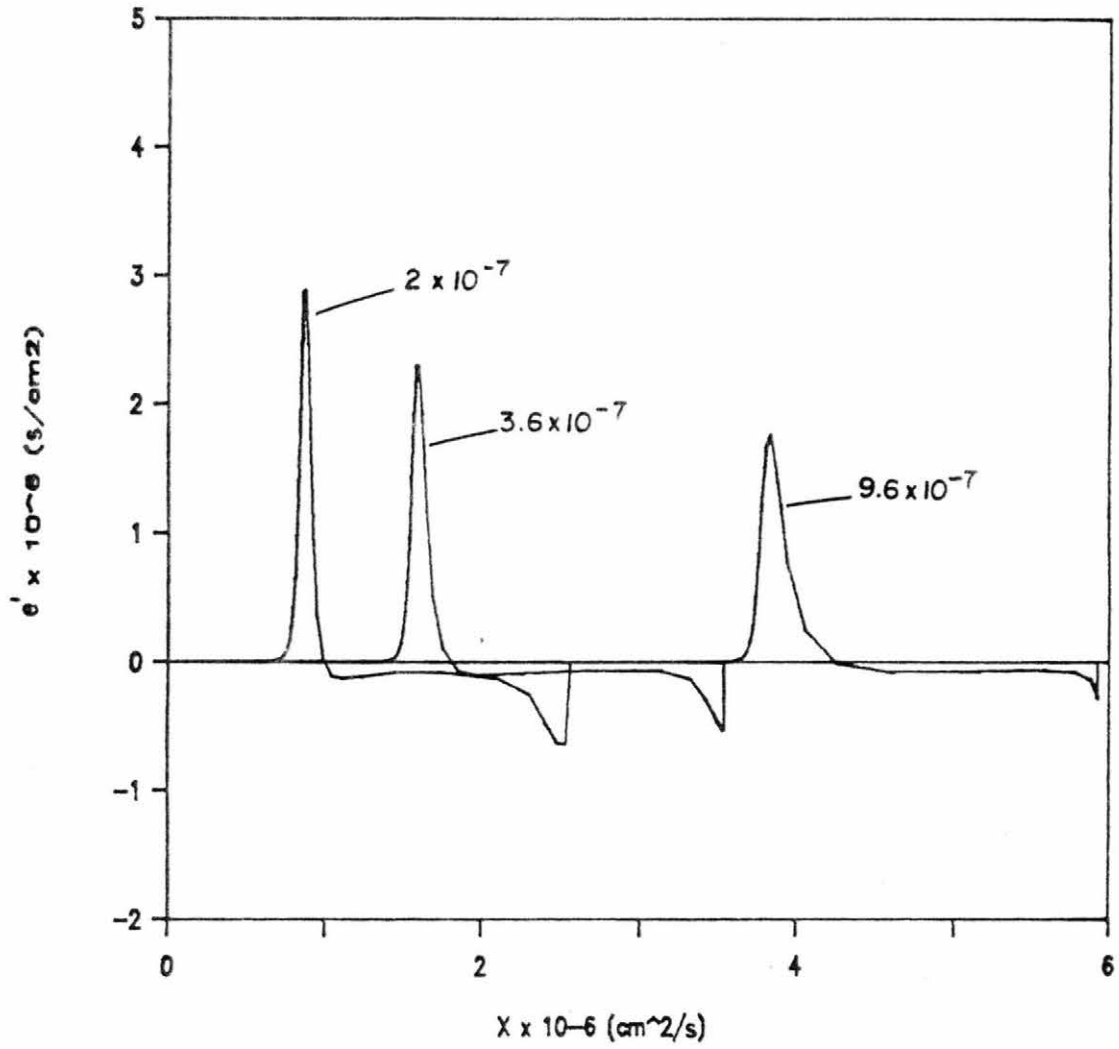


Figure 6.28. Phase transfer for case 6.

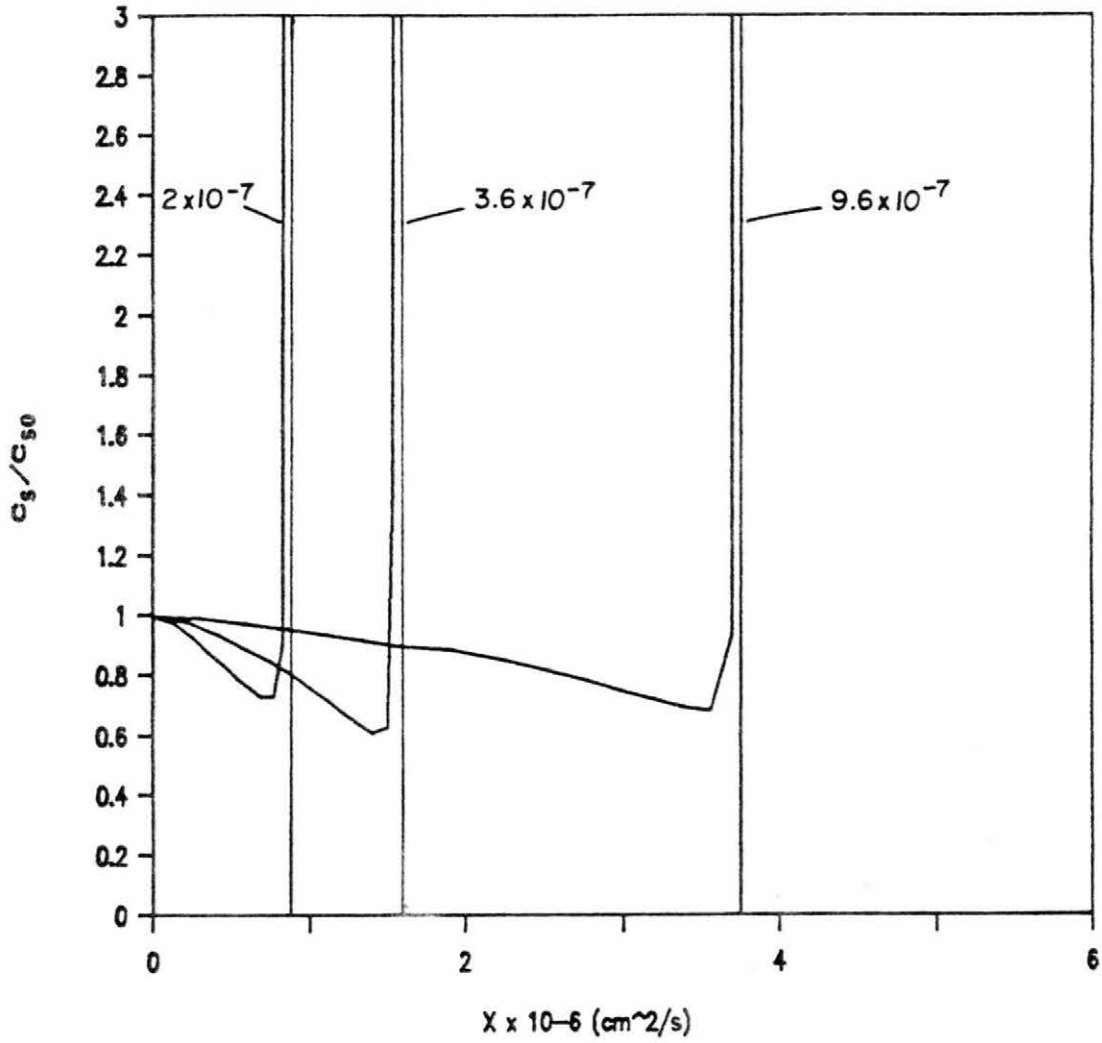


Figure 6.29. Solute Concentration for case 6.

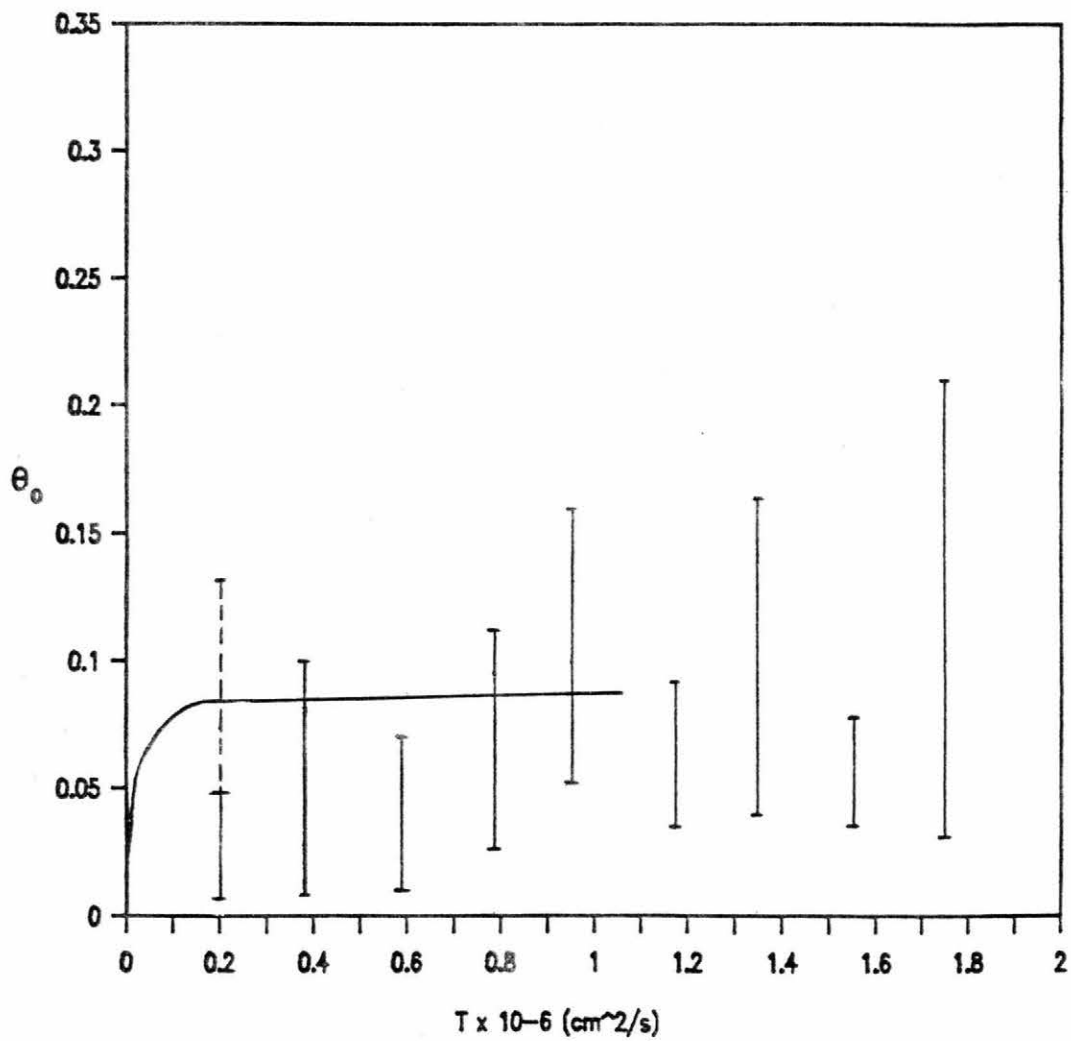


Figure 6.30. Liquid content at the solute front in case 6.

is consistent with the experimental observations as show in Figures 5.12 and 5.13.

#### Sorption with a Resident Solution

The last case will examine constant flux sorption into a media with a low initial liquid content. The normal diffusivity functions (Eq. (6.1)), for Lurgi retorted oil shale will be used. The fraction flow function calculated for case 5 will be used here.

Liquid content Profile. The liquid content profiles are presented in Figure 6.31. The vapor nose is present, but greatly reduced from case 6. The profiles have a shape similar to the profiles reported by Grismer, as shown in Figure 2.5. The calculated time to varying inlet contents is plotted in Figure 6.32. This graph is similar, but plots slightly above case 6.

Seepage Velocity. The seepage velocity for case 7 is shown in Figure 6.33. Due to the initial liquid content, the seepage velocity tends to drop rapidly in in the nose.

Phase Transfer. Figure 6.34 presents the phase transfer for case 7. Comparing this graph to Figure 6.28 shows that the initial solution tends to reduce the maximums of evaporation and condensation and lengthens the region where condensation occurs. This is similar to the difference between cases 3 and 5.

Solute Transport. Figure 6.35 plots the invading solute concentration for case 7. Comparing this figure with the liquid content profiles (Figure 6.31) shows that the invading solute is retarded in the profile, but not concentrated. This is exactly what was observed by Grismer, and shown in Figure 2.5. The slight amount of initial liquid prevents the concentration of the invading solute.

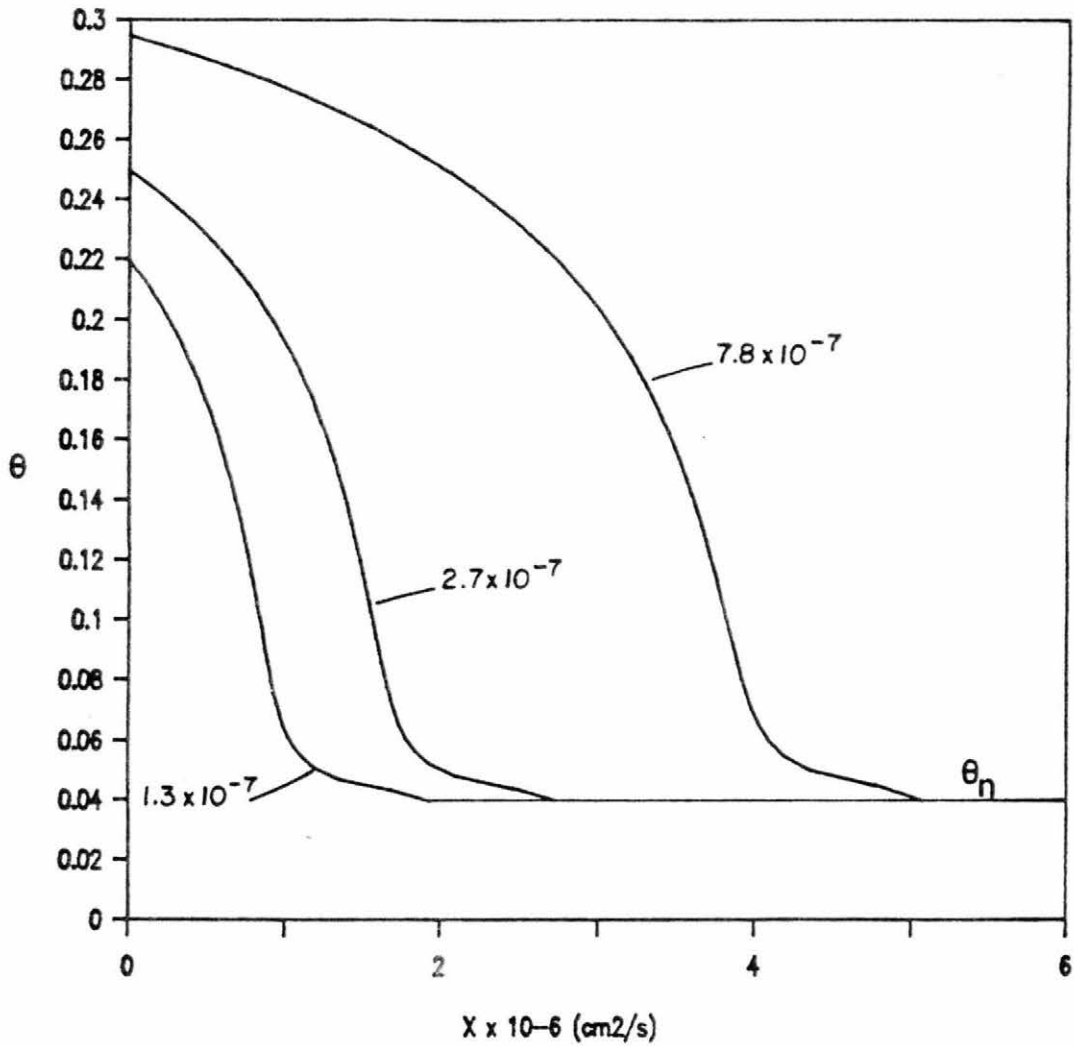


Figure 6.31. Liquid content profile for case 7.

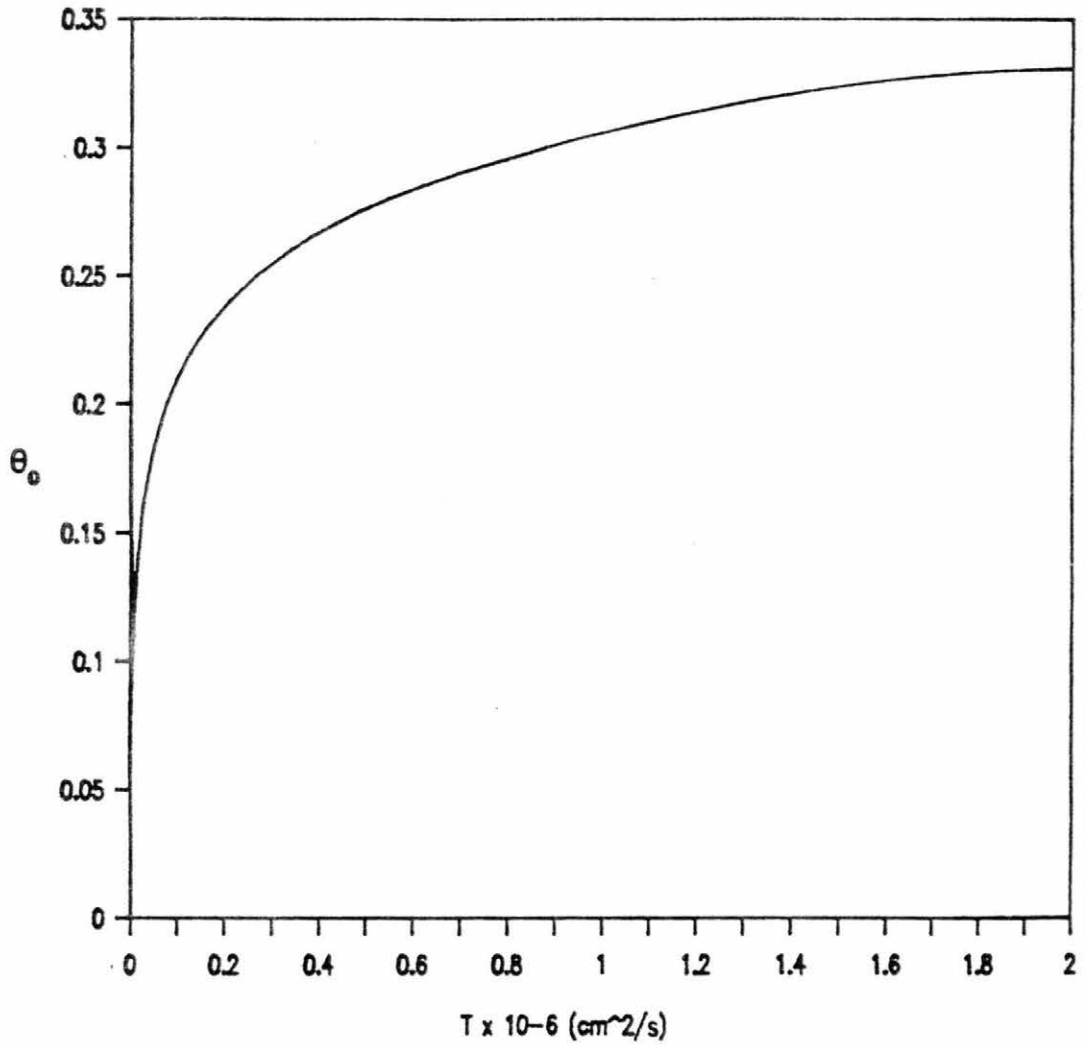


Figure 6.32. Time to inlet liquid content for case 7.

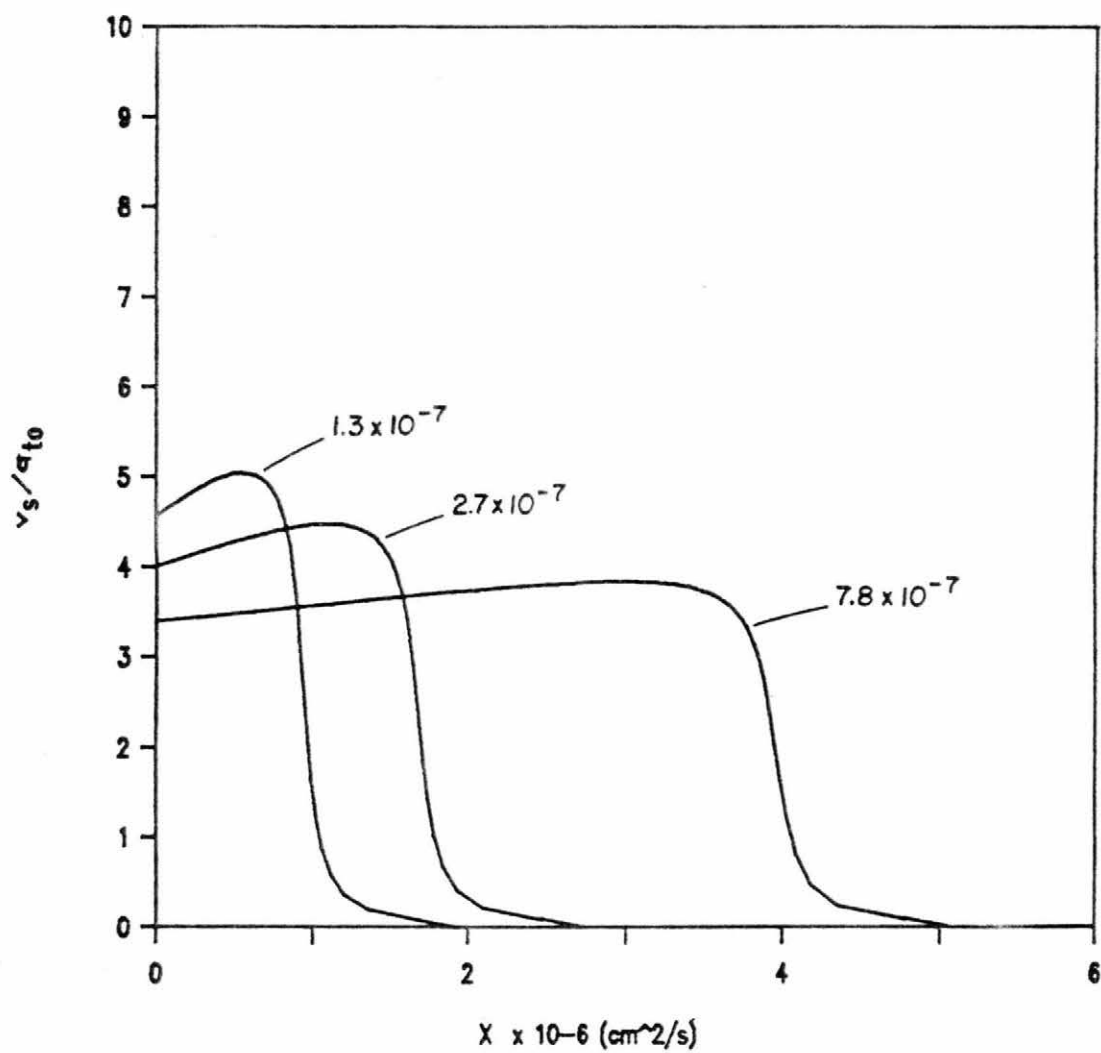


Figure 6.33. Seepage velocity for case 7.

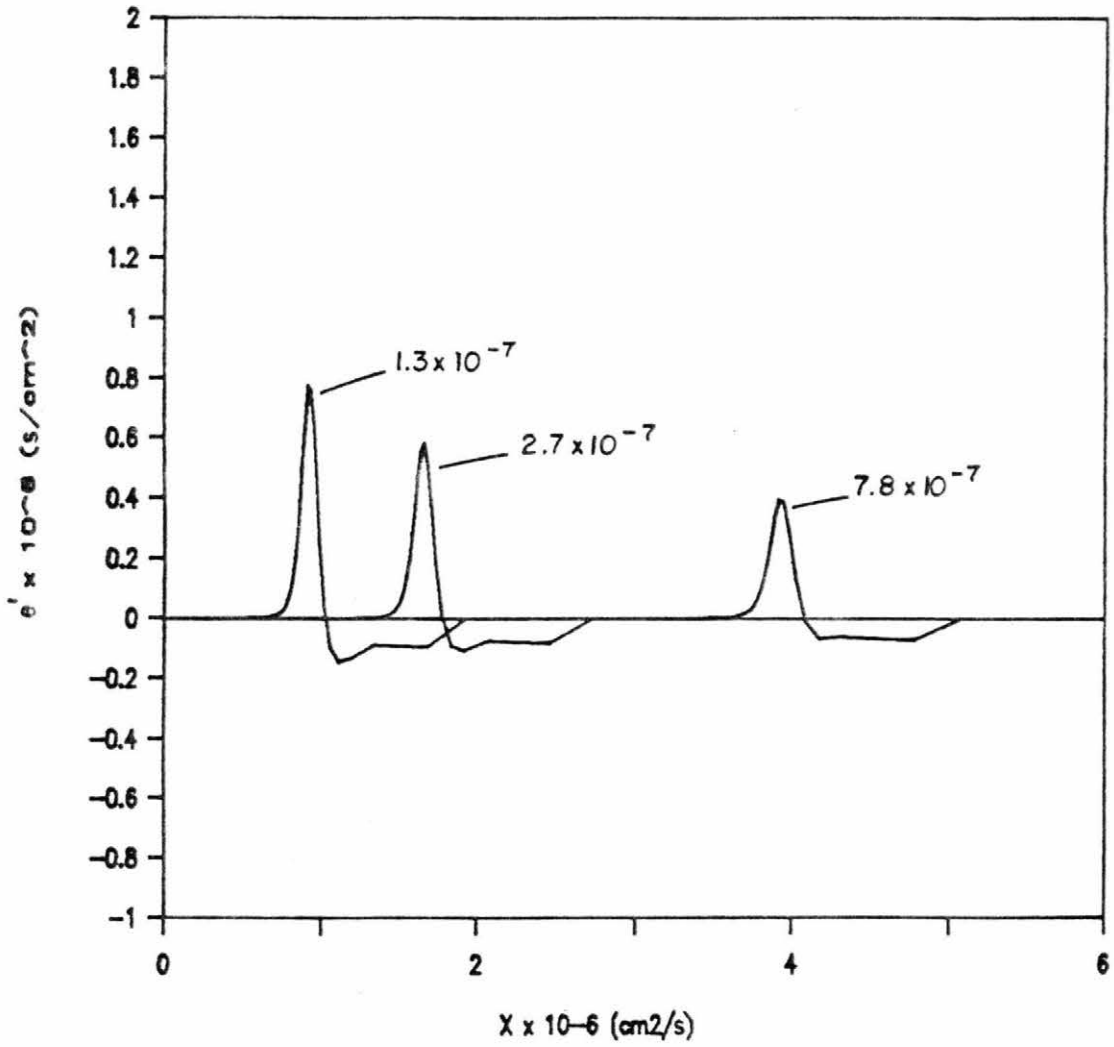


Figure 6.34. Phase transfer for case 7.

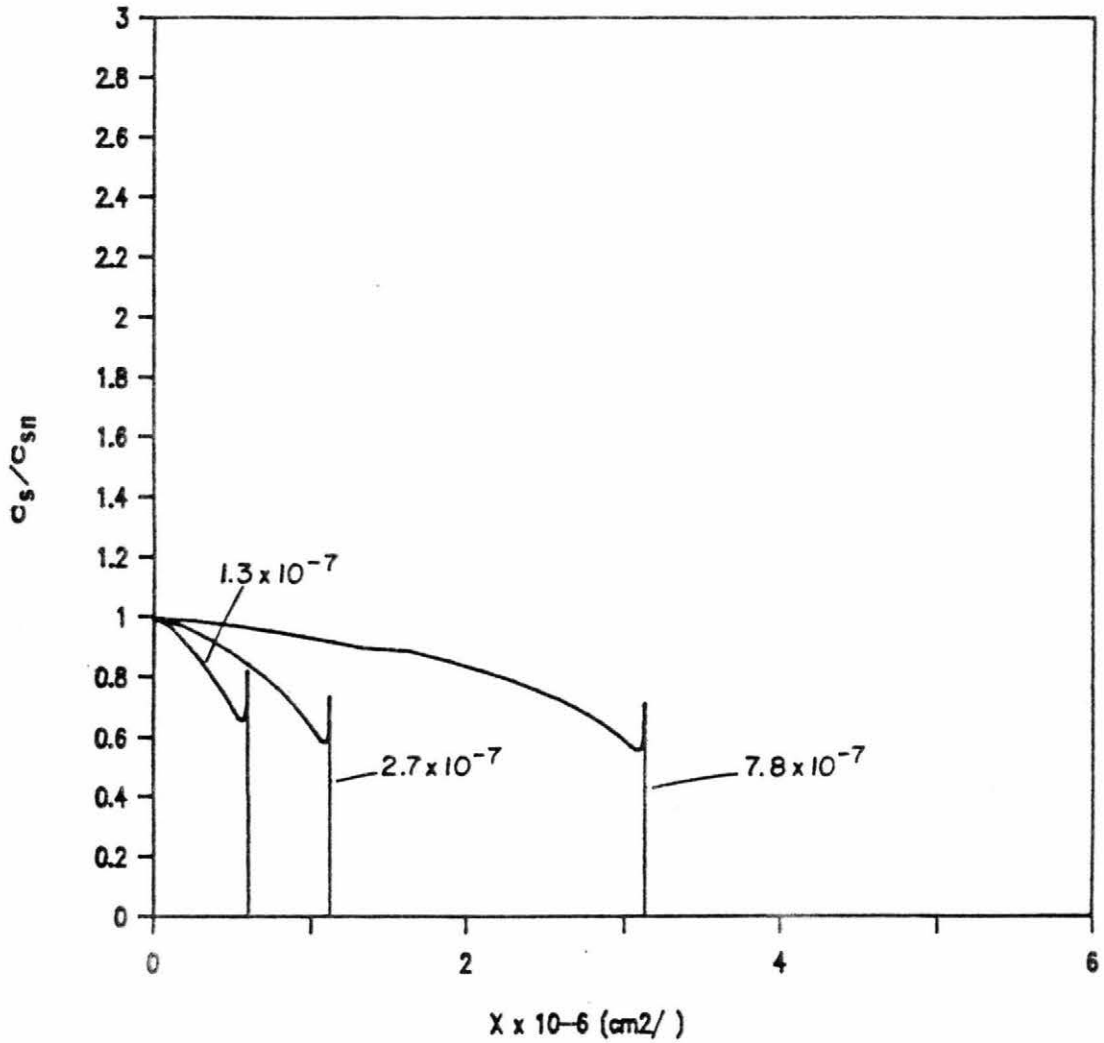


Figure 6.35. Invading solute concentration for Case 7.

Figure 6.36 presents the resident solute concentration. The solute is first concentrated and then diluted. This profile differs from case 5 in that no plateau of elevated concentration is formed.

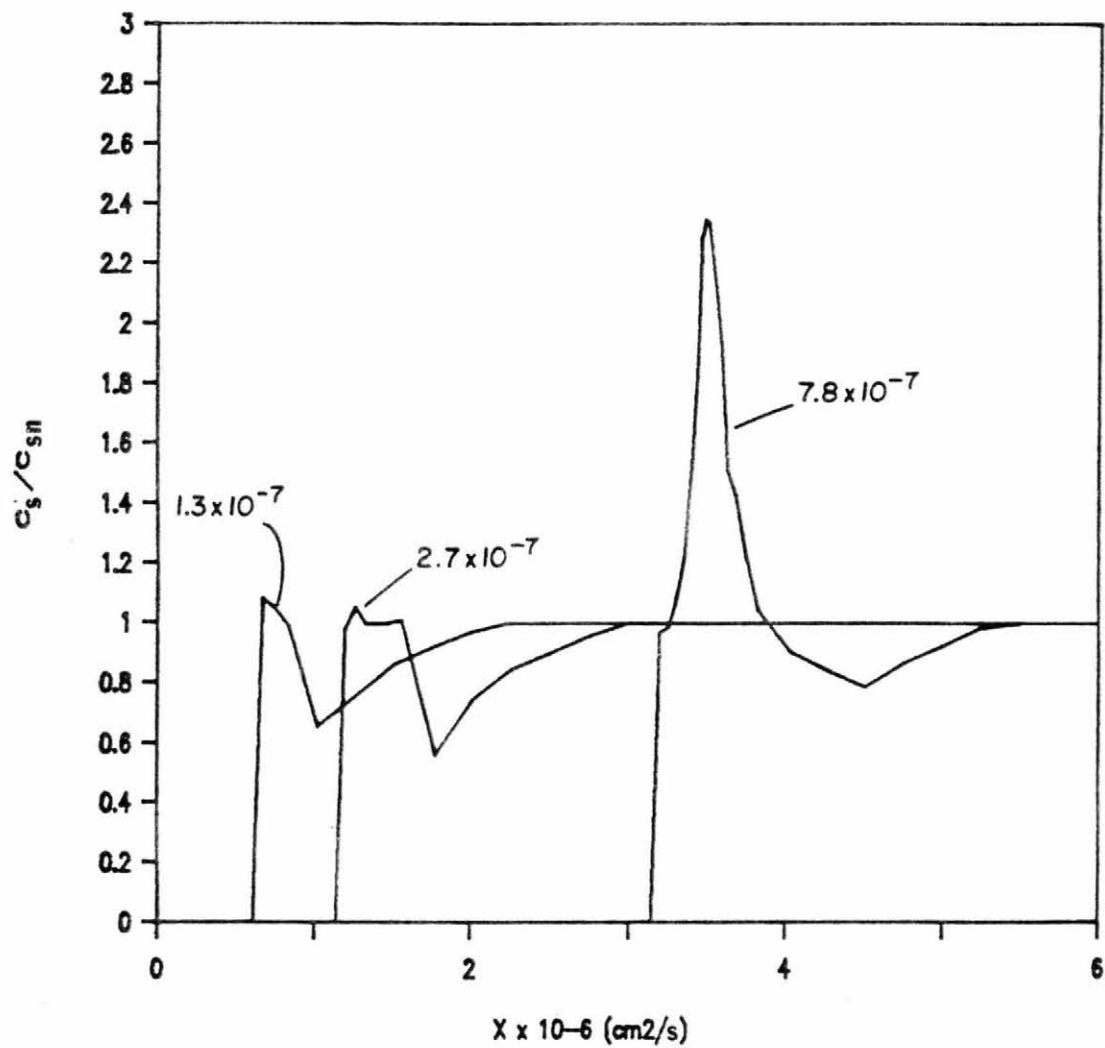


Figure 6.36. Resident solute concentration for case 7.

## Chapter 7

### SUMMARY, CONCLUSIONS AND RECOMMENDATIONS

#### SUMMARY

In relatively dry porous media, water is transported by both liquid bulk flow and vapor diffusion. The two phase transport of the volatile solvent affects the convective transport of nonvolatile solutes. The primary focus of this dissertation is the effect of solvent vaporization on the transport of a nonvolatile solute. To the author's knowledge, this is the first investigation to be undertaken on this subject.

The theory of combined liquid-vapor transport has been critically examined and expanded. The existing theory was found to be adequate for description of total isothermal solvent transport. However, new relations were developed which allow for the explicit calculation of the separate phase transport, and phase transfer in transient flow systems. Phase transfer (evaporation and condensation) was found to induce large gas-phase bulk flow. While the induced gas volumetric flows were large, the convection of solvent vapor was small relative to vapor diffusion in the water-air system examined. Specific criteria were developed to test for the significance of convection by induced gas flow in other systems.

A new theory of transient solute transport by a volatile solvent was developed. The theory allows for solute convection in the liquid phase, dispersion, and phase transfer of solvent. An explicit

assumption of the theory is that solute convection occurs at all water contents above that associated with a monolayer liquid solvent coverage of the porous media. The solute dispersion is assumed to be a function of liquid content and may be zero at non-zero liquid contents.

Analytical and numerical solutions for transient, horizontal transport of solute by a volatile solvent, in a homogeneous, isothermal porous media were obtained. For constant liquid-content boundary conditions, a complete and exact, semi-analytical solution to the governing equation of solvent transport was obtained. The method uses fractional flow concepts developed by Phillip (1973). An analytical solution for solute transport in a volatile solvent subject to the constant solute concentration boundary condition, was obtained for the simplified condition of no solute dispersion.

For constant liquid flux boundary conditions, an approximate analytical solution to the equations governing solvent flow was obtained. The method uses measured or assumed values of the fractional flow function, and transformed spatial and temporal coordinates developed by While et al. (1979). A numerical solution method was developed to calculate the solute flux in this flow. The technique takes maximum advantage for the analytical solution of the solvent flow.

Water and solute transport were measured in relatively dry Lurgi retorted oil shale. The experiments used the dual source gamma ray attenuation system developed by Grismer (1984). Constant flux sorption of solution into dry material was used throughout. The results obtained were similar to results obtained by Grismer in soils. A region of solute free water at low liquid contents was observed to develop ahead of a region of solution during the experiments.

Hydraulic diffusivity was obtained for the entire liquid content range. Using an independently measured water characteristic, the unsaturated hydraulic conductivity was also calculated.

The analytical and numerical solutions developed were applied to replicate the experimental conditions and data taken from the literature. The solutions show that the relative magnitudes of the separate transport coefficients produce many of the flow features observed in experimental data. Significant liquid transport can occur in regions without apparent solute transport. The regions of pure water are only an artifact of the transient experiments. That is, the pure water region would not be seen under steady state conditions. The new theory was also able to explain the increased resident solute concentrations observed by Smiles et al. (1978), and the increased concentration of invading solute observed by Grismer (1984).

These developments represent an addition to the understanding of solute transport in unsaturated systems. The methods and results can be applied to other problems in multiple phase transport such as hazardous waste disposal, mine reclamation and soil leaching.

## CONCLUSIONS

The following specific conclusions have been made for the conditions examined here. For any constant liquid content boundary condition case:

1. All solvent transport parameters maintain similitude with respect to the Boltzman variable, including the phase transfer.

2. If the coefficient of solute dispersion is only a function of liquid content, the solute concentration will also maintain similitude with respect to the Boltzman variable.
3. The ratio of the seepage velocity at a liquid content, to the velocity of the particular liquid content  $B(\theta)$ , is constant for given boundary conditions and predicts the location of the solute front.

For the case of constant content sorption into initially dry columns:

4. The fractional flow function  $F(\theta)$  is increased by vapor diffusion.
5. Vapor diffusion reduces the liquid convection and seepage velocities by reducing the gradient of solution content.
6. The phase transfer tends to be limited to narrow regions of evaporation and condensation.
7. The effects of water vapor transport on solute transport are insensitive to the actual values of vapor diffusion.
8. The invading solute will be concentrated behind the solution content where  $B(\theta)$  is equal to unity.
9. Induced gas convection can be shown to be negligible for the cases examined.

For the case of constant content sorption into a column with low initial liquid content with a resident solute:

10. The fractional flow function  $F(\theta)$  is only slightly increased by the vapor diffusivity.
11. Vapor transport effects are reduced significantly.
12. While the evaporation is limited to a narrow position, the condensation is spread out over a broad area.

13. The invading solute will be restricted behind the region of  $B(\theta)=1$ , but the increase in solute concentration above injection levels will be trivial.
14. The resident solute will be restricted to the region where  $B(\theta)\leq 1$ . It will be concentrated above initial values near the position of  $B(\theta)=1$ , and diluted somewhere beyond that point.
15. The results of Smiles et al. (1978), can be explained by the theory developed here.

For the constant flux sorption of solution:

16. The measured  $F(\theta)$  function is closely approximated by the  $F(\theta)$  function calculated for constant liquid content boundaries.
17. Calculated liquid contents, fluxes and phase transfer, are very similar to the conditions calculated for constant liquid content boundary conditions with the same inlet liquid content.

For the constant flux sorption of solution into an initially dry material:

18. Measured profiles, and time to inlet liquid content are closely approximated by the calculated profiles.
19. The invading solute will be concentrated by the flow processes to solution contents above a relative constant value.
20. The theory developed here predicts within measurement error, the liquid content of the solute front.

For constant flux sorption into a sample with a low initial solution content:

21. The invading solute is not concentrated above the inlet concentration.
22. The resident solute is both concentrated above and dilute below the initial value.
23. The results of Grismer (1984) can be explained by the theory developed here.

#### RECOMMENDATIONS

Three recommendations for further work follow from this research. Each of these recommendations could develop into a major study in its own right and provide additional insight into the processes of solute transport by a volatile solvent. The recommendations are:

1. Further explore the influence of induced gas bulk flow on vapor transport. The possibility of convective dispersion of water vapor at low Peclet numbers should be examined. In particular the conditions where convective transport of vapor becomes significant should be determined. It is possible that under nonisothermal conditions, the gas bulk flow will be much larger, and may be one of the causes of the enhanced vapor transport reported in the literature.
2. Develop analytical or numerical solutions for the complete solute transport equations (Eqs. 4.33 and 4.54), including the dispersion term. This should strengthen many of the conclusions made here.
3. Perform laboratory experiments to completely verify the predictions made here. In particular the predictions concerning the constant liquid content boundary displacement of a resident solute need additional verification. Likewise,

the theory developed here can be applied to desorption processes. Properly conducted desorption experiments may bring forth additional knowledge.

## REFERENCES

- Anderson, D.M. and Low, P.F., 1958. The Density of Water Adsorbed by Lithium-, Sodium-, and Potassium-Bentonite. *Soil Sci. Soc. Am. Proc.* 22:99-103.
- Bear, J., 1972. *Dynamics of Fluids in Porous Media*. American Elsevier, New York.
- Bird, R.B., Stewart, W.E., and Lightfoot, E.N., 1960. *Transport Phenomena*. John Wiley and Sons, Inc. New York.
- Bond, W.J., and Smiles, D.E., 1983. Influence of Velocity on Hydrodynamic Dispersion During Unsteady Soil Water Flow. *Soil Sci. Am. J.* 47:438-441.
- Bond, W.J., Gardiner, B.N., and Smiles, D.E., 1982. Constant-Flux Adsorption of a Tritiated Calcium Chloride Solution by a Clay Soil with Anion Exclusion. *Soil Sci. Soc. Am. J.* 46:1133-1137.
- Boulier, J.F., Touma, J., and Vauclin, M., 1984. Flux-Concentration Relation-Based Solution of Constant-Flux Infiltration Equation: I Infiltration into Nonuniform Initial Moisture Profiles. *Soil Sci. Soc. Am. J.* 48:245-251.
- Bruce, R.R. and Klute, A., 1956. The Measurement of Soil Moisture Diffusivity. *Soil Sci. Soc. Am. Proc.* 20:458-462.
- Brunauer, S., Emmett, P.H., and Teller, E., 1938. Adsorption of Gases in Multi-Molecular Layers. *J. Am. Chem. Soc.* 60:309-319.
- Cass, A., Cambell, G.S., and Jones, T.L., 1984. Enhancement of Thermal Water Vapor Diffusion in soil. *Soil Sci. Soc. Am. J.* 48:25-32.
- Chemical Rubber Company, 1986. *CRC Handbook of Chemistry and Physics*. Chemical Rubber Company, West Palm Beach Fla.
- Childs, E.C., and George, N.C., 1950. Permeability of Porous Materials. *Proc. Royal Soc. (London)* 201A:392-399.
- Corey, A.T., 1977. *Mechanics of Heterogeneous Fluids in Porous Media*. Water Resources Pub., Fort Collins, CO.
- DeVries, D.A., 1950a. Some Remarks on Heat Transfer by Vapour Movement in Soils. *Trans. 4th Intern. Cong. Soil Sci.* 2:38-41.
- DeVries, D.A., 1950b. Some Remarks on Gaseous Diffusion in Soils. *Trans. 4th Intern. Cong. Soil Sci.* 2:41-43.

- Golder Associates, 1983. Movement of Water through a Processed Oil Shale Pile. Report to AMOCO/Rio Blanco Oil Shale Co., March.
- Elrick, D.E., Laryea, K.B., and Groenvelt, P.H., 1979. Hydrodynamic Dispersion During Infiltration of Water into Soil. Soil Sci. Soc. Am. J. 43:856-865.
- Emmett, P.H., Brunauer, S., and Love, K.S., 1937. The Measurement of Surface Areas of Soils and Soil Colloids by the Use of Low Temperature Van Der-Waals Adsorption Isotherms. Soil Sci. 45:57-65.
- Grismer, M.E., 1984. Water and Salt Movement in Relatively Dry Soils. Ph.D. Dissertation, Department of Agricultural and Chemical Engineering, Colorado State University, Fort Collins, Colorado.
- Grismer, M.E., McWhorter, D.B., and Klute, A., 1986. Determination of Diffusivity and Hydraulic Conductivity in Soils at Low Water Contents from Nondestructive Transient Flow Observations. Soil Sci. 141:10-19.
- Grismer, M.E., McWhorter, D.B., and Klute, A., 1986. Monitoring Water and Salt Movement in Soils at Low Solution Contents. Soil Sci. 141:163-171.
- Hadas, A., 1977. Evaluation of Theoretically Predicted Thermal Conductivities of Soils Under Field and Laboratory Conditions. Soil Sci. Soc. Am. J. 41:460-466.
- Heistand, R.N., 1985. Estimating Solid Wastes from Oil Shale Facilities. Proceedings at the Eighteenth Oil Shale Symposium. Colorado School of Mines Press, Golden, CO.
- Jackson, R.D., 1964a. Water Vapor Diffusion in Relatively Dry Soil: I. Theoretical Considerations and Sorption Experiments. Soil Sci. Soc. Am. Proc. 28:172-176.
- Jackson, R.D., 1964b. Water Vapor Diffusion in Relatively Dry Soil: II. Desorption Experiments. Soil Sci. Soc. Am. Proc. 28:464-466.
- Jackson, R.D., 1964c. Water Vapor Diffusion in Relatively Dry Soil: III. Steady-State Experiments. Soil Sci. Soc. Am. Proc. 28:467-470.
- Jackson, R.D., 1965. Water Vapor Diffusion in Relatively Dry Soil: IV. Temperature and Pressure Effects on Sorption Diffusion coefficients. Soil Sci. Soc. Am. Proc. 29:144-148.
- Jury, W.A., and Lety, J. Jr., 1979. Water Vapor Movement in Soil: Reconciliation of Theory and Experiment. Soil Sci. Soc. Am. J. 43:823-827.
- Karathanasis, A.D., and Hajek, B.F., 1982. Quantitative Evaluation of Water Adsorption on Clay soils. Soil Sci. Soc. Am. J. 46:1321-1325.

- Kemper, W.D., 1961. Movement of Water as Effected by Free Energy and Pressure Gradients: I. Application of Classic Equations for Viscous and Diffusive Movements to the Liquid Phase in Finely Porous Media. *Soil Sci. Soc. Am. Proc.* 25:255-265.
- Kemper, W.D., Maasland, E.L. and Porter, L.K., 1964. Mobility of Water Adjacent to Mineral Surfaces. *Soil Sci. Soc. Am. Proc.* 28:164-167.
- Klute, A., 1952. Some Theoretical Aspects of the Flow of Water in Unsaturated soils. *Soil Sci. Soc. Proc.* 16:144-148.
- Klute, A., 1986. Water Retention Laboratory Methods. In: *Am. Soc. of Ag. Mono. No. 9. Methods of Soil Analysis, Part 1. Physical and Mineralogical Methods*, 2nd ed.
- Krupp, H.K., Biggar, J.W., and Nielsen, D.R., 1972. Relative Flow Rates of Salt and Water in Soil. *Soil Sci. Soc. Am. Proc.* 36:412-417.
- Langer, G., Roathe, A., Roethe, K-P, and Gelbin, D., 1978. Heat and Mass Transfer in Packed Beds-III Axial Mass Dispersion. *Inter. J. of Heat and Mass Transfer* 21:751-759.
- Laryea, K.B., Elrick, D.E., and Robin, M.J.L., 1982. Hydrodynamic Dispersion Involving Cationic Adsorption During Unsaturated, Transient Water Flow in Soil. *Soil Sci. Soc. Am. J.* 46:667-671.
- Marcus, D., Sangrey, D.A., and Miller, S.A., 1984. Environmental Effects of Cementation Process on Spent Shale Leachates. Presented at the SME-AIME Annual Meeting, Los Angeles, CA, Feb. 26-Mar.1.
- McWhorter, D.B., 1971. Infiltration Affected by Flow of Air. *Hydrology Papers*, Colorado State University, Fort Collins, Colorado.
- McWhorter, D.B., and Brown, G.O., 1985a. Adsorption and Flow of Water in Nearly Dry Lurgi Retorted Oil Shale. Unpublished report prepared for Standard Oil Company, AMOCO Research Center, Colorado State University, February.
- McWhorter, D.B., and Brown, G.O., 1985b. Liquid and Vapor Transport Coefficients for Retorted Oil Shale. *Proceedings of the 18th Oil Shale Symposium*. Colorado School of Mines Press, Golden, Colorado.
- McWhorter, D.B., and Sunada, D.K., 1977. *Groundwater Hydrology and Hydraulics*. Water Resources Pub., Fort Collins, CO.
- Mooney, R.W., Keenan, A.G., and Wood, L.A., 1952. Adsorption of Water Vapor by Montmorillonite. II. Effect of Exchangeable Ions and Lattice Swelling as Measured by X-ray Diffraction. *J. Am. Chem. Soc.* 74:1371-1374.

- Nakano, M., and Miyazaki, T., 1979. The Diffusion and Nonequilibrium Thermodynamic Equations of Water Vapor in Soils under Temperature Gradients. *Soil Sci.* 128:184-188.
- Nazareth, V.A., 1984. A Laboratory Column Leach Test for Oil Shale Solid Wastes. Ph.D. Dissertation, Department of Agricultural and Chemical Engineering, Colorado State University, Fort Collins, CO.
- Orchiston, H.D., 1954. Adsorption of Water Vapor: I. Soils at 25°C. *Soil Sci.* 76:453-465.
- Orchiston, H.D., 1954. Adsorption of Water Vapor: II. Clays at 25°C. *Soil Sci.* 78:463-480.
- Orchiston, H.D., 1955. Adsorption of Water Vapor: III. Homonic Montmorillonites at 25°C. *Soil Sci.* 79:71-78.
- Phillip, J.R., 1955. The Concept of Diffusion Applied to Soil Water. *Proc. Natl. Acad. Sci. (India)* 24A:93-104.
- Phillip, J.R., 1957. Evaporation and Moisture and Heat Fields in the Soil. *J. Meteorology* 14(4):354-366.
- Phillip, J.R., and DeVries, 1957. Moisture Movement in Porous Materials Under Temperature Gradients. *A.G.U. Trans.*, 38(2):222-231.
- Phillip, J.R., 1973. On Solving the Unsaturated Flow Equation: I. The Flux-Concentration Relation. *Soil Sci.* 116:328-335.
- Phillip, J.R., and Knight, J.H., 1974. On Solving the Unsaturated Flow Equation: III New Quasi-Analytical Technique. *Soil Sci.* 117:1-13.
- Pilz, J., 1982. The Saturated and Unsaturated Shear Strength of Spend Oil Shale. Ph.D. Dissertation, Department of Civil Engineering, Colorado State University, Fort Collins, CO.
- Porter, L.K., Kemper, W. D., Jackson, R.D., and Stewart, B.A., 1960. Chloride Diffusion in Soils as Influenced by Moisture Content. *Soil Sci. Soc. Am. Proc.* 24:460-463.
- Quik, J.P., 1955. Significance of Surface Areas Calculated from Water Vapor Sorption Isotherms by Use of the B.E.T. Equation. *Soil Sci.* 80:423-430.
- Reddell, D.L., and Sunada, D.K., 1970. Numerical Simulation of Dispersion in Groundwater Aquifers. *Hydrol. Pap.* 41, Colorado State University, Fort Collins, CO.
- Richards, L.A. (Ed.), 1954. Diagnostic and Improvement of Saline and Alkali Soils. USDA Agricultural Handbook No. 60. U.S. Government Printing Office, Washington, DC.
- Rio Blanco Oil Shale Project, 1976. Detailed Development Plan, Tract C-a. Vol. 3, Mining, Processing and Support Facilities.

- Rio Blanco Oil Shale Project, 1977. Revised Detailed Development Plan, Tract C-a. Vol. 2, Mining, Processing and Support Facilities.
- Rio Blanco Oil Shale Company, 1981. Tract C-a, Modification to the Detailed Development Plan. Lurgi Demonstration Project.
- Robin, M.J.L., Laryea, K.B., and Elick, D.E., 1983. Hydrodynamic Dispersion During Adsorption of Water by Soil. *J. Hydrol.* 65:333-348.
- Rollins, R.L., Spangler, M.G., and Kirkham, D., 1954. Movement of Soil Moisture under a Thermal Gradient. *Highway Res. Board Proc.* 33:492-508.
- Rolston, D.E., Kirkham, D., and Nielsen, D.R., 1969. Miscible Displacement of Gases Through Soil Columns. *Soil Sci. Soc. Am. Proc.* 33:488-492.
- Rose, D.A., 1963a. Water Movement in Porous Materials: I. Isothermal Vapor Transfer. *Brit. J. App. Phys.* 14:256-262.
- Rose, D.A., 1963b. Water Movement in Porous Materials: II. The Separation of the Components of Water Movement. *Brit. J. App. Phys.* 14:491-496.
- Rose, D.A., 1968a. Water Movement in Porous Materials: III. Evaporation of Water from Soil. *Brit. J. App. Phys., Series(2)* 1:1779-1791.
- Rose, D.A., 1968b. Water Movement in Dry Soils: I. Physical Factors Affecting Sorption of Water by Soil. *J. of Soil Sci.* 19:81-93.
- Ruthren, D.A., 1984. Adsorption and Adsorption Processes. John Wiley and Sons, New York.
- Smiles, D.E., Phillip, J.R., Knight, J.H., and Elrick, D.E., 1978. Hydrodynamic Dispersion During Adsorption of Water by Soil. *Soil Sci. Soc. Am. J.* 44:229-234.
- Smiles, D.E., Perroux, K.M., Zegelin, S.J., and Raats, P.A.C., 1981. Hydrodynamic Dispersion During constant Rate Adsorption of Water into Soil. *soil Sci. Soc. Am. J.* 45:453-458.
- Smiles, D.E., and Gardiner, B.N., 1982. Hydrodynamic Dispersion During Unsteady, Unsaturated Water Flow in Clay Soil. *Soil Sci. Soc. Am. J.* 46:9-14.
- Smiles, D.E., and Phillip, J.R., 1978. Solute Transport During Adsorption of Water by Soil: Laboratory Studies and Their Practical Implications. *Soil Sci. Soc. Am. J.* 42:537-544.
- Stigter, D., 1980. Self Diffusion and Viscosity of Water in Clays. *Soil Sci.* 130:1-6.

- Van Brakel, J., and Heertjes, P.M., 1974. Analysis of Diffusion in Macroporous Media in Terms of a Porosity, A Tortuosity and a Constrictivity Factor. *Int. J. Heat Mass Transfer* 17:1093-1103.
- Van Schaik, J.C., and Kemper, W.D., 1966. Chloride Diffusion in Clay-Water Systems. *Soil Sci. Soc. Am. Proc.* 30:22-25.
- Watson, K.K., and Jones, M.J., 1982. Hydrodynamic Dispersion During Absorption in a Fine Sand. 1. The Constant Concentration Case. *Water Resour. Res.* 18:91-100.
- White, I., 1979. Measured and Approximate Flux-Concentration Relations for Adsorption of Water by Soil. *Soil Sci. Soc. Am. J.* 43:1074-1080.
- White, I., Smiles, D.E., and Perroux, K.M., 1979. Adsorption of Water by Soil: The Constant Flux Boundary Condition. *Soil Sci. Soc. Am. J.* 43:639-664.
- Wilson, J.L., and Gelhar, L.W., 1974. Dispersive Mixing in a Partially Saturated Porous Medium. Tech. Rep. 191, Ralph M. parsons Lab. for Water Resour. and Hydrodyn. Mass. Inst. of Technol., Cambridge, MA, 1974.
- Wilson, J.L., and Gelhar, L.W., 1981. Analysis of Longitudinal Dispersion in Unsaturated Flow. I. The Analytical Model. *Water Resour. Res.* 17:122-129.

## APPENDIX

## EXPERIMENTAL DATA

Table A.1 Particle size distribution of Lurgi retorted shale (Figure 5.1).

---

Size mm	% Finer
5.00	0
2.00	8.37
0.991	37.15
0.841	41.78
0.701	44.87
0.589	47.21
0.495	49.06
0.246	57.10
0.147	60.30
0.074	65.52
0.061	68.95
0.045	71.35

---

Table A.2. Water characteristic for Lurgi retorted oil shale (Figure 5.3).

	$h_c$ cm	$\theta$	
		Wetting	Drainage
Pressure Cell	$9.00 \times 10^1$	0.480	-
	$3.11 \times 10^2$	0.449	0.483
	$6.85 \times 10^2$	0.256	0.470
	$2.07 \times 10^3$	0.205	0.421
	$4.04 \times 10^3$	0.100	0.349
	$9.00 \times 10^3$	0.117	0.309
	$1.47 \times 10^4$	-	0.383
Vapor Sorpton*	$3.00 \times 10^3$	0.175	-
	$2.74 \times 10^4$	0.973	-
	$4.92 \times 10^4$	0.090	-
	$7.40 \times 10^4$	0.082	0.118
	$2.00 \times 10^5$	0.063	0.087
	$3.50 \times 10^5$	0.046	0.075
	$5.75 \times 10^5$	0.042	0.066
	$8.66 \times 10^5$	-	0.059
	$1.13 \times 10^6$	0.030	0.058
	$3.18 \times 10^6$	0.016	0.032
$3.86 \times 10^6$	0.014	-	

\*Vapor sorption  $h_c$  are adjusted by 2500 cm to account for the osonic head.

Table A.3. Water vapor sorption isotherms for Lurgi retorted shale (Figure 5.4).

Solution	Relative Humidity	Adsorption g/g	Desorption g/g
NaOH	0.061	0.0103	-
ZnCl <sub>2</sub>	0.100	0.0113	0.0227
K <sub>2</sub> CO <sub>3</sub>	0.436	0.0215	0.0413
Mg(NO <sub>3</sub> ) <sub>2</sub>	0.542	-	0.0424
NaNO <sub>2</sub>	0.649	0.0296	0.0473
NaCl	0.758	0.0373	0.0535
KCl	0.850	0.0448	0.0621
KNO <sub>3</sub>	0.931	0.0591	0.0830
Ca(H <sub>2</sub> PO <sub>4</sub> ) <sub>2</sub>	0.948	0.0646	-
KH <sub>2</sub> PO <sub>4</sub>	0.963	0.0695	-
K <sub>2</sub> Cr <sub>2</sub> O <sub>7</sub>	0.980	0.125	-



Table A.4. (continued).

Scan	9		10		11		12	
Time (hrs)	216		244		287		337	
Influx (gm)	0		0		0		0	
Length (cm)	$\theta$	$C_s$	$\theta$	$C_s$	$\theta$	$C_s$	$\theta$	$C_s$
0.5	0.195	0.169	0.194	0.166	0.166	0.195	0.159	0.200
1.0	0.179	0.182	0.172	0.187	0.153	0.221	0.154	0.206
1.5	0.168	0.135	0.148	0.159	0.137	0.171	0.132	0.179
2.0	0.087	0.016	0.081	0.034	0.079	0.050	0.079	0.061
2.5	0.041	0	0.046	0	0.055	0	0.063	0
3.0	0.034	0	0.041	0	0.042	0	0.043	0
3.5	0.027	0	0.032	0	0.032	0	0.029	0
4.0	0.024	0	0.022	0	0.028	0	0.030	0
4.5	0.025	0	0.025	0	0.030	0	0.031	0
5.0	0.015	0	0.022	0	0.021	0	0.025	0
5.5	0.017	0	0.021	0	0.025	0	0.040	0
6.0	0.010	0	0.014	0	0.019	0	0.018	0
6.5	0.009	0	0.011	0	0.015	0	0.021	0
7.0	0	0	0.010	0	0.015	0	0.018	0
7.5	0	0	0	0	0	0	0.015	0
Scan	13		14		15		16	
Time (hrs)	384		503		624		720	
Influx (gm)	0		0		0		0	
Length (cm)	$\theta$	$C_s$	$\theta$	$C_s$	$\theta$	$C_s$	$\theta$	$C_s$
0.5	0.156	0.204	0.135	0.233	0.117	0.268	0.105	0.301
1.0	0.149	0.213	0.125	0.255	0.114	0.276	0.101	0.314
1.5	0.135	0.169	0.121	0.183	0.108	0.204	0.102	0.205
2.0	0.082	0.055	0.071	0.085	0.072	0.081	0.068	0.088
2.5	0.060	0	0.049	0	0.057	0	0.050	0
3.0	0.046	0	0.037	0	0.052	0	0.042	0
3.5	0.034	0	0.033	0	0.037	0	0.031	0
4.0	0.030	0	0.032	0	0.032	0	0.032	0
4.5	0.033	0	0.031	0	0.030	0	0.035	0
5.0	0.031	0	0.026	0	0.028	0	0.029	0
5.5	0.027	0	0.028	0	0.029	0	0.031	0
6.0	0.023	0	0.022	0	0.026	0	0.027	0
6.5	0.022	0	0.024	0	0.023	0	0.026	0
7.0	0.027	0	0.022	0	0.029	0	0.026	0
7.5	0.017	0	0.023	0	0.018	0	0.018	0
8.0	0.010	0	0.009	0	0.013	0	0.017	0
9.0	0.011	0	0.017	0	0.018	0	0.024	0
10.0	0.003	0	0.002	0	0.007	0	0.009	0

Table A.4. (continued)

Scan	17		18		19		20	
Time (hrs)	864		1008		1331		1880	
Influx (gm)	0		0		0		0	
Length (cm)	$\theta$	$C_s$	$\theta$	$C_s$	$\theta$	$C_s$	$\theta$	$C_s$
0.5	0.091	0.350	0.082	0.391	0.085	0.373	0.070	0.455
1.0	0.090	0.353	0.089	0.353	0.081	0.386	0.085	0.363
1.5	0.091	0.238	0.087	0.242	0.080	0.252	0.083	0.239
2.0	0.068	0.082	0.060	0.112	0.061	0.093	0.067	0.081
2.5	0.053	0	0.050	0	0.050	0	0.049	0
3.0	0.047	0	0.045	0	0.047	0	0.046	0
3.5	0.032	0	0.029	0	0.023	0	0.024	0
4.0	0.032	0	0.031	0	0.025	0	0.025	0
4.5	0.030	0	0.034	0	0.029	0	0.026	0
5.0	0.023	0	0.029	0	0.023	0	0.026	0
5.5	0.038	0	0.034	0	0.034	0	0.033	0
6.0	0.029	0	0.030	0	0.026	0	0.029	0
6.5	0.026	0	0.027	0	0.027	0	0.031	0
7.0	0.027	0	0.025	0	0.025	0	0.025	0
7.5	0.019	0	0.024	0	0.020	0	0.018	0
8.0	0.017	0	0.020	0	0.016	0	0.019	0
9.0	0.028	0	0.027	0	0.025	0	0.029	0
10.0	0.014	0	0.016	0	0.014	0	0.011	0
Scan	21							
Time (hrs)	2500							
Influx (gm)	0							
Length (cm)	$\theta$	$C_s$						
0.5	0.073	0.433						
1.0	0.077	0.401						
1.5	0.082	0.255						
2.0	0.052	0.125						
2.5	0.037	0						
3.0	0.026	0						
3.5	0.020	0						
4.0	0.021	0						
4.5	0.026	0						
5.0	0.018	0						
5.5	0.026	0						
6.0	0.017	0						
6.5	0.023	0						
7.0	0.024	0						
7.5	0.017	0						
8.0	0.006	0						
9.0	0.022	0						
10.0	0.016	0						

Table A.5. Liquid content and solute concentration for Run 2.

Scan	1		2		3		4	
Time (hrs)	12		24		36		48	
Influx (gm)	1.26		1.04		1.15		1.39	
Length (cm)	$\theta$	$C_s$	$\theta$	$C_s$	$\theta$	$C_s$	$\theta$	$C_s$
0.5	0.134	0.115	0.181	0.119	0.176	0.156	0.245	0.125
1.0	0.047	0.098	0.095	0.150	0.137	0.142	0.193	0.132
1.5	0.009	0	0.010	0.046	0.066	0.024	0.114	0.117
2.0	0	0	0.006	0	0.019	0	0.027	0
2.5	0	0	0.007	0	0.014	0	0.016	0
3.0	0	0	0	0	0.005	0	0.012	0
3.5	0	0	0	0	0.005	0	0.003	0
4.0	0	0	0	0	0	0	0.000	0
4.5	0	0	0	0	0	0	0.009	0
Scan	5		6		7		8	
Time (hrs)	59		73		84		96	
Influx (gm)	0.93		1.14		0.96		1.18	
Length (cm)	$\theta$	$C_s$	$\theta$	$C_s$	$\theta$	$C_s$	$\theta$	$C_s$
0.5	0.262	0.124	0.272	0.126	0.268	0.134	0.273	0.135
1.0	0.232	0.122	0.249	0.125	0.256	0.129	0.264	0.132
1.5	0.158	0.124	0.210	0.119	0.239	0.121	0.247	0.129
2.0	0.053	0	0.080	0.059	0.162	0.082	0.221	0.102
2.5	0.027	0	0.033	0	0.041	0	0.066	0.027
3.0	0.015	0	0.021	0	0.021	0	0.031	0
3.5	0.012	0	0.014	0	0.022	0	0.025	0
4.0	0.011	0	0.010	0	0.017	0	0.012	0
4.5	0.017	0	0.008	0	0.021	0	0.019	0
5.0	0	0	0.002	0	0.006	0	0.001	0
5.5	0	0	0	0	0.002	0	0.000	0
6.0	0	0	0	0	0.001	0	0.005	0

Table A.5. (continued).

Scan	9		10		11		12	
Time (hrs)	108		121		131		145	
Influx (gm)	1.29		1.94		1.40		2.24	
Length (cm)	$\theta$	$C_s$	$\theta$	$C_s$	$\theta$	$C_s$	$\theta$	$C_s$
0.5	0.287	0.132	0.307	0.132	0.309	0.132	0.335	0.127
1.0	0.270	0.134	0.310	0.123	0.292	0.135	0.312	0.131
1.5	0.262	0.131	0.304	0.120	0.292	0.130	0.314	0.127
2.0	0.248	0.111	0.287	0.110	0.284	0.119	0.310	0.116
2.5	0.206	0.054	0.265	0.093	0.288	0.101	0.302	0.109
3.0	0.040	0	0.182	0.018	0.258	0.057	0.276	0.092
3.5	0.021	0	0.045	0	0.095	0	0.257	0.038
4.0	0.019	0	0.023	0	0.036	0	0.096	0
4.5	0.011	0	0.010	0	0.032	0	0.033	0
5.0	0.007	0	0.005	0	0.014	0	0.019	0
5.5	0.004	0	0	0	0.013	0	0.017	0
6.0	0.009	0	0.001	0	0.014	0	0.018	0
6.5	0	0	0	0	0.009	0	0.011	0
7.0	0.003	0	0.002	0	0.010	0	0.007	0
7.5	0.002	0	0	0	0.002	0	0.007	0
8.0	0	0	0	0	0	0	0.005	0
Scan	13		14		15		16	
Time (hrs)	157		169		180		193	
Influx (gm)	2.00		2.23		2.75		5.90	
Length (cm)	$\theta$	$C_s$	$\theta$	$C_s$	$\theta$	$C_s$	$\theta$	$C_s$
0.5	0.317	0.138	0.347	0.127	0.386	0.117	0.368	0.133
1.0	0.311	0.136	0.334	0.128	0.369	0.119	0.359	0.131
1.5	0.311	0.134	0.339	0.125	0.377	0.116	0.378	0.126
2.0	0.307	0.125	0.338	0.118	0.371	0.113	0.394	0.116
2.5	0.293	0.123	0.321	0.117	0.355	0.113	0.366	0.120
3.0	0.284	0.108	0.312	0.107	0.344	0.105	0.365	0.112
3.5	0.266	0.080	0.301	0.091	0.324	0.100	0.353	0.111
4.0	0.262	0.025	0.301	0.062	0.331	0.083	0.349	0.105
4.5	0.064	0.009	0.273	0.013	0.315	0.043	0.341	0.089
5.0	0.025	0	0.050	0	0.317	0	0.345	0.061
5.5	0.022	0	0.025	0	0.048	0	0.331	0.027
6.0	0.020	0	0.023	0	0.027	0	0.330	0
6.5	0.010	0	0.019	0	0.020	0	0.072	0
7.0	0.017	0	0.020	0	0.019	0	0.020	0
7.5	0.015	0	0.012	0	0.006	0	0.018	0
8.0	0.004	0	0.003	0	0.007	0	0.005	0
9.0	0.002	0	0	0	0	0	0	0

Table A.5. (continued).

Scan		17
Time (hrs)		198
Influx (gm)		5.95
Length (cm)	$\theta$	$C_s$
0.5	0.477	0.096
1.0	0.455	0.108
1.5	0.459	0.109
2.0	0.469	0.105
2.5	0.437	0.106
3.0	0.438	0.102
3.5	0.433	0.099
4.0	0.416	0.098
4.5	0.394	0.093
5.0	0.392	0.083
5.5	0.380	0.066
6.0	0.390	0.038
6.5	0.360	0.010
7.0	0.324	0
7.5	0.028	0
8.0	0.021	0
9.0	0.003	0
10.0	0	0